T.R.
EGE UNIVERSITY
Graduate School of Applied and Natural Science

TUNGSTEN OXIDE MODIFIED ELECTRODES AND THEIR ELECTROCATALYTIC APPLICATIONS

PhD Thesis

İrem ÇAKAR DAVASLIOĞLU

Supervisor: Prof. F. Nil ERTAŞ

Co-Supervisor: Prof. Dr. Süleyman KOÇAK

Chemistry Department

İzmir

2021

T.R.
EGE UNIVERSITY
Graduate School of Applied and Natural Science

TUNGSTEN OXIDE MODIFIED ELECTRODES AND THEIR ELECTROCATALYTIC APPLICATIONS

İrem ÇAKAR DAVASLIOĞLU

Supervisor: Prof. F. Nil ERTAŞ
Co-Supervisor: Prof. Dr. Süleyman KOÇAK

Chemistry Department
Analytical Chemistry Third Cycle Programme

İzmir
2021

EGE ÜNİVERSİTESİ FEN BİLİMLERİ ENSTİTÜSÜ

ETİK KURALLARA UYGUNLUK BEYANI

EÜ Lisansüstü Eğitim ve Öğretim Yönetmeliğinin ilgili hükümleri uyarınca Doktora Tezi olarak sunduğum "***Tungsten Oxide Modified Electrodes And Their Electrocatalytic Applications (Tungsten Oksit Modifiye Elektrotlar Ve Elektrokatalitik Uygulamaları)***" başlıklı bu tezin kendi çalışmam olduğunu, sunduğum tüm sonuç, doküman, bilgi ve belgeleri bizzat ve bu tez çalışması kapsamında elde ettiğimi, bu tez çalışmasıyla elde edilmeyen bütün bilgi ve yorumlara atıf yaptığımı ve bunları kaynaklar listesinde usulüne uygun olarak verdiğimi, tez çalışması ve yazımı sırasında patent ve telif haklarını ihlal edici bir davranışımın olmadığını, bu tezin herhangi bir bölümünü bu üniversite veya diğer bir üniversitede başka bir tez çalışması içinde sunmadığımı, bu tezin planlanmasından yazımına kadar bütün safhalarda bilimsel etik kurallarına uygun olarak davrandığımı ve aksinin ortaya çıkması durumunda her türlü yasal sonucu kabul edeceğimi beyan ederim.

11 / 11 / 2021

İmzası

İrem Çakar Davaslıoğlu

ÖZET

Tungsten Oksit Modifiye Elektrotlar ve Elektrokatalitik Uygulamaları

ÇAKAR DAVASLIOĞLU, İrem

Doktora Tezi, Kimya Anabilim Dalı
Analitik Kimya Doktora Programı
Tez Danışmanları: Prof. Dr. Fatma Nil ERTAŞ
Prof. Dr. Süleyman KOÇAK
Kasım 2021, 98 sayfa

Nano yapılı geçiş metalleri ve oksitleri, üstün katalitik özelliklerinden dolayı fonksiyonel malzemeler olarak ilgi çekmektedir. Bu tezde, çeşitli elektrotlar üzerinde biriken tungsten oksitin elektrokatalitik etkisinin araştırılması ve diğer metal nanoparçacıklarla oluşturduğu kompozitlerinin incelenmesi amaçlanmıştır. Bu amaçla, camsı karbon elektrot üzerine WO_x türleri elektrokimyasal biriktirildikten sonra sinerjik etki arayışı ile platin nanopartiküller ile dekore edilmiştir. Bu yenilikçi elektrotların karakterizasyon çalışmalarının ardından, katalitik performansları oksijen indirgeme reaksiyonu (ORR) için denenmiştir. ORR sinyalinde gözlenen sinerjik etki, kompozitin hiper d-hipo-d etkileşimine bağlanmıştır. Kompozit yapıdaki tungstenin karışık değerlikli yapısı da katalitik aktiviteye önemli katkıda bulunmuştur. Yöntemin analitik uygulaması, günlük kullanılan dezenfektan analizine alternatif bir yol olarak hidrojen peroksit için enzimatik olmayan sensör geliştirmeyi kapsamaktadır.

Tezin ikinci bölümünde, WO_x ile modifiye edilmiş kalem ucu grafit elektrotlar, 5 mM ferrisiyanür iyonlarının varlığında Elektrokimyasal empedans spektroskopi (EIS) ölçümlerine dayalı olarak Okratoksin A (OTA) tayini için aptasensör üretimi için destek malzemesi olarak kullanılmıştır. 5-amino aptamerin (NH_2-Apt) EDC/NHS mekanizması ile kovalent bağlanma verimi, adsorpsiyon yoluyla elektrot yüzeyine bağlanan NH_2-Apt ile elde edilen sonuçlar karşılaştırılarak, doğrulanmıştır. Yük aktarım direncindeki (R_{ct}) farklılıklar, metal oksit film üzerindeki -OH grupları aracılığıyla EDC/NHS mekanizmasının etkinliğini açıkça göstermiştir. Daha sonra, OTA tespiti için çalışma koşulları ile çözelti parametreleri (tungstat iyon konsantrasyonu, pH ve aptamer derişimi) optimize edilmiştir. Bir diğer mikotoksin olan Zearalenon (ZEA) kullanılarak seçicilik sınanmış ve nanomolar seviyelerde kalibrasyon grafikleri oluşturulmuştur.

Tezin son bölümünde, tungsten oksit film titanyum nanotüpler (TNT) üzerine elektro-biriktirme ile kompozit film oluşturulduktan sonra uygun potansiyelde çeşitli azo boyar maddelerinin Fotoelektrokatalitik bozunması incelenmiştir. Bu ikili oksit filminin Rodamin B bozunmasına uygulama koşulları optimize edilmiş ve bozunma mekanizmasını netleştirmek için kinetik çalışmalar da yapılmıştır. Sonuç olarak, TNT ve WO_3 arasındaki sinerjik etkileşim, üstün bir katalitik aktivite sumaktadır ve modifiyerin kimyasal özelliklerinden kaynaklanan güneş ışımasında kullanım için bir potansiyel arz etmektedir.

Tungsten oksidin elektrokatalitik aktivitelerinin farklı yönleri olarak değerlendirilerek, literatürde bu tür çalışmalara katkıda bulunacak verilerin üretimi gerçekleştirilmiştir.

Anahtar sözcükler: Voltammetri, Oksijen indirgenme tepkimesi, Tungsten oksit, EIS, aptasensör, Fotoelektrokatalitik bozunma, Rodamin B.

ABSTRACT
TUNGSTEN OXIDE MODIFIED ELECTRODES AND THEIR ELECTROCATALYTIC APPLICATIONS

ÇAKAR DAVASLIOĞLU, İrem

PhD in Chemistry Department (Analytical Chemistry)
Supervisor: Prof. Dr. Fatma Nil ERTAŞ
Co-Supervisor: Süleyman KOÇAK
November 2021, 98 pages

Nanostructured transition metals and their oxides are considered as attractive functional materials due to their outstanding catalytic properties. In this thesis, it was aimed to search the electrocatalytic effect of tungsten oxide deposited on several electrodes and to study its composites with other metal nanoparticles. For this purpose, glassy carbon electrode was for electrochemical deposition of WO_x species along with platinum nanoparticles in pursue of synergic effect and following the characterization studies, catalytic performances of the novel electrodes have been tested for oxygen reduction reaction (ORR). The synergic effect was attributed to the hyper d- hypo-d interaction of the composite. Multivalent character of the tungsten species in the composite has also contributed to the significant catalytic activity. Analytical application of the method covers the non-enzymatic sensor development for hydrogen peroxide as an alternative way for daily used disinfectant analysis.

In the second part of the thesis, pencil graphite electrodes modified with WO_x was used as a support material for aptasensor fabrication for the detection of Ochratoxin A (OTA) based on the Electrochemical Impedance Spectroscopic (EIS) measurements in the presence of 5 mM ferricyanide ions. Covalent binding efficiency of NH_2-Apt by EDC/NHS mechanism was confirmed by comparing the results obtained with NH_2-Apt bound to the electrode surface through adsorption. The differences in R_{ct} levels clearly indicated the efficiency of the EDC/NHS mechanism probably via -OH groups on the metal oxide film. Then, the solution parameters (tungstate ion concentration, pH and aptamer concentration) along with operating conditions have been optimized for OTA detection. Selectivity was ensured by using another mycotoxin, Zearalenone (ZEA) and the calibration graphs have been constructed in nanomolar levels.

In the final part of the thesis, tungsten oxide film has been electrodeposited on the titanium nanotubes (TNT) and then, by setting the potential at an appropriate value, the composite film was applied for the Photoelectrocatalytic (PEC) degradation of several azo dyes. The application conditions of this binary-oxide film to Rhodamine B degradation have been optimized and kinetic studies were also carried out to clarify the degradation mechanism. In conclusion, synergic interaction between the TNT and WO_3 offers a superior catalytic activity and display a potential for the use in solar irradiation inherited from the chemical properties of the modifier.

Overall studies can be evaluated as different aspects of electrocatalytic activities of tungsten oxide have been clarified in this thesis to contribute the studies of this kind in the literature.

Keywords: Voltammetry, Oxygen Reduction Reaction Tungsten oxide, EIS, aptasensor, photoelectrocatalytic degradation, Rhodamine B.

ÖNSÖZ

Birçok insanın farkında olmasa da hayatının hemen hemen her anında yer alan elektrokimyasal süreçlere, bu tezde yürüttüğüm çalışmalarım aracılığıyla katkıda bulunmaktan ötürü mutlu ve gururluyum.

Yüksek lisans çalışmalarım sırasında geçiş metallerinin katalitik etkinliklerinin birçok alanda kullanımına tanıklık ettikten sonra doktora sürecimde ERTAŞ araştırma grubumuzda daha önceden çalışılmamış Tungsten geçiş metali ile elektrokimyasal ve elektrokatalitik süreçlere nasıl bir katkı yapabiliriz sorusuyla yola çıktım.

Bu yolda ilerlerken yürüttüğüm çalışmalar, tungsten oksit kaplı modifiye yüzeylerin, Platin nanoparçacıkların getirdiği sinerjik etkiyle de desteklendiğinde, çözünmüş oksijenin indirgenmesine yönelik reaksiyonlarda iyi bir katalitik etkinlik sağladığını ortaya koymuştur. Bu bulgu sayesinde tungsten oksit ve Pt modifiye yüzeyler enzimsiz bir sensör olarak değerlendirilerek Kovid-19 pandemisine bağlı olarak günümüzde sıkça kullanılan dezenfektanlardaki hidrojen peroksit tayini mümkün kılınmıştır. Tezimin ikinci ve en çok önemsediğim kısmında da doğru ve etkin bir şekilde izlenmediği sürece, hepimizin beslenme düzenine girmesi çok mümkün olan mikotoksinlerden Okratoksin-A tayinine yönelik bir aptasensör geliştirilmiştir. Tezimin son kısmında da Tungsten Oksit ile modifiye edilen Titanyum nano tüpler ile, UV ışık altında tekstil sektöründe sıkça kullanıldığı bilinen azo boyar maddelerden Rodamin B'nin zararsız bir türüne dönüştürülerek çevreye olan olumsuz etkilerinin azaltılması mümkün kılınmıştır.

Bilimin hiçbir zaman durmayacağının ve yapmış olduğum çalışmalarımın ufak da olsa katkılarının bilincinde olarak, bu tezde sunduğum verilerin benden sonra gelecek genç arkadaşlarıma da yön vermesini ve bu sayede bilimi daha öteye taşımalarını diliyorum.

2013 yılında başlayarak, iş hayatımla birlikte yürüttüğüm bu tez sürecinde bu aşamaya gelmem, bana olan desteklerini bir an olsun geri çekmeyen sevgili hocalarım Prof. Dr. Nil ERTAŞ ve Prof. Dr. Süleyman KOÇAK sayesinde mümkün olmuştur. Sayın Hocam Prof. Dr Pınar KARA KADAYIFÇILAR ve sevgili arkadaşlarım Doç. Dr. K. Volkan ÖZDOKUR ve Dok. Öğr. İrem AYDIN KIRLANGIÇ'a çalışmalarımdaki desteklerinden ötürü minnettarım.

Bu tez çalışması kapsamında yürütülen 2018-FEN-036 kodlu projem için gerekli maddi desteği sağlayan Ege Üniversitesi Bilimsel Araştırma Enstitüsüne de çok teşekkür ederim.

İZMİR İrem ÇAKAR DAVASLIOĞLU

11/11/2021

CONTENTS

	Page
Özet	v
Abstract	vii
Önsöz	ix
Contents	xiii
Figure List	xvi
Table List	xxii
Abbreviations and Symbols	xxiii
1. INTRODUCTION	1
1.1. Chemical and Electrochemical Properties of Tungsten oxide	1
1.2. An Overview of Electrochemistry and Electroanalytical Methods	3
1.3. Catalysis and Electrocatalysis	5
1.4. Electrocatalysis in Oxygen Reduction	8
1.5. Catalytic Activity of Transition Metal Oxides in ORR	10
1.6. The Role of ORR in Electrochemical Biosensor Technologies	16
1.7. Principles of Sensing Systems Based on EIS	21
1.8. Determination of Ochratoxin A in Food Samples	24
1.9. Photoelectrocatalysis	29
1.10. Photoelectrocatalytic Degradation of Azo Dyes	31
1.11. Aim of the PhD Thesis	33

CONTENTS (CONTINUE)

	Page
2. EXPERIMENTAL	35
2.1 Apparatus	35
2.2 Reagents	35
2.3 The Procedure for ORR Studies Carried Out with GCE	36
2.3.1. CV Deposited Electrodes	37
2.3.2. Pulsed Deposited Electrode	37
2.3.3. Biosensor development	38
2.4 The Procedure for Aptasensor Studies Carried Out with PGE	39
2.4.1. Modification of Pencil Graphite Electrodes	39
2.4.2. Aptamer Immobilization	40
2.4.3. EIS Measurement Procedure	41
2.5 Photoelectrocatalytic Studies with TNT Electrode	41
2.5.1. Preparation of TNT for PEC Studies	42
2.5.2. PEC Degradation System for Dye Solutions	43
3. RESULTS AND DISCUSSION	45
3.1 ORR Studies with WO_3 Modified Glassy Carbon Electrode	45
3.1.1. Cyclic Voltammetric Deposition Studies	45

CONTENTS (CONTINUE)

Page

3.1.2. Pulsed Deposition Studies 57

3.1.3 Analytical Applications of GCE/WOx-Pt Electrodes 66

3.1.3.1 Enzymatic Applications of GCE/WOx-Pt Electrode 66

3.1.3.2 Non-Enzymatic Applications of GCE/WOx-Pt Electrode 67

3.2. EIS Studies with Pencil Graphite Electrodes 73

3.2.1. Studies with 5'-Amino Aptamer 73

3.2.2. Studies with 5'-Thiol Aptamer 86

3.3. PEC Studies with Titanium Nanotube Electrode 88

3.3.1 Preparation and Characterization of TNT/WO_3 Electrode 88

3.3.2 PEC Studies for Screening Dyes 90

3.3.3. Kinetic Study 95

4. CONCLUSION 97

REFERENCES 99

ACKNOWLEDGEMENT 113

ÖZGEÇMİŞ 116

FIGURES LIST

Page

Figure 1.1 Catalytic applications of tungsten oxide 2

Figure 1.2 Current-potential characteristics of the hydrogen and oxygen reduction and oxidation reactions at the electrodes (Kühl and Strasser, 2016). 6

Figure 1.3 General illustration of a volcano plot 7

Figure 1.4 Trassati's volcano plot for the HER in acidic media at different electrodes (Quaino et al., 2014). 8

Figure 1.5 Volcano plot for the ORR. 9

Figure 1.6 The techniques used for electrochemical deposition. 11

Figure 1.7 Transition metals with electronic configuration (Reithmaier et al., 2011). The metals studied so far by the group were framed. 15

Figure 1.8 The main parts of a biosensing system 17

Figure 1.9 Enzymatic glucose oxidation at the electrode surface 20

Figure 1.10 Schematic representation of EIS system 22

Figure 1.11 The main components of Nyquist plot (Randviir and Banks, 2013). 23

Figure 1.12 Chemical structure of ochratoxin A 25

Figure 1.13 Degradation mechanism in PEC system (Cao et al., 2017). 29

Figure 1.14 Types of electrodes and catalytical reactions studied in the thesis 32

Figure 2.1 Three electrode system consisting of the GCE as the working electrode, Ag/AgCl as the reference electrode and a Pt wire as the auxiliary electrode. 34

Figure 2.2 Representation of modification and measurements steps used for ORR studies 38

Figure 2.3 Preparation of catalase immobilized GCE/WOx-Pt electrode 39

FIGURES LIST CONTINUE

Page

Figure 2.4 The mechanism of carbodiimide chemistry via EDC/NHS for binding of NH_2-Aptamer **40**

Figure 2.5 Modification and measurements steps for aptasensor development **41**

Figure 2.6 The procedure used for the TNT preparation **42**

Figure 2.7 Images of A) titanium foil used for TNT preparation and the TNT obtained by the procedure, B) Ti foil and TNT electrodes modified with WOx by electrodeposition **43**

Figure 2.8 Schematic illustrations of experimental set up for PEC studies **43**

Figure 3.1 A) Cyclic voltammograms obtained for the cell containing 0.15 M Na_2WO_4 in 0.5 M H_2SO_4 containing 0.08 M H_2O_2 at a scan rate of 50 mV s^{-1}, **B)** The images of the electrodes. **46**

Figure 3.2 Cyclic voltammograms of GCE/WO_x in pH:5,0 BR Buffer a) purged with nitrogen gas and b) saturated with oxygen gas. Potential range: 0.8 – (-0.5) V Scan rate: 50 mVs^{-1} **46**

Figure 3.3 Consecutive cyclic voltammograms of GC electrodes in 0.001 M Pt^{2+} ions in 0.01 M H_2SO_4 solution in the potential range of 1.0 – (-0.5) V with scan rate of 50 mVs^{-1} **47**

Figure 3.4. The catalytic response of GCE/Pt modified electrode in pH:5,0 BR Buffer purged with nitrogen gas and b) saturated with oxygen gas. Scan rate: 50 mVs^{-1} **48**

Figure 3.5 Cyclic voltammograms of GCE/Pt/WO_x electrode in 0.05 M WO_4^{2-} in 10^{-2} M H_2SO_4 **49**

Figure 3.6. The catalytic response of GCE/Pt/WO_x electrode in pH:5,0 BR Buffer purged with nitrogen gas and b) saturated with oxygen gas. Scan rate: 50 mVs^{-1} **49**

Figure 3.7 The catalytic response of GCE/WO_x/Pt modified electrode in pH:5,0 BR Buffer a) purged with nitrogen gas and b) saturated with oxygen gas. Scan rate: 50 mVs^{-} **50**

FIGURES LIST CONTINUE

Page

Figure 3.8 Cyclic voltammograms of co-deposition of WOx and Pt nanoparticles on the GCE in the potential range of 1.0 – (-0.5) V with scan rate of 50 mVs^{-1} 50

Figure 3.9 Cyclic voltammograms recorded for comparison of a) GCE/WOx, b) GCE/Pt, c) GCE/Pt/WOx and d) GCE/WOx-Pt electrode performances for the ORR in pH:5.0 BR Buffer. 51

Figure 3.10 Consecutive cyclic voltammograms in deposition of GCE/WOx-Pt from the deposition solution containing 0.001 M Pt^{2+} ions in 0.01 M H_2SO_4 and tungstate ions to maintain the molar ratio of a) 1:10; b) 1:25; c) 1:50; d) 1:75 and e) 1:100 in the potential range of 1.0 – (-0.5) V with scan rate of 50 mVs^{-1}. 53

Figure 3.11 The catalytic responses of GCE/WOx-Pt prepared in different molar ratios towards the reduction of oxygen dissolved in pH:5,0 BR Buffer. a) 1:10 b) 1:25 c) 1:50 d) 1:75 e) 1:100 Potential range: 0.8 – (-0.5) V Scan rate: 50 mVs^{-1} 54

Figure 3.12 The catalytic responses of GC/WOx-Pt modified electrodes in pH:5,0 BR Buffer in the potential range of 0.8 – (-0.5) V at a scan rate of a) 10 b) 25 c) 50 d) 75 e) 100 mV s^{-1} 55

Figure 3.13 Comparison of ORR signals of GCE/WO_x-Pt modified surfaces obtained in BR buffer in a pH range of a) 2.0 b) 5.0 c) 7.0 d) 9.0 and e) 11.0. Scan rate: 50 mV/s 56

Figure 3.14 Schematic diagram of pulsed deposition parameters 57

Figure 3.15 Pulsed potential deposition current response by time by changing the potential from 0,2 V to -0.5 V with 3 seconds of pulse duration for 100 times. 58

Figure 3.16 The ORR responses of the pulsed deposited GC/WOx-Pt electrodes and GCE/Pt electrode prepared by different procedures. Scan rate: 50 Mv s^{-1} 59

FIGURES LIST CONTINUE

Page

Figure 3.17 The 2.500 times magnified SEM images of A) CV and B) Pulsed deposited GC/WO_x-Pt electrodes 62

Figure 3.18 The 20.000 times magnified SEM images of A) Cyclic deposited and B) Pulsed deposited GC/WO_x-Pt electrodes 63

Figure 3.19 The EDX results of the cyclic and pulsed deposited GC/WO_x-Pt electrodes 64

Figure 3.20 XPS spectra for CV deposited GCE/WOx-Pt, (a) survey spectrum (b-f) fitted high-resolution spectra of b) C1s, c) O1s, d) W4f and e) Pt4f. 65

Figure 3.21 Chronoamperograms recorded for the catalase biosensor based on GCE/WOx after the addition of 1 mM H_20_2 to the cell 66

Figure 3.22 Chronoamperograms recorded for the catalase biosensor based on GCE/WO_x-Pt after the addition of 1 mM H_20_2 to the cell 67

Figure 3.23 Cyclic voltammograms recorded at GCE/WO_x-Pt in 0.05 M H_20_2 solution. Cycle number was indicated on the voltammograms. 68

Figure 3.24 Chronoamperograms recorded at GCE/WO_x-Pt at various potentials after injection of 5 mM H_2O_2 at every 60 second. 68

Figure 3.25 Performances of GCE/WO_x-Pt electrode in a) pH 7.0 PBS buffer and b) pH 9.0 Boric acid buffer solutions containing 0.5 mM H_2O_2 in the cell. 69

Figure 3.26 Chronoamperograms recorded at 0V by injecting standard solutions of H_2O_2 in a concentration range of 0.1- 1.0 mM every 60 s. 70

Figure 3.27 Calibration curves for H_2O_2 in a concentration range of 0.1-1.0 mM. 70

Figure 3.28 Details of standard addition technique used in sample analysis 71

Figure 3.29 Calibration curves for H_2O_2 in a concentration range of 0.5 - 2.0 mM. 71

FIGURES LIST CONTINUE

Page

Figure 3.30 Schematic representation of signal formation in Amino-Aptasensor 73

Figure 3.31 Cyclic voltammograms recorded in pH 7.4 BR buffer solution containing 5 mM $Fe(CN)_6]^{3-/4}$ at a a) bare PGE, b) PGE/WO_x (CV), c) NH_2-Apt-PGE/WO_x, d) After blocking with 1% BSA, and after interaction with e) OTA and f) VEGf . 74

Figure 3.32 The Nyquist graphs of amino-aptasensor based on modification from 0.005 M Na_2WO_4 by using A) CV and B) PD techniques; where a) PGE/WO_x b) NH_2-Apt-PGE/WO_x, c) after blocking with BSA, and after interaction with d) OTA and e) ZEA. 75

Figure 3.33 The R_{ct} values measured for the amino-aptasensor prepared by depositing from solutions containing 0.005 M WO_4^{2-} ion and applying CV or PD techniques 76

Figure 3.34 The R_{ct} values measured for the amino-aptasensor prepared by depositing from solutions containing 0.005, 0.030 and 0.075 M WO_4^{2-} ion and applying CV or PD techniques. 78

Figure 3.35 The effect of Na_2WO_4 concentrations on the difference in charge transfer resistances of the aptasensors prepared on bare and WOx deposited electrodes by either CV or PD technique. 79

Figure 3.36 The performances of the aptasensors prepared in the absence and presence of EDC/NHS mechanism 80

Figure 3.37 The effect of aptamer concentration on the charge transfer resistances of the aptasensors prepared on PGE/WOx (PD) from 0.075 M Na_2WO_4 solution. 81

Figure 3.38 The effect of aptamer concentration on the Rct values of OTA and ZEA 81

Figure 3.39 The effect of aptamer concentration on the R_{ct} values of OTA and ZEA 81

FIGURES LIST CONTINUE

Page

Figure 3.40 The 20.000 times magnified SEM images of A) bare PGE, B) CV and C) Pulsed deposited PGE/WOx electrodes 83

Figure 3.41 SEM images of the electrodes in each stage of the aptasensor fabrication procedure. 84

Figure 3.42 The Rct values obtained for the set of OTA solution for calibration and VEGf (1 nM) for non-specific interactions. 85

Figure 3.43 Calibration curve for OTA 85

Figure 3.44 a) Effect of OTA concentration on the DRct levels measured and b) the calibration curve constructed for OTA 86

Figure 3.45 Schematic representation of signal formation in Thiol-Aptasensor 86

Figure 3.46 Performances of the NH_2-Apt immobilized PGE/WO_x electrode and SH-Apt immobilized PGE/WO_x/Au electrode 87

Figure 3.47. Cyclic voltammograms recorded at a scan rate of 50 mV s^{-1} in 0.01 M H_2SO_4 and 0.1 M H_2O_2 mixture containing 0.15 M tungstate ion for five repetitive cycles. 89

Figure 3.48 SEM images of A) bare TNT and TNT/WO_3 composite electrode prepared by cycling the potential between −0.75 –0.5 V for B) 2 cycles and C) 4 cycles D) EDX spectra of B. 89

Figure 3.49 A) XPS survey spectra, B) TNT-WO_3 composite electrode and C) the scan of oxygen. 90

Figure 3.50 The change in the PEC Degradation percentages of the azo dyes by time where the anode material is a) bare TNT and b) TNT/WO_3 electrodes, c) without UV irradiation. 90

Figure 3.51 Photocurrent profiles of TNT/WO_3 composite electrode in 6 mg L^{-1} RhB solution 91

Figure 3.52 The effect of tungstate ion concentration in fabrication of TNT/WO_3 on the PEC degradation efficiency of RhB 92

FIGURES LIST CONTINUE

Page

Figure 3.53 The effect of cycle number used in the deposition step on the time dependent degradation efficiency of RhB 94

Figure 3.54 The effect of the solution pH on the absorbance of 6 mg L^{-1} RhB solution 94

Figure 3.55 PEC degradation of RhB solutions in various concentrations. 95

Figure 3.56 First order kinetic of RhB degradation for three different concentrations. 96

TABLES LIST

Page

Table 1.1. Thermodynamic electrode potentials of ORR at different media (Si et al, 2014) 9

Table 1.2 Analytical characteristics of non-enzymatic methods for hydrogen peroxide 19

Table 1.3 The advantages and disadvantages of antibodies and aptamers 24

Table 1.4 Analytical properties of Electrochemical Aptasensors Developed for OTA. 27

Table 1.5. PEC Degradation of azo dyes at different metal oxide anode materials. 31

Table 3.1. Peak characteristics of GCE/WOx-Pt towards the ORR 54

Table 3.2 Peak height and peak potentials of GCE/WO_x-Pt modified electrodes obtained by differentiating the deposition scan rate. 55

Table 3.3 Peak characteristics of the ORR signal obtained at GCE/WO_x-Pt in different pH media 56

Table 3.4 Procedures for preparing GCE/WO_x-Pt and GCE/Pt electrodes by PD technique. 58

Table 3.5 The ORR peak characteristics of GCE/WO_x-Pt and GCE/Pt electrodes prepared via pulsed deposition technique. 60

Table 3.6 The ORR peak characteristics of the GCEs modified with transition metal oxides 61

ABBREVIATIONS AND SYBMBOLS

AdCSV: Adsorptive Cathodic Stripping Voltammetry

ASV: Anodic Stripping Voltammetry

$C_{d:}$ Double layer capacitance

CV: Cyclic voltammetry

θ: phase angle a

DFT: density functional theory

DP: Differential pulse

E^o: Standard cell potential

EIS: Electrochemical impedance spectroscopy

GCE: Glassy carbon electrode

GOx: glucose oxidase (GOx) enzyme

HER: Hydrogen evolution reactions

HOR hydrogen oxidation reactions

HRTEM: High-resolution transmission electron microscopy

LOD: Limit of detection

η: Overpotential

NH_2-Apt: 5'-Amino Aptamer

OER: oxygen evolution reaction

ORR: Oxygen reduction reaction

OTA Ochratoxin A

ABBREVIATIONS AND SYBMBOLS (CONTINUE)

PD: Pulsed Deposition

PEC: Photoelectrocatalysis

PGE: Pencil Graphite Electrodes

PyOx: Pyranose oxidase enzyme

RhB: Rhodamine B.

TNT: Titanium nanotubes

WO_x: Non-stoichiometric tungsten oxide where $WO_{3-\delta}$ ($0 < \delta < 1$)

SEM: scanning electron microscopy

SH-Apt: 5'-Thiol Aptamer

SPCE: screen-printed carbon electrodes

SW: square wave

X_c: capacitive reactance given below

XPS: X-ray photoelectron spectroscopy

XRD: X-ray diffraction

Z: Impedance

1. INTRODUCTION

1.1. Chemical and Electrochemical Properties of Tungsten oxide

Over the past three decades, nanostructured transition−metals and their oxides are considered as one of the most attractive functional materials due to their outstanding catalytic, magnetic, optical properties. In their electronic structure, the s-shells of positive metallic ions are always full while the d-shells are partly filled and this electronic configuration is responsible from their unique properties such as good electrical characteristics, high dielectric constants and their wide bandgaps (Guo et al., 2015).

Tungsten or wolfram is a transition metal with electronic configuration of [Xe] $4f^{14}5d^{4}6s^{2}$ and its name is originated from the Swedish "*tung sten"* meaning heavy stone (https://www.rsc.org, 2021). Tungsten oxide is an intermediate product obtained in the recovery of tungsten from its minerals.

Tungsten has several oxide forms including stoichiometric WO_2 and WO_3 and **non-stoichiometric** WO_x which has $WO_{3-\delta}$ ($0 < \delta < 1$) forms. The crystal structure of WO_3 is temperature dependent and the most common structure of WO_3 is monoclinic. WO_3 is an n-type semiconductor with moderate band gap energy (2.4–2.8 eV). Therefore, it exhibits high optical absorption within the visible region (Peleyeju and Viljoen, 2021).

Tungsten oxide has attracted great attention over the past two decades due to its high stability in acid solution and its outstanding catalytic performances in electrochromic devices (Rozman et al., 2020), in gas sensors (Dong et al., 2020), and energy storage systems (Shinde and Jun, 2020).

As shown in **Figure 1.1**, WO_3 has also been utilized in hydrogen evolution reactions (HER) (Xie et al., 2020), in photoelectrocatalytic degradation of organic pollutants in water (Peleyeju and Viljoen, 2021), photoelectrocatalytic water splitting (Zhao et al., 2019) and in fabrication of supercapacitors (Yao et al., 2017).

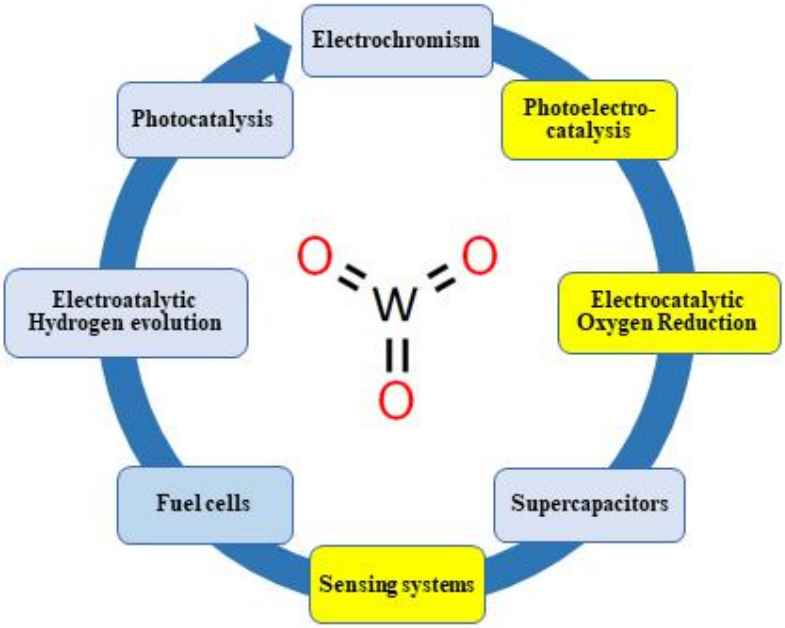

Figure 1.1 Catalytic applications of tungsten oxide

In this thesis, it was aimed to search the electrocatalytic effect of tungsten oxide deposited on carbon-based electrodes and to study its composites with other metal nanoparticles in pursue of any synergetic effect for electrocatalytic activity towards the highlighted reactions. Following the characterization studies with scanning techniques, catalytic performances of the novel electrodes have been tested upon several reactions for analytical applications including oxygen reduction reaction (ORR), photoelectrocatalytic degradation reactions and in biosensor fabrication.

The common point of these application areas is that they are based on electrochemical techniques. Therefore, next section gives a brief information about electrochemistry and electrocatalysis followed by the literature survey on transition metal oxides and their use in ORR.

The use of transition metal oxides in photoelectrocatalytic degradation of organic compounds and their applications in electrochemical sensor technologies were also covered. Special attention was paid on electrochemical deposition conditions of metal oxide film formation and its modification with metallic nanoparticles. Finally, the main procedures in biosensor technologies and the techniques used in monitoring the biocomponent response were summarized.

1.2. An Overview of Electrochemistry and Electroanalytical Methods

In analytical point of view, determination of organic and inorganic substances is very important in clinical, food and environmental samples along with quality control studies in industry (Girault, 2004). For this purpose, the methods based on electroanalytical and especially voltammetric techniques have gained an importance in chemical analysis as it allows for on-site analysis with the production of portable devices at a low cost. In order to comprehend these methods, it is necessary to know electrochemistry and the underlying principles (Nişli and Ertaş, 2010).

Electrochemistry is essentially the science that focuses on the transfer reactions of charged particles such as ions or electrons at the electrode-solution interface. In relation to the thermodynamic and kinetic properties of electrode reactions, the current imbalance in the electrical double layer leads to a potential difference. This potential difference of the interface can be measured with the help of a second electrode which is called as the reference electrode. For current measurements, another electrode, called as auxiliary or counter electrode, is required to undertake current passage (Tural et al., 2003).

The simplest way to classify electrochemical methods is to consider the location where the events that generated the analytical signal occurred. Thus, method groups including events related to the main solution (bulk) and events developing on the electrode-solution interface emerged. The latter group includes the most common methods developed so far where the changes in the current passing through the working electrode are monitored under controlled potential. Microelectrodes are used as working electrodes to increase polarization.

Although there are two main variables here, the development of a large number of methods can be attributed to the use of timing as another variable during the application of the excitation signal and current sampling.

For a redox reaction given as $Ox + ne^- \rightleftharpoons R$, Nernst equation (Eq. 1.1) establishes a relationship between the standard cell potential (E^o) and the activity of the oxidized (a_{ox}) or reduced (a_R) species.

$$E = E^o + \frac{0{,}059}{n} \log \frac{a_{Ox}}{a_R} \qquad \text{(Eq. 1.1)}$$

This equation applies to equilibrium conditions and reversible systems. In general, **reversibility** defines the position where the reaction easily changes direction in response to the change in conditions. In electrochemical reactions, this term is used for situations where the electrode reaction changes direction rapidly and therefore the reaction takes place very quickly in both directions even small changes in potential.

Voltammetric methods developed using the three-electrode system allowed more sensitive measurements with the use of the **differential pulse** (DP) technique in the 1970s. DP techniques, based on the differences of the capacitive and faradic current over time, enabled us to perform more sensitive analyses down to sub micromolar concentrations. Studies are ongoing to increase the sensitivity of existing voltammetric methods and to develop novel methods.

There are two options to improve the sensitivity in voltammetry: by increasing the rate of signal-to-noise ratio or the faradaic current itself. The latter can be accomplished by using stripping techniques that are carried out by accumulating the electroactive type on the electrode surface electrolytically or by adsorption, and then stripping by changing the potential in anodic or cathodic direction (Zoski, 2007).

One of this kind of method developed is called as the **Anodic Stripping Voltammetry** (ASV) where the metal ion is deposited on the electrode surface under controlled potential for a predetermined time and then, the potential is scanned in anodic direction by applying linear or DP scan modes. The anodic peak obtained is used for quantification of the accumulated metal ions. In method development stage, solution parameters along with the operational parameters such as deposition time and potential along with the scan rate should be optimized (Wang, 2006).

In **Adsorptive Cathodic Stripping Voltammetry** (AdCSV), the metal ion or an organic substance is complexed with a suitable ligand and adsorbed on the electrode surface. Following the accumulation step, the potential is scanned in cathodic direction by applying linear, DP or square wave (SW) modes. The limit of detection (LOD) of the method can be lowered down to 10^{-10} M.

Further increase in the sensitivity can be attained by **catalytic methods** where the substance deposited on the electrode surface is oxidized with an oxidant in the solution phase and reduce again at the electrode, thereby increasing the current. Basic information about the catalysis in electrochemistry is given next.

1.3. Catalysis and Electrocatalysis

The phenomenon of facilitating the oxidation of hydrogen on platinum surface was first observed in the 1820s and Berzelius called this phenomenon as **Catalysis** in 1835 (Nakiboğlu, 2010). The material used in the catalysis, i.e., **catalyst**, increases the rate of chemical reactions but not consumed in the process.

Electrocatalysts, on the other hand, increases the rate of electron transfer between the molecule and the electrode and it may function at electrode surfaces. In some cases, the electrode surface itself behaves like a catalyst. Pioneering study on this area was conducted by Bowden and Rideal who studied the overpotential for hydrogen evolution at several metals as a function of current density and then the **electrocatalysis** term was coined by Kobozev in 1936 (Açıkyıldız et al., 2014). Since then, many catalytic and electrocatalytic systems have been searched.

Electrocatalysis is closely related with heterogeneous catalysis, and the transformation of the molecule follows certain routes over electrode surface modified with the catalyst. The reaction rate can be defined as the number of electrons passed between the reactant and the electrode and therefore, it is related with the current passed through the circuit (Duca and Koper, 2021).

In an electrochemical cell including an anode and a cathode immersed in an electrolyte solution, a sufficient voltage must be applied between the electrodes to obtain current. The difference between the applied potential and the equilibrium potential defines the **overpotential** ($\eta = E - E_{eq}$) and a good electrocatalyst should display high current density at low overpotential.

High specific area provides larger surface available for adsorption of the ions or molecules involved in the electrode process. Therefore, the electrode material, type of the electrocatalyst, and its specific surface area are crucial for the catalytic activity.

Electrocatalysis is one of the most important application areas of modern electrochemistry, particularly in energy conversion systems, electrolysis cells and electroanalysis. Clean energy storage and conversion studies have been dedicated to improving the electrocatalytic activity of cathode and anode materials in water splitting and fuel cell technologies. The main reactions involved are the oxygen reduction reaction (ORR), and hydrogen evolution reaction (HER) and of the anode materials for oxygen evolution reaction (OER) and hydrogen oxidation reactions (HOR) as illustrated in **Figure 1.2** (Kühl and Strasser, 2016).

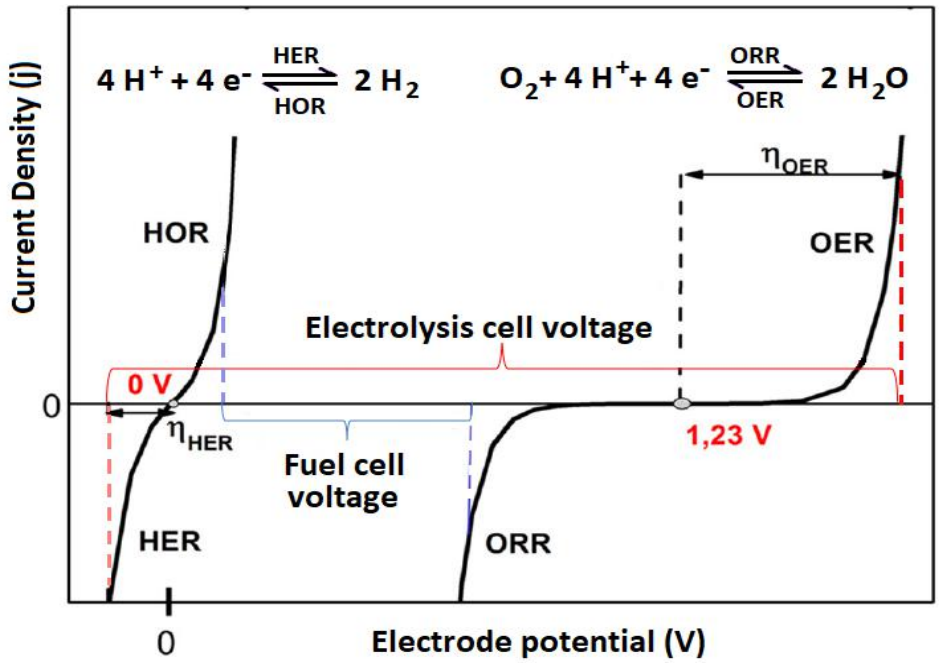

Figure 1.2 Current-potential characteristics of the hydrogen and oxygen reduction and oxidation reactions at the electrodes (Kühl and Strasser, 2016).

The voltammetric signals of the oxygen and hydrogen redox electrodes intersect at 0 and 1.23 V, respectively corresponding to their equilibrium potential. The cell voltage required in the electrolysis of water is the sum of standard electrode voltage E^o and the overpotentials of HER and OER denoted as η_{HER} and η_{OER}, respectively (Eq. 2). On the other hand, fuel cell voltage obtained equals to the standard electrode potential minus the overpotentials of HOR and ORR designated as η_{HOR} and η_{ORR}, respectively (Eq. 3).

$$E_{electrolysis} = E^o + \eta_{HER} + \eta_{OER} \quad \text{(Eq. 1.2)}$$

$$E_{fuel\ cell} = E^o - \eta_{HOR} - \eta_{ORR} \quad \text{(Eq. 1.3)}$$

According to the **Figure 1.2**, to decrease the overpotential for the ORR is the key point for the conversion and storage systems and extensive catalysis research have been carried out to solve this issue in the last two decades.

An electrocatalyst can be heterogeneous such as a noble metal surface, or homogeneous like an enzyme. Widely used material for both cathodic and anodic processes is platinum however, its high cost and deterioration in chlorine production limits its use. Therefore, cost-effective alternatives are extensively being searched including alloys, carbon-based or polymer based metallic composites.

An electrocatalytic reaction that undergoes at the electrode-surface interface may involve several steps including adsorption of the reactant on the catalyst, electron transfer accompanied by chemical reaction and then, desorption of the product back to the solution. This is the basis of the Sabatier principle (Reithmaier et al., 2011). According to this principle, the strength of the adsorption bond of the reactant to the electrode substrate should not be too high or too low but, intermediate value to obtain an optimal electrocatalytic activity. A weaker bond results in less activity while higher strengths lead the retention of the product blocking the active sites on the electrode surface.

Sabatier principle is usually illustrated as a **volcano plot** where the current density is plotted against the adsorption energy giving a maximum like a volcano as introduced by Balandin in 1969. As shown in **Figure 1.3**, the plot has an ascending side where the binding energy of the reactant is increased and a descending side where the interaction is too strong to desorb the product.

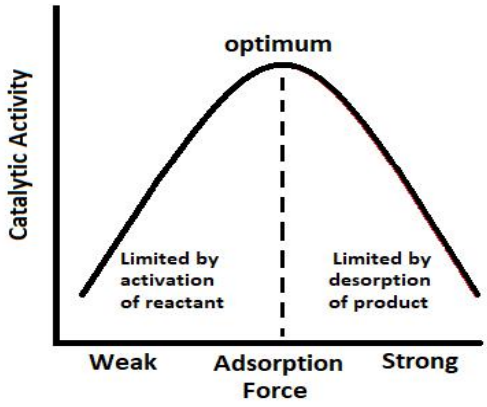

Figure 1.3 General illustration of a volcano plot

The plot in **Figure 1.4** shows the volcano curve for hydrogen evolution reaction and the plot gives a maximum indicating that the platinum is the optimum catalyst for the hydrogen gas evolution (Quaino et al., 2014). In the descending side transition metals mostly covered with oxide reduces the overall reaction rate and the catalytic activity is limited by desorption of hydrogen gas due to the strong adsorption of the hydrogen molecule to the electrode.

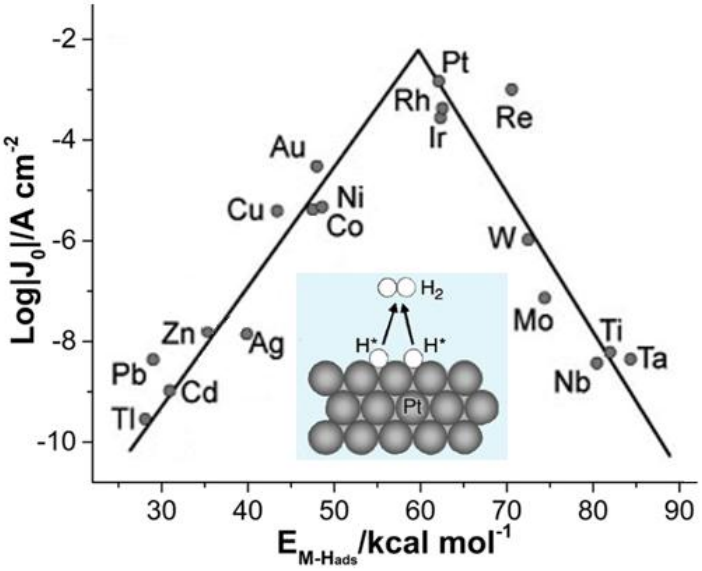

Figure 1.4 Trassati's volcano plot for the HER in acidic media (Quaino et al., 2014).

Volcano plot is a practical way to predict the activity of heterogeneous catalysts and its modern versions use adsorption energies calculated by density functional theory (DFT) (Quaino et al., 2014). These plots have been constructed for other important reactions such as ORR as given in next section.

1.4. Electrocatalysis in Oxygen Reduction

In addition to being one the most important reactions in biological processes, such as respiration, oxygen reduction reaction (ORR) also plays an important role in energy-converting systems including metal-air batteries and more recently fuel cells (Si et al., 2014).

Mainly two pathways are suggested for this reaction; first mechanism may be based on the direct four-electron transfer from oxygen gas to water as given in the figure. Alternative mechanism suggests two electrons transfer from oxygen to hydrogen peroxide for aqueous acidic electrolytes. In alkaline solutions, super oxide ion might be formed by transferring one electron as given in **Table 1.1.**

Table 1.1 Thermodynamic electrode potentials of ORR at different media **(**Si et al, 2014**)**

Electrochemical ORRs							**E (V vs SHE)**	**Electrolyte**
O_2	+	$4H^+$	+	$4e^-$	⇌	$2H_20$	1.229	Aqueous acidic soln
O_2	+	$2H^+$	+	$2e^-$	⇌	H_20_2	0.70	
H_2O_2	+	$2H^+$	+	$2e^-$	⇌	$2H_20$	1.76	
O_2	+	$2H_2O$	+	$4e^-$	⇌	$4OH^-$	0.401	Alkaline soln.
O_2	+	H_2O	+	$2e^-$	⇌	$HO_2^- + OH^-$	-0.065	
HO_2^-	+	H_2O	+	$2e^-$	⇌	$3OH^-$	0.867	

The kinetics of the ORR is slow and therefore, a cathode catalyst is required. Again, volcano plot constructed for the ORR can give an insight for the catalyst choice. As can be seen from the **Figure 1.4**, platinum is the most efficient catalysts. However, there might be a small amount of intermediates, such as peroxide and its high cost limits their use in commercially viable fuel cells.

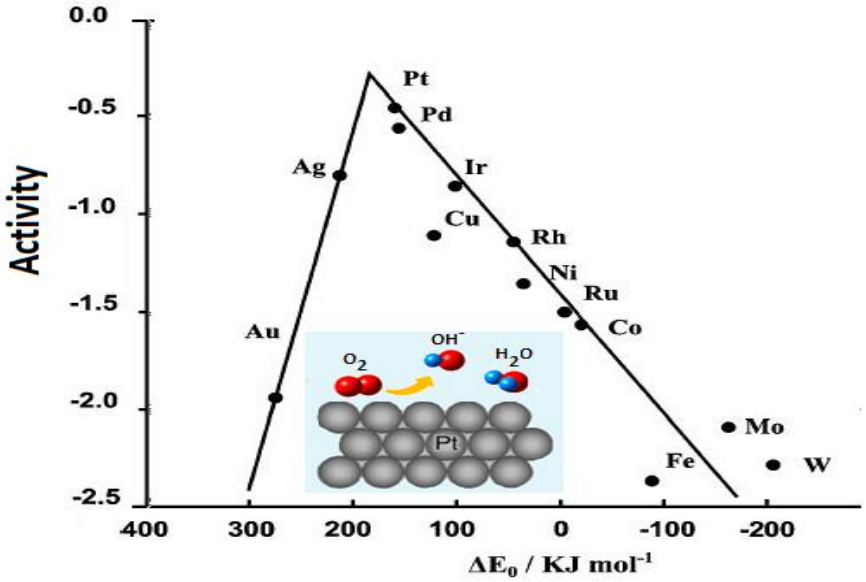

Figure 1.5 Volcano plot for the ORR at various electrodes.

Over the past decades, huge efforts were made on developing alternative catalysts, including other noble metals and alloys but, their high cost limits their wide use.

Alternatively, the combination of nonprecious metals, carbonaceous materials, transition metal chalcogenides, and transition metal carbides have been evaluated (Wang et al., 2018).

Catalyst development strategies include increasing the intrinsic activity of the material along with the number of active sites on the surface (Seh et al., 2017). For this purpose, theoretical and experimental studies must be combined to understand these electrochemical transformations.

The binding energy of a reactant to the electrode surface depends on the electronic structure of the metallic surface (Guo et al., 2015). For example, in the HER mechanism given above, hydrogen gas adsorbs onto the Pt surface by interaction of the hydrogen 1s state with the platinum 6s band and this interaction creates one filled and an empty antibonding molecular orbital.

On the other hand, the metal d-band hybridizes with the bonding (σ) orbital of the reactant to form bonding (d-σ) and antibonding (d-σ)* states. The former state is full for the noble metals, but the later state is affected by the electronic structure of the metal at the electrode surface and as this state is getting weaker as it is filled. Transition metals have full s shells while the d−shells are not filled which gives them unique electronic properties. These metals have various oxidation states, and their oxides are becoming popular being the most versatile functional materials.

1.5. Catalytic Activity of Transition Metal Oxides in ORR

Transition metal oxides have been studied as non-precious metal electrocatalysts for ORR as they can form chemical bonds with dissolved oxygen through their d orbitals. Their catalytic activity depends on the occupancy degree of their outer shells (Reithmaier et al., 2011).

The metals with hyper d orbitals such as Pt, Pd, Ni, Co, Ru are rich in electrons in outer shells and display considerable catalytic activity. Other metals with hypo d orbitals such as Ti, Zr, W and Mo are rather poor catalyst but, their combinations with hyper-d-electronic transition metals create synergistic effect forming rather stable intermetallic phases. This intermetallic **hypo-d –hyper-d** electronic combination can be compared to Lewis's acid-base definition where the hyper-d elements serve as the base, while the hypo-d elements correspond to the acid counterpart.

Type of supporting material is also important providing good dispersion and avoiding the agglomeration of the metallic nanoparticles. Titanium and/or titania (TiO_2) contributes to this hypo-hyper d-interaction explained above. Carbon based supports provides a platform for adsorption and dispersion of Pt metal nanoparticles and is affected by the acid–base properties of the substrate.

Transition metals whose electrode potential is more negative than hydrogen evolution potential cannot be deposited electrochemically from their aqueous solutions. For instance, molybdate anion, formed in the intermediate step, has a stable structure and the electrode potential shifts to more negative potentials. Therefore, molybdenum cannot be deposited in a metallic state unless special cell conditions are met (Chou et al., 2006).

In electrochemical deposition of such metal oxides, the surface structure or the valence of the metal and therefore the catalytic activity can be controlled by changing the deposition parameters. In deposition step, the potential or current is kept constant, or more frequently controlled accumulation is provided by linear scans at a given scan rate in a predetermined potential range.

Cyclic voltammetry (CV) is frequently used for this purpose but, in recent years; Pulsed Deposition (PD) technique in which potential pulses are applied during electrochemical deposition is becoming more popular. With this technique, active accumulation nuclei are formed on the electrode surface and a better distribution is observed compared to other techniques (Lee et al., 2013). **Figure 1.6** shows the applied pattern for both deposition technique.

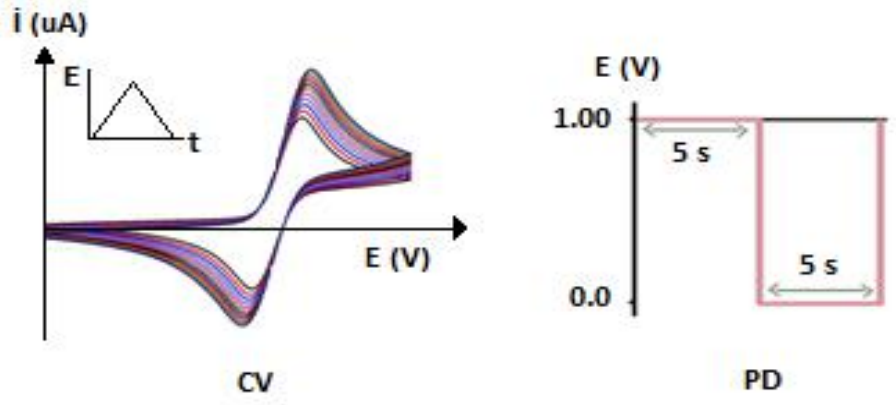

Figure 1.6 The techniques used for electrochemical deposition.

In a study carried out by Liu et al., structural analysis of the MoO_3 thin film deposited on the electrode surface by the CV technique in acidic conditions has revealed that central metal ion has different valences being Mo(VI) and Mo(V) (Liu et al., 1999). This non-stoichiometric film converts to a conductive layer by capturing protons or other cations to the structure in the form $[MoO_{3-x}(OH)_x]$ called as bronze which has catalytic activity for a large number of redox species.

In a former study carried out in this lab it was shown that blue oxide film on can be obtained glassy carbon electrode (GCE) via successive cycling the potential in aqueous Na_2MoO_4 solution prepared in pH 2.0 sulfuric acid (Koçak et al., 2013). X-ray photoelectron spectroscopic (XPS) examination of the oxide film has revealed the formation of mixed-valence oxide by CV technique.

In the last decade, several studies based on increased electrocatalytic activity of inorganic oxides with noble metal catalysts have been reported. In another study carried out in this lab, the catalytic activity of the molybdenum oxide layer deposited on a GCE further modified by decorating with Pt nanoparticles was investigated (Çakar et al., 2013). This GCE/MoOx/Pt electrode was used as a platform for the ORR and higher current density was obtained at more positive potentials due to the **hypo d–hyper d** combinations between metal and metal oxide. The best response toward dissolved oxygen was obtained with an electrode prepared by cycling the potential in a range of 1.05 to −0.25 V at a scan rate of 20 mV/s for successive 10 cycles in a deposition solution with a mole ratio of 1:90 Pt:Mo.

Close inspection of the film has revealed that the noble metal nanoparticles have been dispersed evenly over the oxide layer which prevents their agglomeration. In addition, the oxide layer is reported to increase the chemisorption and catalytic properties of Pt particles in agreement with a former study (Gan et al., 2007).

In a continuation study, the electrode performance towards the ORR in a weak acidic environment was examined and the influence of the deposition technique on the chemical and morphological properties of the resultant binary catalyst was compared with PD technique. (Yavuz et al., 2015). GCE/MoOx/ Pt surfaces prepared by PD technique have displayed higher catalytic activity to the ORR than the CV counterpart and even better than bare Pt disk electrode, probably due to the higher dispersion of the deposits.

Another transition metal oxide that has wide use in electrochemical energy storage systems is manganese dioxide. Environmentally friendly MnO_2 offers superior electrochemical performance at a low cost and therefore it is widely used in batteries. The mechanism was elucidated that the electrode interacts with dissolved oxygen adsorbed on carbon to form the oxygen radical via Mn(III)/Mn(IV) pair (Zhou et al., 2006).

Electrochemically synthesized MnO_2 structures in these batteries perform better than chemically synthesized oxides and the technique used for electrochemical deposition also determines the surface morphology (Lee et al., 2013). The scanning electron microscopic (SEM) images of the film obtained indicate that CV accumulation resulted in the formation of nanorods while the PD has leaded the formation of needle like nanostructures.

In another study, it has been reported that Pt nanoparticles decorated on this oxide layer increase the electrocatalytic activity of the formed bimetallic catalyst towards the oxidation of formic acid (El Deab, 2012).

Similarly, GCE/MnO_x-Pt electrode was used for the ORR in buffered solutions (Özdokur et al., 2014). The electrode has demonstrated better electrocatalytic activity towards the ORR than the bare Pt disk due to the larger surface area of MnO_x preventing the agglomeration of Pt nanoparticles.

In addition to the single transition metal oxides in conjunction with a noble metallic nanoparticle, their binary combinations have also displayed high catalytic activity (Tang et al., 2006). This synergistic effect between the binary metal oxides has been assigned to the improvement of their redox properties. Such combination of transition metals into MnO_x compounds has been investigated extensively to enhance the charge storage properties and a pseudo capacitive behavior was reported for the Mn/Mo oxide film (Nakayama et al., 2005).

Electrocatalytic efficiency of co-deposited transition metal oxides can be further increased by the incorporation of hyper d-electronic of noble metals. A continuation study in this lab has been designed to fabricate the MnO_x-MoO_x film co-deposited by PD technique and the film was further decorated with Pt nanoparticles in pursue of electrocatalytic activity both in anodic and cathodic directions in alkaline and weak acidic solutions, respectively.

In the former study, electrocatalytic performance of the electrode for formaldehyde oxidation which have a potential candidate for fuel cell applications was verified (Özdokur et al., 2016a). It was reported that PD technique is responsible for the homogenous distribution of Pt nanoparticles over the mixed metal oxides.

In the latter study, this synergistic effect was utilized in cathodic region and the electrocatalytic activity of the mixed metal oxide combined with Pt nanoparticles towards the ORR was investigated (Özdokur et al., 2016b). In both studies this binary metal oxide electrode has acted as a good catalyst revealing the dual function of such combinations.

Nowadays, cobalt oxides attract attention due to their unique properties and exceptional electrocatalytic activity for various compounds. In a rather recent study, cobaltous oxide was deposited on the GCE by using the CV and PD techniques and decorated with Pt nanoparticle to reveal any enhancement in electrocatalytic activities (Kuşçu et al., 2020). The deposition solution composition along with the operating conditions were optimized by monitoring the ORR signal in pH 5.0 acetate buffer.

Figure 1.7 shows the transition metal oxides and their combinations with noble metals so far studied in the lab. In the search for other alternatives, experimental studies should agree with theoretical approaches and considering that the stability of hypo-hyper d compounds is increased in the direction of 3d → 5d, the stability of the intermetallic compound also increases in this direction (Reithmaier et al., 2011). In this case, stable intermetallic compounds in each transition metal sequence are Pt-Hf, Pd-Zr and Ni-Ti.

Next study was designed to use of zirconia-based electrocatalytic surface for the ORR coupled with Pd nanoparticles (Kuşci et al., 2018). The electrode surface was characterized by using SEM, X-ray diffraction (XRD) and XPS analysis. The catalytic effect of the developed electrode was found to be superior towards dissolved oxygen in alkaline and weak acidic media for energy conversion studies as well as sensing purposes.

21 Sc $[Ar]3d^14s^2$	22 Ti $[Ar]3d^24s^2$	23 V $[Ar]3d^34s^2$	24 Cr $[Ar]\ 3d^54s^1$	25 Mn $[Ar]3d^54s^2$	26 Fe $[Ar]3d^64s^2$	27 Co $[Ar]3d^74s^2$	28 Ni $[Ar]3d^84s^2$	29 Cu $[Ar]3d^{10}4s^1$	30 Zn $[Ar]3d^{10}4s^2$
39 Y $[Kr]4d^15s^2$	40 Zr $[Kr]4d^25s^2$	41 Nb $[Kr]4d^35s^2$	42 Mo $[Kr]4d^55s^1$	43 Tc $[Kr]4d^55s^2$	44 Ru $[Kr]4d^75s^1$	45 Rh $[Kr]4d^85s^1$	46 Pd $[Kr]4d^{10}$	47 Ag $[Kr]4d^{10}5s^1$	48 Cd $[Kr]4d^{10}5s^2$
57 La $[Xe]6s^25d^1$	72 Hf $[Xe]5d^26s^2$	73 Ta $[Xe]5d^36s^2$	74 W $[Xe]5d^46s^2$	75 Re $[Xe]5d^56s^2$	76 Os $[Xe]5d^66s^2$	77 Ir $[Xe]5d^76s^2$	78 Pt $[Xe]5d^96s^1$	79 Au $[Xe]5d^{10}6s^1$	80 Hg $[Xe]5d^{10}6s^2$

Figure 1.7 Transition metals with electronic configuration (Reithmaier et al., 2011). The metals studied so far by the group were framed.

Another binary metal oxide modified electrodes developed so far are the GCE/CuOx-MoOx/Pd (Özdokur et al., 2018) and GCE/CNT/VOx-RuO_x/Pt (Karaca and Koçak, 2021) fabricated via CV and PD techniques, respectively. Former electrode has displayed catalytic activity towards to dissolved oxygen in alkaline medium while the latter has given superior performance towards oxidation of hydrazine a promising candidate for energy conversion systems.

In a rather recent study, the synthesis of mixed oxide films of manganese and vanadium on a GCE was achieved by electrochemical pulsed deposition and the electrode was formerly modified with multiwall carbon nanotubes (MWCNT) to increase the surface area (Akoğulları et al., 2020). The electrode was characterized with SEM, XPS, XRD and High-resolution transmission electron microscopy (HRTEM). The GCE/CNT/MnO_x−VO_x film was further decorated with gold nanoparticles to enhance the catalytic activity. The effect of medium pH on the ORR signal was studied in the range of 2.0–12.0 and the best results were obtained in pH 5.0 acetate buffer solution.

Tungsten oxide has attracted attention recently due to its exceptional optical and electrochemical properties. WOx can form hydrogen tungsten bronzes (H_xWO_3, $0.3< x <0.5$) and this species was found stable in acidic media which allow them to use in strongly acidic fuel cells. (Wang and Dong, 1994). Similarly, improved electrocatalytic activity was observed for Pt/C catalysts modified with WOx activity for the ORR (Hernandez-Pichardo et al., 2015).

Transition metal oxide-based catalysts encountered in the literature are usually designed for the energy conversion systems (Özdokur et al., 2019). On the other hand, the ORR signal can also be utilized in sensor technologies and photoelectrocatalytic activities as well. Next section gives these applications of such systems.

1.6. The Role of ORR in Electrochemical Biosensor Technologies

A **chemical sensor** is a device that can convert a chemical signal into an analytical signal with the help of a transducer, which converts the energy from one form to another, via the interaction between the target analyte and the sensing material placed in the system (Naresh and Lee, 2021). So far, the most popular sensors are based on electrochemical transducers which includes at least two electrode system, including working and the reference electrode.

In amperometric sensors where the current is monitored, an additional electrode called counter electrode should be included in the sensing system for a reliable response. An ideal sensor should display sensitive and selective response to a particular analyte over a wide range with high precision. Therefore, the type of working electrode is crucial for analytical point of view.

In addition to the traditional metallic electrodes, carbon-based electrodes are widely used in sensor design and fabrication, recently due to their high conductivity and ease of chemical modification at a low cost (Wang, 2006). Among the various types of carbonaceous materials, pencil graphite electrode (PGE), glassy carbon electrode (GCE) and screen-printed carbon electrodes (SPCEs) are more popular in sensor and biosensor technologies allowing selective and sensitive analysis. Besides, these electrode surfaces can be easily modified with nanomaterials and polymeric film structures to lower the overvoltage required for the process to improve the sensitivity and selectivity.

Sensitive and reliable analysis of reactive oxygen species, especially, hydrogen peroxide is of high importance in food security, environmental monitoring, and biomedical analysis (Žalnėravičius et al., 2019). Hydrogen peroxide determination at a bare carbon electrode, however, requires high overvoltage and therefore, the electrode surface is modified with several nanomaterials or polymeric film structures to lower the potential and increase the signal to improve the sensitivity and selectivity as well.

Oxygen and hydrogen peroxide are of importance in biological processes as well since these species are the main components of oxidase enzyme-based analysis. As given in **Figure 1.8,** substrate (glucose) concentration can be determined via their concentration in the cell after the enzymatic reaction (Wang, 2006).

A pioneering study on this area was designed by Clark and Lyons in 1962 to measure glucose in blood samples via detection of oxygen consumed by the enzyme-catalyzed reaction at an oxygen electrode. In this study, glucose oxidase (GOx) enzyme was immobilized onto the electrode via a semipermeable dialysis membrane. The term **Biosensor** was coined thereafter.

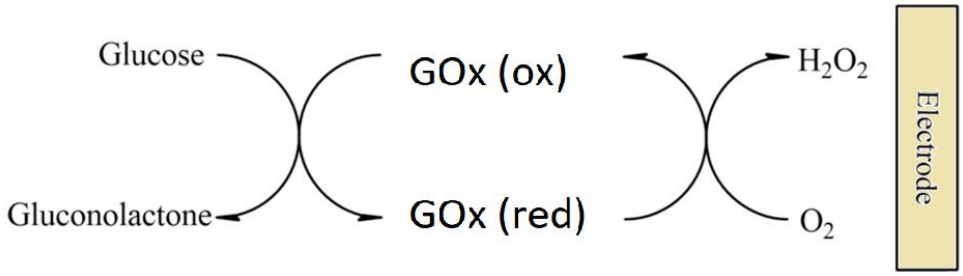

Figure 1.8 Enzymatic glucose oxidation at the electrode surface

Oxygen reduction reaction at a bare carbon electrode requires high overvoltage and therefore, various approaches have been explored for the electrode modification. The use of MnO_2 modified carbon-based electrodes in biosensing applications over hydrogen peroxide formation in both neutral and slightly alkaline media have been reviewed (Beyene et al., 2004). In the biosensor studies based on SPCE, the carbon ink incorporated with MnO_2 was printed on a ceramic support for the detection of biologically important compounds such as glucose and lactate.

In addition to the peroxide signal, reduction signal of oxygen left over from the enzymatic reaction can be utilized for biosensing studies since the differences in the peak current are directly proportional to the substrate concentration. This approach was first used in pioneering study of Clark for glucose detection where the oxygen diffused through a Teflon membrane and left over from the interaction with glucose oxidase was measured at Pt electrode (Wang, 2016).

Transition metal oxide electrodes are proven to be a good platform for biosensor fabrication. GCE/MoOx/Pt electrode for instance, was used for glucose determination by immobilizing glucose oxidase enzyme (GOx) onto the electrode surface (Çakar et al., 2013). The current differences in the ORR signal at 0.25 V was monitored against the glucose concentration and the calibration curve was found comparable to that of other biosensors modified with Au nanoparticles or CNTs as electrical connectors between the electrode and the redox center of GOx.

In another study, pyranose oxidase (PyOx) enzyme was immobilized onto the GCE/MnOx-Pt electrode which is known to have catalytic activity for the ORR (Özdokur et al., 2014). The enzyme was bridged by ionic liquid unit in the pursuit of a stable and rapid response with a high sensitivity. This biosensor was found very stable which allows them to be used in automated systems.

Highly selective enzymatic sensors have been developed in last two decades but, the main disadvantages of these sensors are the enzyme instability and sensitivity to temperature changes along with the high cost.

On the other hand, several nanoparticles which has an activity to mimic the natural peroxidase enzyme, the synthesis and applications of these artificial enzyme mimetics has been utilized in development of **non-enzymatic** sensors for hydrogen peroxide. Satisfactory performance can be attained by synthesizing uniform size and shape of nanostructures with high surface area and high catalytic activity.

Graphene-based nanostructured materials as electrocatalysts in enzymeless sensor development have been reviewed (Zhang and Chen, 2017). **Table 1.2** summarizes the featured characteristics of the non-enzymatic chemical sensors developed for hydrogen peroxide detection.

As can be followed from the table, electrocatalytic activity of the core-shell nanoparticles has provided an easy way to prepare relatively inexpensive and more stable amperometric hydrogen peroxide sensors. Their comparable sensitivity with enzymatic biosensors makes them a good alternative for detection of hydrogen peroxide in real samples.

Non-enzymatic sensor applications are not limited to hydrogen peroxide. Quantification methods of cholesterol (Derina et al., 2020), creatinine (Kumar et al., 2021) and glucose (Dong et al., 2021) by using non-enzymatic sensing technologies have been reviewed recently.

Table 1.2 Analytical characteristics of non-enzymatic methods for hydrogen peroxide

Electrode	**Cell content**	**Working Potential**	**Linear range LOD**	**Reference**
$CoWO_4$	0.1M NaOH	0.2 V (vs Hg/HgO)	LOD: 10.7 µM	Liao et al., 2015
GO/Au@Pt@Au	0.1 M PBS (pH: 7.4)	-0.3 V (vs SCE)	0.5 - 110 µM LOD: 0.25 µM	Li et al., 2016
Ag@Pt–G/GCE	0.2 M saline PBS (pH: 7.2)	−0.35 V (vs SCE)	5 - 12400 µM LOD: 0.9 µM	Liu et al., 2016
$CuFe_2O_4$/RGO/CPE	0.1 M PBS (pH: 7.4)	−0.350 V (vs Ag/AgCl)	2–200 µM LOD: 0.52	Benvidi et al., 2017
Te Nps/GCE	0.1 M PBS (pH: 7.0)	CV:-1.5-1.5 V (40 mv/s)	0.67 to 8.04 µM LOD: 0.3 µM	Manikandan et al., 2017
Pd NP-Cu	1 M PBS	1.2 V (vs $HgSO_4$)	100–2000 µM LOD: 2.1 µM	Yang et al., 2017
Cu@PtPd/C	0.05 M PBS (pH 7.4)	−0.10 V (vs Ag/AgCl)	5–250 µM LOD: 0.37 µM	Gutierrez et al., 2018.
Pt/MoS_2/Ti	0.1 M PBS (pH: 7.4)	-0.6 V (vs SCE)	10 - 160 µM LOD: 0.87 µM	Žalnėravičius et al., 2019

Today **Biosensor** refers to an analytical device involving a bioreceptor i.e., biological sensing element that can recognize the target substrate such as enzymes, cells, aptamers, DNA, and antibodies (**Figure 1.9**). By the aid of great progress in nanoscience and electronic sensing systems, biosensor technology has great advancement in biomedicine, food safety, drug discovery, and environmental monitoring of many substances.

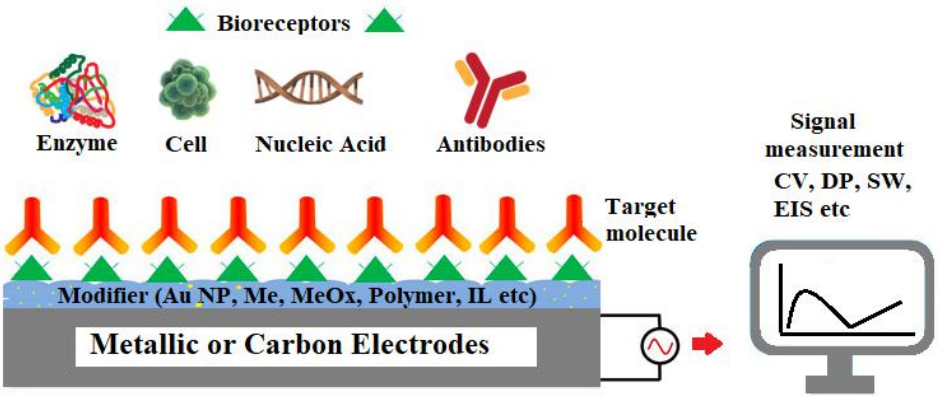

Figure 1.9 The main parts of a biosensing system

Metal oxide films constitute the platform on the electrode surface for their immobilization. In a study, mixed metal oxide film electrode, GCE/MnOx-MoOx/Pt, prepared by PD technique was treated with a cell (G. oxydans cellular paste) to create the bioactive layer. This biosensor was utilized for ethanol detection via recording the oxygen signal left over from bacterial metabolism in the presence of the substrate (Özdokur et al., 2016b). The performance of the biosensor developed was found superior to other developed biosensors in terms of response time and detection range.

Similarly, the GCE/CNT/MnOx-VOx/AuNP electrode was utilized as a platform for the immobilization of GOx enzyme with the aid of chitosan and in the presence of an ionic liquid (Akoğulları et al., 2020). After optimizing the related parameters, the biosensor was reported to display a linear range for glucose between 0.1–1.0 mM and the LOD was calculated as 0.02 mM.

In a more recent study, GCE/CoOx/Pt electrode was utilized for tyrosinase immobilization with gelatin and the influence of solution and operational parameters for phenol detection was optimized for phenol detection in micromolar levels (Kuşçu et al., 2020). Several metal oxides including ZnO, FeO, TiO_2, ZrO_2, MgO etc. have been used for application in biosensors over their electrochemical behavior (Rahman et al., 2010).

In addition to the amperometric biosensors, **impedimetric sensors** are becoming popular. Next heading gives brief information on the main principles of Electrochemical Impedance Spectroscopy (EIS) and its applications in aptamer-based sensor developments. Specific applications of this technique to a mycotoxin i.e., Ochratoxin A (OTA) were also covered.

1.7. Principles of Sensing Systems Based on EIS

Impedance (Z) is defined as the opposition force to electrical current in a circuit like the resistance (R) and its unit is also the same as ohm. The main difference from the resistance is that impedance can be seen only in AC circuits (Gamry, 2021).

In an electrochemical cell, the interfacial region at the electrode surface consists of an electric double layer. Within this very thin double layer, a large potential gradient develops. The double layer resembles a parallel-plate capacitor where the charge (q) is proportional to the potential difference(E) and the double layer capacitance (C_{dl}) in farads given as $q = C_{dl}\, E$. Considering the resistance of the solution to the movement of a charged species along with the double layer capacitance, the cell can be imagined as an RC circuit where the impedance occurs due to the reactance (X) and resistance as given below.

$$Z^2 = R^2 + X_c^2 \qquad \text{(Eq.1. 4)}$$

In this equation, X_c represents the capacitive reactance given below

$$X_c = ½\, \pi f\, C_{dl} \qquad \text{(Eq. 1.5)}$$

where the f is the frequency of the AC current. Therefore, the impedance varies according to the frequency. Impedance has a phase angle (θ) and it is represented by using real and imaginary values such as $R + ik$.

EIS provides to visualize the actual electrical double layer structure of a modified electrode and it is utilized for elucidating interfacial behavior of electrodes over a century for purposes such as corrosion analysis and monitoring the fuel cell performances and today, biomonitoring of biologically important compounds.

The EIS technique is based upon complex mathematical transforms. The operational impedance is the complex ratio of the voltage and current in an AC circuit (Eq. 1.6). Here, j is the imaginary component and ω is the frequency: (Randviir and Banks, 2013).

$$Z\,(j\omega) = V\,(j\omega) / I\,(j\omega) \qquad \text{(Eq. 1.6)}$$

In EIS system, a fixed sinusoidal voltage is applied to the cell containing the analyte in a proper electrolyte solution (**Figure 1.10**). This voltage is selected by the type of the analyte.

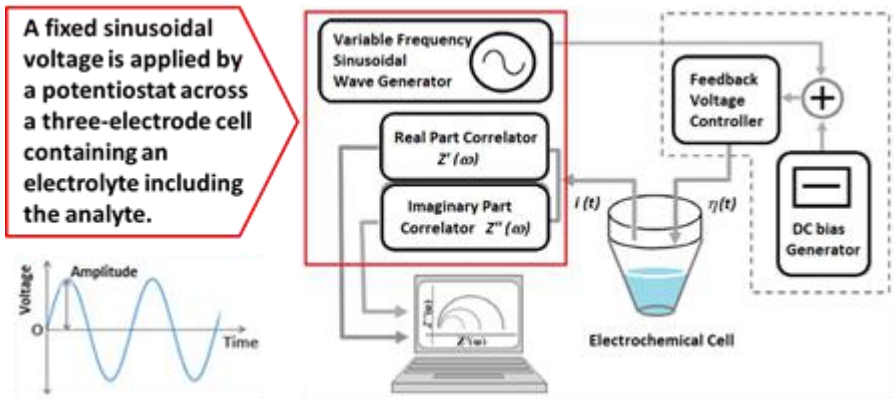

Figure 1.10 Schematic representation of EIS system

For biological applications, a composite electrode is prepared to attract target analytes which alters the conductivity of the electrode by blocking electrode surface. In such systems, since a **redox probe** such as potassium ferricyanide or hexamine-ruthenium (III) chloride are used, the potential is chosen to suit these mediators.

The current flow through the cell is recorded and then, converted into an impedance value by the software built in the system. This process is repeated across the frequency range used and the real and imaginary components are plotted against each other to obtain **Nyquist plots**. Then, we can calculate the resistances of the solution and charge transfer resistances along with the Warburg impedance from these plots (**Figure 1.11**). Since the solution resistance does not change with the frequency, it can be calculated from the intersection of the axis at the highest frequency. Charge transfer resistance, on the other hand, is dependent on the frequency and can be calculated from the intersection with the real axis in kinetically controlled region.

As can be followed from the top of the figure, Randles circuit which simulates the EIS experiment, consists of C_{dl}, the solution resistance (R_s) and charge transfer resistance (R_{ct}), along with the Warburg impedance (Z_w) that accounts for the diffusion of ions in solution to compensate for the difference in concentration caused by the electrochemical reaction.

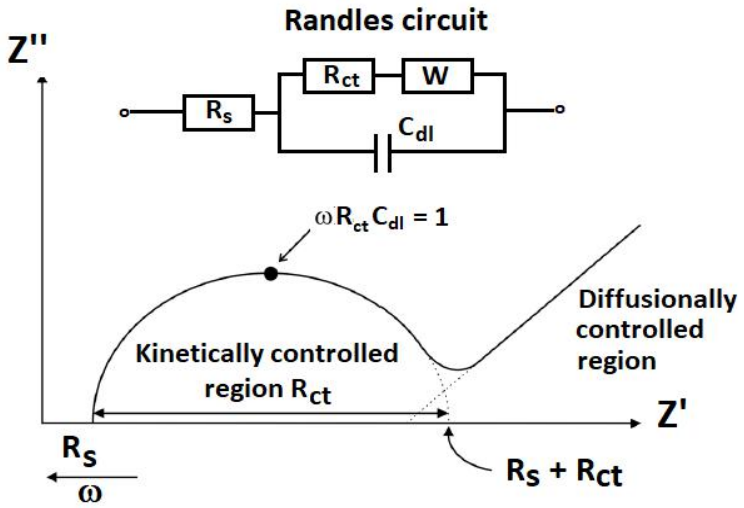

Figure 1.11 The main components of Nyquist plot (Randviir and Banks, 2013).

EIS has been widely utilized in development of **DNA biosensors**. Nyquist plots are drawn to compare the effect of electrode modifications in 1 mM $[Fe(CN)_6]^{3+/4+}$. Charge transfer resistance which appears as a larger semi-circle in the plot changes upon addition of the analyte. Single use screen printed electrodes (SPEs) are usually utilized for the specific detection of analytes where the three-electrode system is insulated by a film to prevent short-circuit.

Since 2000, functional nanomaterials have been integrated into the electrode surface and resulting nanobiosensors have made a significant advancement in the sensing prob technologies with enhanced sensitivity and selectivity. Vast number of research have been reported for biological and chemical applications via different types of label-free biosensors including enzymatic biosensors genosensors, immunosensors and, aptasensors (Munoz et al., 2017).

There are two types of affinity probes used for sensing systems are protein-based antibodies and oligonucleotide-based aptamers. Aptamers are single-stranded oligonucleotides and display several advantages over antibodies being stable in extreme conditions such as pH and temperature. In addition, they can be easily modified with functional groups (Chen et al., 2017). They are available with accurate and reproducible chemical production called Systematic Evolution of Ligands by Exponential Enrichment (SELEX). Like antibodies, aptamers exhibit high affinity to specific targets and act as molecular recognition elements by folding themselves into distinct structures. **Table 1.3** summarizes the advantages and disadvantages of both biorecognition elements.

Table 1.3 The advantages and disadvantages of antibodies and aptamers

	Advantages	**Disadvantages**
Antibodies 	• High affinity and selectivity • High immunogenicity	• Denaturation under temperature and extreme pH conditions • Limited storage conditions • In-vivo biological production
Aptamers 	• High affinity and selectivity • In-vitro production • No denaturation under temperature and extreme pH conditions • Long-term storage	• Low immunogenicity

Therefore, increasing number of **aptasensors** have been designed for the detection of a wide range of analytes targets including antibiotics detection (Chen et al., 2017), plant pathogen detection (Khater et al., 2017), cancer relevant biomolecules (Yang et al., 2021) such as lung cancer (Kıvrak et al., 2020), prostate cancer (Ghorbani et al., 2019), diagnosis of cardiovascular diseases (Azzouz et al, 2021) and for detection of mycotoxins (Guo et al., 2021). Next section gives a brief information on the mycotoxin and ochratoxin A, and analytical methods developed for their determination in food samples.

1.8. Determination of Ochratoxin A in Food Samples

Mycotoxins are fungal secondary metabolites, and these fungal toxins are classified as mutagenic and carcinogenic (Goud et al., 2018). Generally, the crops used as food resources are often exposed to a variety of mycotoxins which are produced at inconvenient conditions, such as long storage time and temperature, humidity, etc.

Currently, more than 300 mycotoxins are known, and among them, Aflatoxins (Afs) are the most toxic that have been designated as a group 1 carcinogen by the International Agency for Prime Archives in Chemistry Research on Cancer (IARC) of the WHO. The other types include zearalenone (ZEA), ochratoxin A (OTA), fumonisins (F) etc.

OTA (**Figure 1.12**) has been classified as a group 2B (possible carcinogenic agents) by IARC (Guo et al., 2021). The target organ of OTA is the kidney; however, it has other toxic effects, including nephrotoxic, teratogenic, and immunotoxic effects on human and animals.

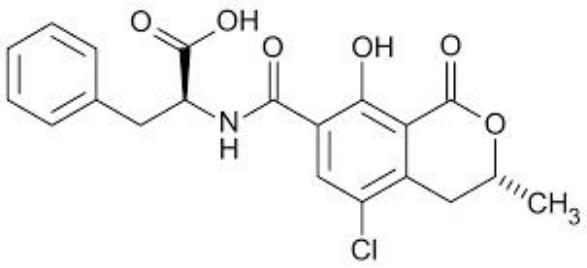

Figure 1.12 Chemical structure of ochratoxin A

European commission's scientific committee for food (SCF) have set up limits for mycotoxins in food commercialized inside the European Union (EU regulation, 2010). EU has established the tolerable weekly intake (TWI) in 120 ng/kg of body weight and the limits established for most OTA-contaminated food products were reported as 10 ng g^{-1} soluble coffee, 10 ng g^{-1} for dried fruits, 3 ng g^{-1} for cereals, 2 ng g^{-1} for wine and grape juice, and spices along with 0.5 g g^{-1} for baby food. Controls in the EU were extended to spices with a limit of 20 ng g^{-1} for paprika, 15 ng g^{-1} for white and black pepper, and 15 ng g^{-1} for their mixtures (Cubero-Leon et al., 2017). Therefore, their analysis is important in food stuffs.

From an analytical chemistry point of view, trace amounts of OTA in those rather complex matrices require a consecutive steps of efficient sample preparation and instrumental detection. Confirmatory and quantitative approaches for the detection of mycotoxins usually include Enzyme-linked immunosorbent assay (ELISA) and chromatographic techniques namely, thin layer chromatography (TLC), high-performance liquid chromatography (HPLC), and liquid chromatography coupled with mass spectrometry (LC–MS) (Guo et al., 2021). Recent progress in chromatographic methods developed for mycotoxins in food was reviewed (Medina et al., 2021).

Dried fruits are important agricultural products and Turkey has a leading position for fig and apricot production and exports in the world. However, regional temperature and climatic conditions along with the water activity of the fruit during ripening, harvesting and drying stages make the product suitable for mycotoxin formation.

OTA incidence and levels in Turkish dried figs have been determined by HPLC in a thesis study carried out in our country (Güler, 2008). Nearly half of the fig samples collected from the Aegean Region in 2003 and 2004 were found to be contaminated and the highest incidences of OTA were found within the range of 0.12-1.0 ng g^{-1}. In another study, dried fruits samples of Iran were analyzed by enzyme linked immunosorbent assay (ELISA) technique and the incidence rates of OTA contamination in dried fig was around 10% (Rahimi and Shakerian, 2013). Only 2.1% of dried fig samples were found higher than maximum tolerance limit accepted by EU being 10 ng g^{-1}.

Chromatographic methods are robust and can be applied to various species but, the requirement for expensive and special instruments along with time consuming and complicated pretreatment steps. As an alternative approach, antibody-based immunoassays have been developed for determination of mycotoxins (Guo et al., 2021).

In the last decade, sensors based on aptamers that can form aptamer/target complexes with very strong affinity and selectivity are more popular for OTA detection in food samples. Electrochemical aptasensors particularly are drawing attention since they provide rapid, portable, and inexpensive systems with high sensitivity and selectivity. Generally, the techniques such as EIS, DPV, CV and square wave voltammetry (SWV) was used in the measurement step.

Table 1.4 gives the details of aptasensor studies based on electrochemical methods. Wu et al. have used a gold electrode modified with the thiol- and MB-(methylene blue) dual-labeled aptamer for ultrasensitive OTA detection (2012). The method was applied for the OTA detection in red wine samples with satisfying recoveries.

In another study, the gold electrode was modified with neutral red electropolymerization and treated with chemically synthesized silver nanoparticles (Ag NPs) to thiolate the aptamer to the surface (Evtugyn et al., 2013). In the presence of OTA, the aptamer/OTA complex has changed the charge transfer resistance (R_{ct}) values of the cell containing ferricyanide ions measured by EIS. The validated method was applied to OTA determination in beer samples with satisfactory recoveries.

Table 1.4 Analytical properties of Electrochemical Aptasensors Developed for OTA.

Measurement Technique/ Medium	**Electrode Modification***	**Aptamer sequence**	**Linear Range/ LOD**	**Sample type/ Sample pretreatment**	**Reference**
SWV -0.2--0.4 V (vs Ag/AgCl), Fr: 60 Hz. /10 mM PBS (pH 7.4) + 20 mM $MgCl_2$	Au/ thiol- and MB dual-labeled aptamer modified	5'MB-GAT CGG GTG TGG GTG GCG TAA AGG GAG CAT CGG ACA-SH-3'.	1-1000 pg mL^{-1} 0.095 pg mL^{-1}	Red wine/diluted with PBS soln. (1:1).	Wu et al., 2012
EIS 0.01M $K_3[Fe(CN)_6]$ and 0.01M $K_4[Fe(CN)_6]$. Amp. 5 mV. Fr: 100 kHz - 0.04 Hz	Au/ poly-Neutral Red and Ag NPs	5'-SH-GAT CGG GTG TGG GTG GCG TAA AGG GAG CAT CGG ACA-3	0.3-30 nM 0.05 nM	Beer/Boiled for 15 min and HEPES + 0.1 M KCl was added	Evtugyn et al., 2013
EIS 0.001M $[Fe(CN)_6]^{-3/-4}$ + 0.1 M KCl. 0.24 V vs Ag/AgCl Fr: 100 kHz−0.1 Hz	SPCE/thionine and IrO_2NPs	5′-GAT CGG GTG TGG GTG GCG TAA AGG GAG CAT CGG ACA AAA AAA AAA NH_2-3′	0.01-100 nM 0.014 nM	White wine/ dilution with buffer	Rivas et al., 2015
EIS 0.001M $[Fe(CN)_6]^{-3/-4}$ at 0.1 V (vs. Ag/AgCl) Amp: 5 mV Fr: 1 kHz to 0.1 Hz	SPCE/Polythiophene-3-carboxylic acid	5′-GAT CGG GTG TGG GTG GCG TAA AGG GAG CAT CGG ACA-3' (NH_2-OTA)	0.31–6.19 nM 0.31 nM	Coffee/extr with methanol+5% aq $NaHCO_3$ under stirring for 60 min → MIP	Zejli et al., 2018
EIS 0.005M $[Fe(CN)_6]^{-3/-4}$ at 0.24 V vs. Ag/AgCl, Fr: 10 kHz to 0.05 Hz	PGE/MnOx (PD)	5′-Amino-C6-GAT CGG GTG TGG GTG GCG TAA AGG GAG CAT CGG ACA-3′.	0.025-1.0 nM 0.025 nM	Grape juice/ diluted in 1:10 ratio by using PBS	Kırlangıç et al., 2021

In addition to the gold disk electrode, disposable carbon-based electrodes are preferred such as screen-printed carbon electrodes (SPCE) and PGEs modified with polymeric films, nano particles, and other nanomaterials to enhance the sensitivity and selectivity. A recent study from the lab has shown that PGE modified with transition metal oxides by CV or DP deposition techniques, provided a promising platform for aptasensor fabrication (Kırlangıç et al., 2021). Among the studied transition metals namely manganese, molybdenum, and tungsten, MnO_x has displayed high selectivity and sensitivity towards OTA detection in grape juice samples.

Considering the role and applications of transition metal oxides in the electrochemical biosensor technologies, a rather limited number of immunosensing and aptasensing studies have been encountered in the literature. Promising results obtained in a former study in the lab on the use of transition metal oxides deposited onto a PGE in aptasensor studies was the driving force to study the WO_x as a platform for OTA detection.

Another catalytic application area is the photoelectrocatalysis. Next section gives the fundamentals of the area and special applications to the photoelectrocatalytic degradation of azo dyes.

1.9. Photoelectrocatalysis

Photoelectrocatalysis (PEC) has been introduced as a promising technique for hydrogen evolution, generating electricity and removal of organic pollutants from water system (Cao et al., 2017). The PEC mechanism includes the activation of the **photocatalyst** which act as the anode in a cell where a suitable potential is applied. In case of the energy of the incident photon ($E = h\nu$) is higher than the bandgap of the semiconductor (E_g), valence electrons are released. These electrons can react with the oxygen dissolved in the solution to form **Reactive Oxygen Species** (ROS).

As illustrated in **Figure 1.13**, both electrons and holes (h^+) generated by the photon can be accelerated to the opposite electrode by application of a small potential. The electrons are driven to the cathode through the external circuit while the holes left behind react with organic molecules in the vicinity of the electrode.

This system is well suited for removing organic pollutants by degradation into non-toxic small molecules. The applied potential contributes to the photocatalytic degradation of the target pollutant and this potential should be chosen between the redox potential of the species and oxygen evolution potential. If the potential is set higher than evolution potential of oxygen, more active species could be formed, and this electrochemically generated oxygen may form H_2O_2 by capturing the photogenerated electrons.

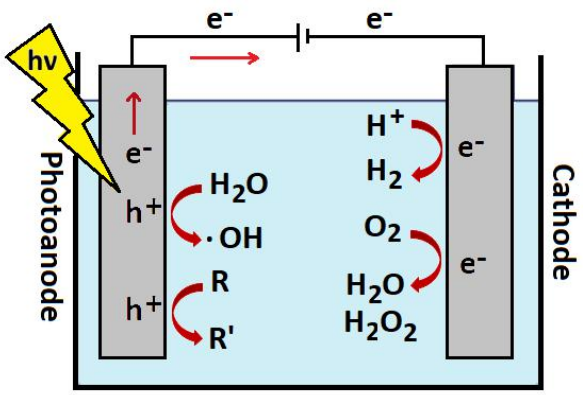

Figure 1.13 Degradation mechanism in PEC system (Cao et al., 2017).

Performance of the system mostly depends on the type of semiconductor used as the photocatalyst and operating conditions. Since the first experiments on the PEC studies, low-cost titanium dioxide (TiO_2) is preferred owing to its high efficiency (Palmas et al., 2021). However, this material is that catalytic active in UV regions. Therefore, fabrication of electrodes responding to visible light has become a critical task. For this purpose, the most investigated films include binary and ternary oxides and organic semiconductors (Cao et al., 2017). The activity of photoanode is affected by the interaction between the electronic characteristics and surface morphology, therefore, titanium nanotube (TNT) arrays (Mor et al., 2006) and nanorod films (Feng et al., 2005) have been extensively utilized for degradation studies.

The PEC performance can be improved by modification of the anode material by either internal doping or surface sensitization (Tang et al., 2018). The latter approach is mostly preferred, and the electrodes are modified with noble metals (Kim et al., 2015), metals (Foura et al., 2017), non-metals (In et al., 2007), and carbonaceous materials as well (Tang et al., 2018).

The coupling of TiO_2 (3.2 eV) with an oxide material containing close band gap energies results in a considerable enhancement of performance. Upon modification of TNT with nanostructured WO_3 (2.8 eV) a significant contribution to visible light absorption, higher hydrophilicity and better adsorption of reactants have been observed (Guaraldo et al., 2016). In addition, as an electron acceptor, integration of WO_3 into the composite increases the Lewis surface acidity. Photo-generated charge carriers can be separated more efficiently by this means. The synthesis technique plays an important role on the catalytic activity of nanostructured tungsten trioxide thin films (Zhu et al., 2016).

By the development of UV and Vis light-responding materials, the application of these photoanodes in the removal of organic contaminants such as pharmaceuticals, endocrine disrupting chemicals and dyes, has become important as an advanced oxidation method. The efficiency of the method depends on the type of the contaminant as well as the photoanode materials and its operation conditions, Next section gives the details of the applications on azo dyes.

1.10. Photoelectrocatalytic Degradation of Azo Dyes

Azo dyes are commonly used due to their chemical stability but due to their toxicity, their removal is an important obligation. Besides the classical methods such as filtration, adsorption and coagulation, advanced oxidation process such as photoelectrocatalytic techniques provide a useful strategy where the organic pollutant is oxidized at the photoanode surface. There are several reviews which cover the recent advances in these applications (Cao et al., 2017, Peleyeju and Viljoen, 2021, Rajput et al., 2021, Garcia-Segura and Brillas, 2017). **Table 1.5** summarizes the anode materials used in removal of dyes in PEC system.

Tungsten oxide-based catalysts for PEC degradation of organic pollutants from water have been recently reviewed (Peleyeju and Viljoen, 2021). WO_3-based catalyst can also act in visible region and its valence band edge (2.6 V vs NHE) affords a necessary potential for removal of organic pollutants including methylene blue (Zeng et al., 2017).

Table 1.5. PEC Degradation of azo dyes at different metal oxide anode materials.

Type of dye	**Anode material**	**Lamp/Applied voltage/Time**	**Dye conc./medium pH**	**Decoloration (%)**	**Ref.**
Acid yellow 1	Boron doped TNT	125 W Hg / 1.2 V (vs. Ag/AgCl)/ 2 h	0.43 mM / pH: 2.0	100%	Bessegato et al., 2015
Methylene blue	$TiO_2/SrTiO_3$	300 W Xe arc/ 0.5 V vs. Ag/AgCl / 20 min	10 mg/L / pH: 5.0	100%	Huang et al., 2014
Methylene blue	WO_3 nanoplate array	500 W Xe arc/ 1.0 V vs. SCE/1.75 h	not given / neutral pH	80%	Zeng et al., 2017
Methyl orange	Monoclinic WO_3	500 W Xe arc / 1.0 V vs. SCE / 3 h	61 µM / 0.1 NaH_2PO_4	95.7%	Zheng et al., 2014
Methyl orange	Graphite/TiO_2/ Ni foam	500 W Xe arc / 2.0 V vs. SCE / 2 h	10 mg/L / 0.1 M Na_2SO_4	99.8%	Jia et al., 2016
Reactive Black 5	TiO_2/WO_3 templates	125 W Hg / 1.0 V vs. Ag/AgCl / 2 h	$5x10^{-5}$ M / pH 2	100%	Guaraldo et al., 2016
Rhodamine B	Slant-placed TiO_2 film	11 W Hg / 1.0 V vs. SCE / 1 h	20 mg/L /pH 2.5	98%	Yao et al., 2012
Rhodamine B	ITO/CNT-TiO_2/ITO	500-W Xe arc / 1.5 V /-	5 mg/L / 1.5 M NaCl	-	Wang et al., 2013
Rhodamine B	$TiO_2/C/Al_2O_3$ membrane	500 W Xe arc / 1.0 V vs. stainless steel	10 mg/L / not given	-	Wang et al., 2015
Rhodamine B	N-doped TiO_2/FTO	20 W UV / 0.52 V vs. graphite /4 h	not given / 0.1 M NaOH	64%	Kothavale et al., 2020

]

In another study, it was reported that the performance of TiO_2 catalyst was enhanced by modifying with WO_3 by sol-gel method, and this effect was attributed to increased Lewis's surface acidity of TiO_2-WO_3 composites (Riboni et al., 2013). By this means the composite can act as an electron acceptor resulting in the enhanced separation efficiency of photo-generated charge carriers. Modifications made by annealing the TNT at a high temperature was noted to destruct its nanotubular structure (Sun et al., 2015).

Electrochemical synthesis, on the other hand, provides a cost-effective method for obtaining films at adjustable thicknesses. A limited number of studies have been noticed in the literature. A binary oxide film was prepared by electrodeposition of WO_3 onto the TNT and then, cathodic reduction was employed to introduce oxygen vacancies into the WO_3-TNT composite film (Wang et al., 2020). The composite film was applied for the PEC degradation of volatile organic compounds at −1.4 V (vs SCE). No study was encountered dealing with degradation of azo dyes by using electrochemically prepared WO_3-TNT composites.

1.11. Aim of the PhD Thesis

Tungsten oxide has attracted great attention over the past two decades due to its high stability in acid solution and its outstanding catalytic performances. Therefore, in this thesis, it was aimed to study the catalytic effects of WOx in diverse application areas. The thesis work consists of three main parts, explained under 3 different electrodes: GCE, PGE and TNT for various applications as illustrated in **Figure 1.14**.

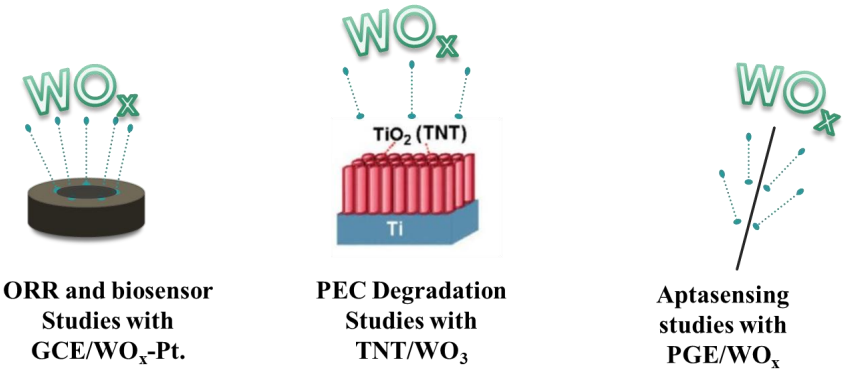

Figure 1.14 Types of electrodes and catalytical reactions studied in the thesis

First part of the thesis deals with electrocatalytic effect of WOx film deposited on the GCE and the synergistic effect of platinum nanoparticles deposited onto the film towards the ORR. Here, the effect of deposition conditions and cell contents have been elucidated in the pursue of best signal formation and these electrodes have been searched for possible application to the enzymatic and non-enzymatic sensor development.

In the **second part** of the thesis, the PGEs have been modified with WOx film as a supporting surface for aptasensor studies. In the light of a former study in this lab, the WOx modified PGEs have been prepared by using different deposition techniques and under optimized conditions, two different aptamers have been bounded to the electrode surface by different strategies. The aptasensor was utilized for OTA detection and their performances have been compared.

In the **third part** of the study, tungsten oxide film has been electrodeposited on the titanium nanotubes (TNT) and then, by setting the potential at an appropriate value, the composite film was applied for the PEC degradation of several azo dyes. The application conditions of this binary-oxide film to Rhodamine B degradation have been searched. By this means different aspects of electrocatalytic activities of tungsten oxide have been elucidated.

2. EXPERIMENTAL

2.1 Apparatus

Voltammetric (CV and PD) and chronoamperometric measurements were carried out by using Autolab PGSTAT. Electrochemical impedance spectroscopy (EIS) measurements were made with Autolab III/FRA2 potentiostat present in Analytical Chemistry Department of Ege University Faculty of Pharmacy. For the ORR studies, a three-electrode system consisting of GCE (BASi, 3 mm diameter, geometric surface area 0.0707 cm^2) as working electrode, a platinum wire (99.99%) as auxiliary electrode and a saturated silver/silver chloride (Ag/AgCl, sat. KCl) as the reference electrode was used (**Figure 2.1**). For surface morphology and chemical composition analysis, Scanning Electron Microscope with Energy Dispersive X-ray Spectroscopy (SEM-EDX) (Zeiss GEMINI 500) and X-ray Photoelectron Spectroscopy (XPS) (Thermo Scientific K-Alpha).

Figure 2.1 Three electrode system consisting of the GCE as the working electrode, Ag/AgCl as the reference electrode and a Pt wire as the auxiliary electrode.

In EIS measurements, Tombow 0.5 mm/2B pencil tips are used as the working electrode. Mettler Toledo S210-Bio Seven Compact was used for the pH measurements. In PEC studies, experimental set up was used in collaboration with Erzincan Binali Yıldırım University Chemistry Department where Keithley 2200-DC power supply was used for anodization of titanium foils. Modified TNT surfaces have been characterized by using Fei Quanta FEG 450 FESEM. UV-A lamp (100 watt, for an intensity of 21,700 µW/cm² at 5 cm or 8,900 µW/cm² at 25 cm distance) delivering high intensity long-wave (365 nm) ultraviolet light produced by Ted Pella Inc. PEC degradation kinetics has been monitored by using PG instruments T 80 Plus for UV-Vis absorbance measurements.

2.2 Reagents

All the reagents used for the electrochemical depositions and measurements were of analytical grade. Ultrapure water obtained from a Millipore water (18.2 MΩ.cm resistivity) system was used. Sodium tungstate dihydrate ($Na_2WO_4.2H_2O$) with a purity of 99.0% and potassium tetrachloroplatinate (II) (K_2PtCl_4) with 46-47% Pt amount was purchased from Acros Organics. $K(AuCl_4)$ salt was purchased Sigma. Hydrogen peroxide, 35% solution (medical extra pure) and sulfuric acid with 95-97% purity were purchased from Merck Company. Solution of 0.005 M sodium tungstate was prepared freshly prior to measurements by dissolving appropriate amount of $Na_2WO_4.2H_2O$ in 0.5 M H_2SO_4. Britton Robinson buffer (BR) solutions were prepared by mixing of equal concentrations (0.04 M) of boric acid (H_3BO_3), orthophosphoric acid (H_3PO_4) and glacial acetic acid (CH_3COOH). The desired pH was adjusted by adding 1.0 M NaOH into the acid mixture solution.

High salt solution used for OTA studies consisted of 1.5 M sodium chloride (NaCl) and 0.001 M magnesium chloride ($MgCl_2$) in phosphate buffer solution (PBS) with a pH of 7.4. $MgCl_2$ and NaCl were both purchased from Merck. PBS was prepared by dissolving adequate amounts of K_2HPO_4 and KH_2PO_4 in ultrapure water. Both reagents were purchased from Merck. The pH was adjusted by adding 1.0 M NaOH into the acid solution.

$K_4[Fe(CN)_6].3H_20$ and KCl used for preparing ferri/ferrocyanide solution was purchased from Sigma Aldrich. The stock solution consisted of 0.01 M $K_4[Fe(CN)_6].3H_20$ and 0.1 M KCl. EDC (1-ethyl-3-(3-dimethylaminopropyl) carbodiimide hydrochloride) and NHS (N-Hydroxy succinimide, 98%) were obtained from Sigma Aldrich. Adequate amounts of both reagents were weighed properly and dissolved in pH 7.4 PBS for preparing EDC/NHS solution.

Ochratoxin A (OTA), albumin bovine serum (BSA) and 2-mercaptoethanol (ME) were purchased from Sigma Aldrich Company. Amino- and thiol-based OTA aptamers were purchased from Heliks Biyoteknoloji Company. The sequence of the aptamers are as follows: 5'-Amino-C6-GAT CGG GTG TGG GTG GCG TAA AGG GAG CAT CGG ACA-3' and 5'- Thiol– GAT CGG GTG TGG GTG GCG TAA AGG GAG CAT CGG ACA 3'.

Photoelectrocatalytic studies have been carried out with titanium nanotubes in collaboration with Erzincan Binali Yıldırım University, Chemistry Department where the titanium foils (0.2 mm, 99.6% purity) was maintained from GoodFellow Cambridge Limited Company. Ethylene glycol (≥99.0% purity), ammonium fluoride, NH_4F (≥98.0 purity) obtained from Sigma Aldrich were used for preparing TNTs. Azo dyes namely, Methylene Blue (MB), Mordant Orange-1 (Alizarin Yellow) and Rhodamine B (RhB) used as model pollutants for PEC degradation studies were purchased from Sigma Aldrich. Stock solutions of each dye (6 ppm) were prepared by dissolving a proper amount dye in ultrapure water.

2.3 The Procedure for ORR Studies Carried Out with GCE

Initially, the GCE was polished with Al_2O_3 slurry on a piece of cloth and then rinsed with pure water. The electrode was placed into a beaker containing 50:50 deionized water and ethanol mixture and subsequently sonicated in an ultrasonic bath for 5 minutes. The electrode was inserted into the measuring cell and the cell contents were deaerated by purging high purity nitrogen and/or oxygen for minimum 10 minutes before each experiment. All experiments were carried out at room conditions.

Catalytic activity of bare GCEs towards ORR was recorded in BR buffer (pH 5.0) via cyclic voltammetry before each study. Different modification steps of bare GCE surface were applied and after each modification, the performances of the modified surfaces were investigated to pursuit a change in the catalytic activity for ORR signals.

Then, the modified electrodes were dipped into BR buffer with a pH of 5.0 and the potential was cycled between 0.8 and -0.5 V at 50 mV/s scan rate. Background catalytic performance of each electrode was measured by purging N_2 from the buffer solution. Then, the same solutions were saturated with O_2 gas and the signal for ORR was recorded for each modified GCE surface to see any difference from the background signal.

In the pursuit of the best composition of metal oxide film with the highest electrocatalytic activity performance, possible order of deposition was tested by applying CV and PD techniques. In the former technique, five different modification procedures have been applied as given below.

2.3.1. CV Deposited Electrodes

GCE/WO_x: The GCE was dipped into a deposition medium containing 0.05 M WO_4^{2-} in 0.01 M H_2SO_4 solution and the potential was scanned from 1.0 to -0.9 V with a 50 mV/s scan rate for ten consecutive cycles. In further studies, deposition conditions were changed by using a deposition solution containing 0.005 M Na_2WO_4 in 0.5 M H_2SO_4 and 0.08 M H_20_2. The potential range was set up between 0.9 V and -0.6 V with a 50 mV/s scan rate.

GCE/Pt: The bare GCE was immersed into 0.001 M Pt^{2+} in 0.01 M H_2SO_4 solution and the deposition was performed by cycling the potential from 1.0 to -0.5 V having a 50mV s^{-1} scan rate for ten consecutive cycles.

GCE/WO_x/Pt: The GCE/WOx obtained was further modified with Pt^{2+} ions for several cycles by scanning the potential from 1.0 to -0.5 V at a rate of 50 mV s^{-1} from a solution consisted of 0.001 M Pt^{2+} in 0.01 M H_2SO_4.

GCE/Pt/WO_x: The bare GCE was firstly modified with Pt NPs by scanning the potential from 1.0 to -0.5 V with a 50 mV s^{-1} scan rate for ten cycles. The deposition medium was changed to tungstate solution and the GCE/Pt was further modified from 0.05 M WO_4^{2-} solution. The potential was scanned from 1.0 to -0.9 V with a 50 mV s^{-1} scan rate for ten cycles.

GCE/WO_x-Pt: Co-deposition of WO_4^{2-} and Pt^{2+} was performed in solution consisted of 0.001 M Pt^{2+} in 0.01 M H_2SO_4. The weighed amounts of tungstate and platinum ions were calculated to obtain a specific mole ratio for Pt:WO_x being 1:10; 1:25; 1:50; 1:75 and 1:100 by keeping the molarity of Pt^{2+} constant and changing the molarity of tungstate ion. The scan rate was 50 mV s^{-1}.

2.3.2. Pulsed Deposited Electrode

GCE/WO_x-Pt (PD): Here, co-deposition of WO_4^{2-} and Pt^{2+} was performed as given above by keeping the mole ratio of Pt:WO_x to be 1:10; 1:25; 1:50; 1:75 and 1:100. Pulsed deposition program was applied where the potential was set to 0.2 V for 3 s and then -0.5 V 5 for 3 s sequentially. This process was run for 50 times. All the procedures have been summarized in **Figure 2.2.**

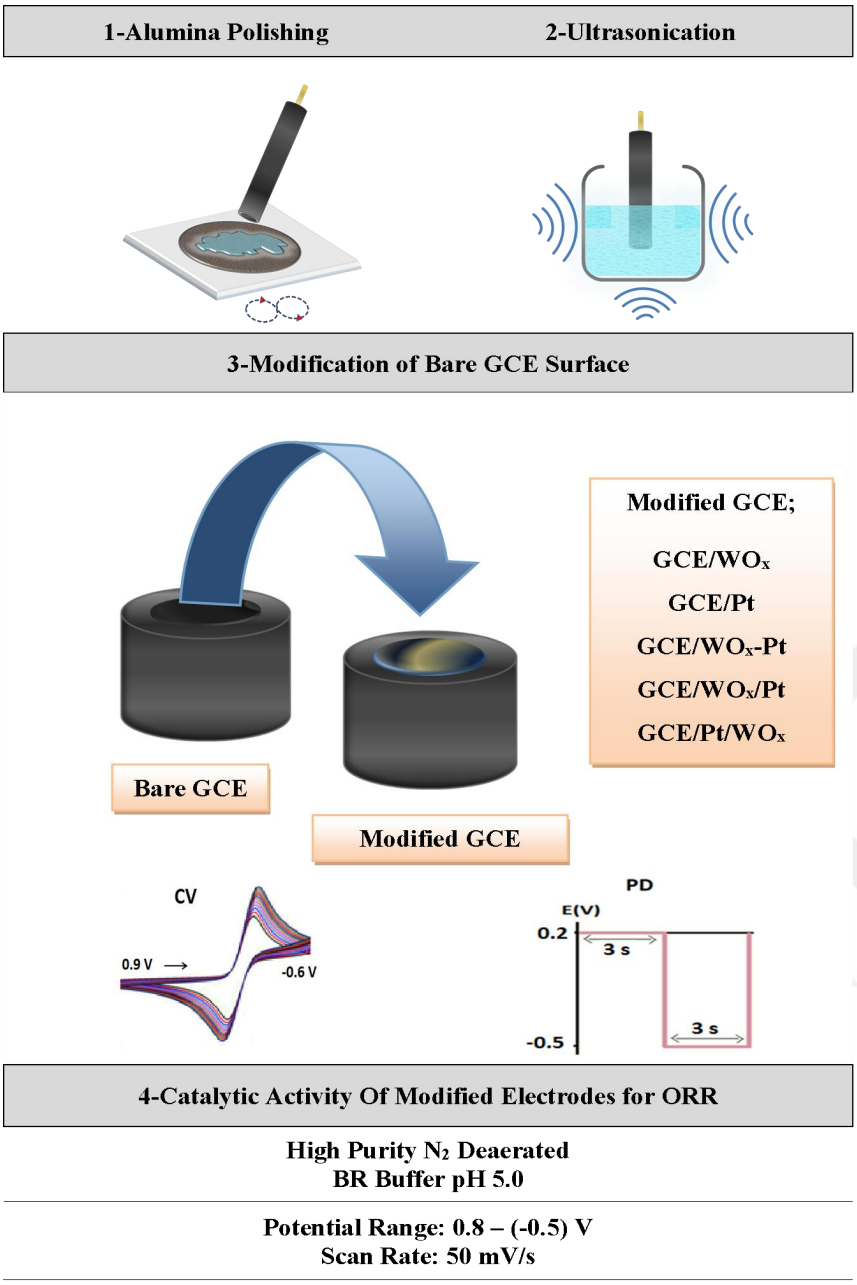

Figure 2.2 Representation of modification and measurements steps used for ORR studies

2.3.3. Biosensor development

As shown in **Figure 2.3**, after the electrode preparation, 0.25 mg catalase enzyme and 0.75 mg gelatin were mixed in 50 mL pH 7.0 PBS and kept in water bath (37°C) to obtain a homogenous mixture. 10 µL of the enzyme-gelatin mixture was immobilized onto GCE/WOx surface and kept in refrigerator (4°C) for one hour. The electrode was immersed in 100 µL glutaraldehyde (%2.5 v/v) solution in pH 7.0 PBS.

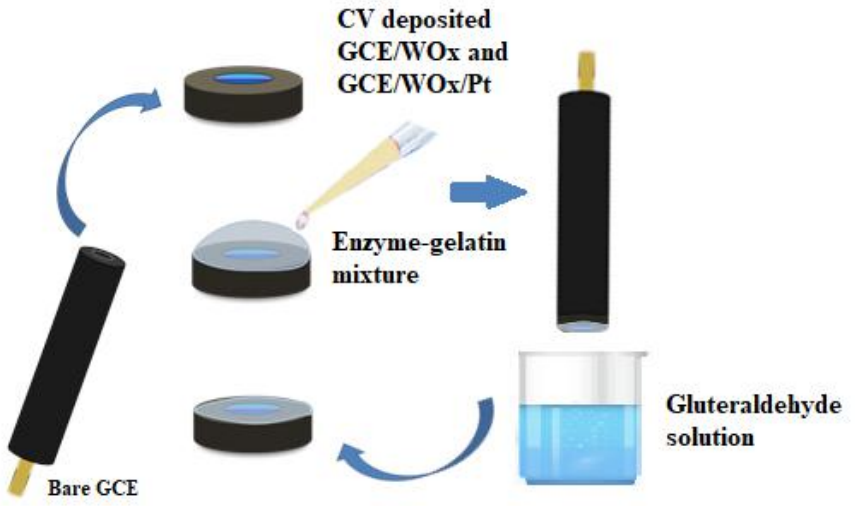

Figure 2.3 Preparation of catalase immobilized GCE/WOx-Pt electrode

2.4 The Procedure for Aptasensor Studies Carried Out with PGE

Aptasensor studies were carried out in Faculty of Pharmacy, Analytical Chemistry Department. The stages of aptasensor preparation and the procedure used in EIS measurements were given below.

2.4.1. Modification of Pencil Graphite Electrodes

First, the bare PGE was conditioned in acetic acid/acetate buffer (pH:4.8) at a potential of 1.4 V for one minute. This anodization step helps to increase the number of carboxylic groups on graphite surface to facilitate the binding of EDC/NHS onto the surface. Then, the bare PGEs were modified as given below.

PGE/WOx (CV): The PGE was immersed in the cell containing 0.075 M Na_2WO_4 in 0.5 M H_2SO_4 and 0.08 M H_20_2. The reference (Ag/AgCl, sat) and counter (Pt) electrodes were connected. The potential range was set up between 0.9 V and -0.6 V with a 50 mVs^{-1} scan rate for 5 consecutive cycles.

PGE/WOx (PD): The PGEs were immersed into the same deposition medium, and the potential was set to 0.2 V for 3 s and then -0.5 V for 3 s sequentially. This process was repeated for 50 times.

PGE/WOx/Au NP: PGE/WOx electrodes prepared above was dipped into the voltammetric cell containing $1.4x10^{-3}$ M Au^{3+} in 0.01 M HCl solution. In PD technique, the potential was set to 0 (5 s) and -0.5 V (5 s) for 50 times.

2.4.2. Aptamer Immobilization

In this thesis, two different aptamers have been used for immobilization onto the PGE/WO_x electrodes: 5'-Amino- Aptamer: 5'-Amino-C6-GAT CGG GTG TGG GTG GCG TAA AGG GAG CAT CGG ACA-3' and 5'-thiol Aptamer: 5'- Thiol– GAT CGG GTG TGG GTG GCG TAA AGG GAG CAT CGG ACA 3'). Immobilization procedures were differed in nature according to the chemical activity of amino- or thiol groups.

Immobilization of amino bearing aptamer (NH_2-Apt) was accomplished via electrodes via carbodiimide chemistry via EDC/NHS mechanism as illustrated in **Figure 2.4**.

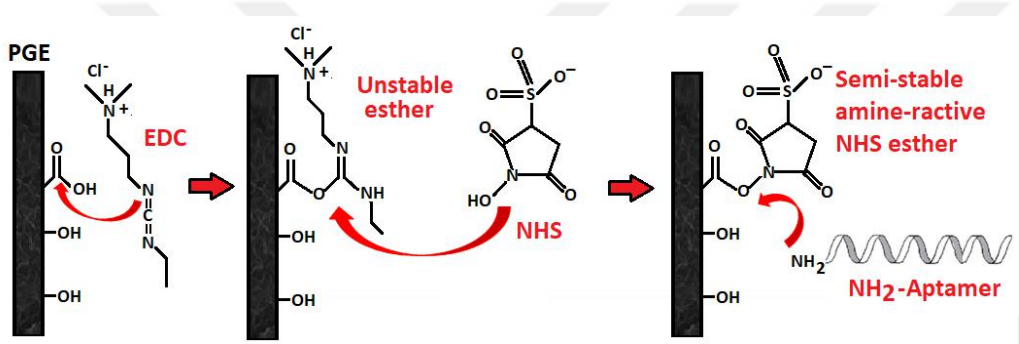

Figure 2.4 The mechanism of carbodiimide chemistry via EDC/NHS for binding of NH_2-Aptamer

The procedure can be followed from **Figure 2.5** where the PGE/WO_x electrodes were immersed into 0.008 M EDC/NHS solutions for an hour to obtain a selective surface to immobilize the OTA aptamer. The electrodes were kept in 0.5 µM aptamer solution for an hour and then, dipped into the PBS (pH 7.4) solution containing 1% BSA to block residual active tips. After blocking step, the electrodes were treated with OTA solution for another one hour. The last step prior to the measurement was to wash the treated electrodes with PBS (pH 7.4) by immersing into the solution for 1-2 seconds.

The 5'-thiol aptamers (SH-Apt) specific to OTA was immobilized onto the PGE/WOx electrode decorated with gold nanoparticles (Au NPs). The PGE/WOx/Au electrodes were incubated in 0.1 µM SH-Apt solution in acetate buffer (pH 4.8) for 1 hour. To prevent non-specific binding, the electrodes was immersed in %1 2-mercaptoethanol (ME) solution for 1 hour and then, it was incubated with OTA in PBS for 1 hour. After the process, the electrodes were dipped into the PBS and allowed to dry in inverted position.

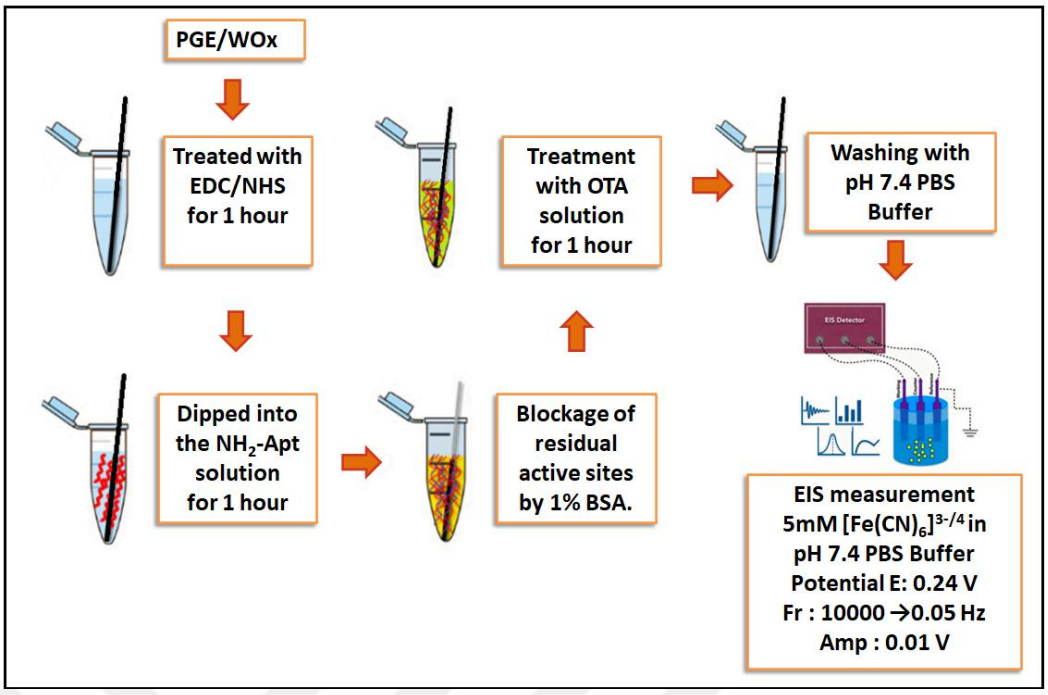

Figure 2.5 Modification and measurements steps for aptasensor development

2.4.3. EIS Measurement Procedure

In the EIS procedure, the applied potential was chosen as 0.24 V based on cyclic voltammogram recorded between 0.8V to -0.5V. The frequency range was 10.000 - 0.05 Hz with an amplitude of 0.01V and the charge transfer resistance (R_{ct}) values for each electrode were recorded.

Quantitation studies were carried out by calculating the differences (ΔR_{ct}) between the R_{ct} value of interaction with the target molecule and after the blocking the residual active sites by a proper reagent given as the below equation.

$$\Delta R_{ct} = R_{ct}\ (Target) - R_{ct}\ (Blocking) \qquad \text{(Eq. 2.1)}$$

2.5 Photoelectrocatalytic Studies with TNT Electrode

Titanium nanotubes (TNTs) have been modified with WO_3 for photoelectrochemical degradation studies in collaboration with the research group in Erzincan Binali Yıldırım University. For this purpose, the TNT arrays were grown by electrochemical anodization method on Titanium foils (0.25 mm, 99.7% purity from Sigma Aldrich) as described earlier (Çırak et al., 2017).

2.5.1. Preparation of TNT for PEC Studies

As shown in **Figure 2.6**, high purity titanium foils were cut in pieces of 1.0 x 3.0 cm and cleaned by ultrasonic agitation sequentially in acetone, isopropyl alcohol, and deionized water for 30 min. Then, it was dipped into the cell containing ethylene glycol, 0.4% (w/w) NH_4F and 5% (w/w) deionized water where the cathode is platinum mesh. Then, 40 V DC potential was applied for 4 hours under magnetic stirring.

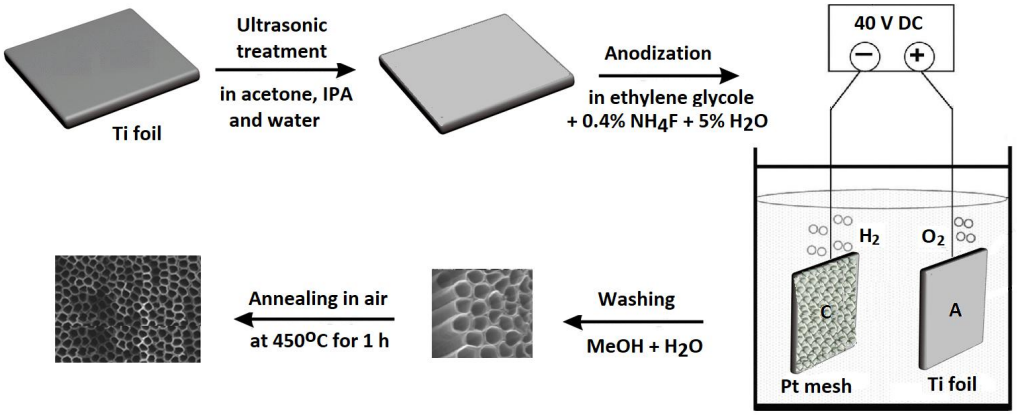

Figure 2.6 The procedure used for the TNT preparation

Following this step, the TNT arrays were cleaned in methanol and water, subsequently for one min to remove any residual. Afterwards, the TNT arrays were annealed at 450°C for 1 h in air ambient for amorphous to anatase phase transition. In the modification step, the TNT electrode with a surface area of 2.0 cm^2 was placed in the cell as the working electrode for subsequent modification and the three-electrode system was completed with an Ag/AgCl as the reference electrode and a Pt wire as the counter electrode.

The voltammetric cell was filled with 50 mL of 0.005 M tungstate solution prepared from Na_2WO_4 .$2H_20$ in 0.5 M H_2SO_4 and 0.08 M H_2O_2 mixture. Then, the potential was cycled between -0.9 V – 0.6 V for several times with a 50 mVs^{-1} scan rate. **Figure 2.7** shows the images of the material used for TNT preparation and modified TNT sample.

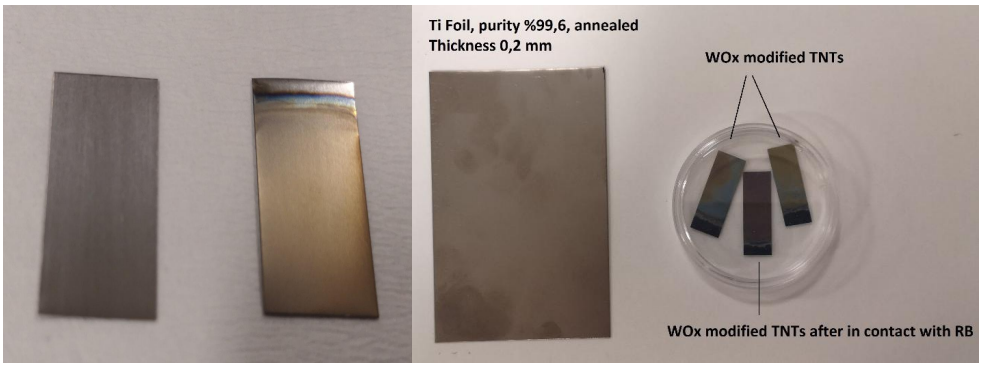

A **B**

Figure 2.7 Images of A) titanium foil used for TNT preparation and the TNT obtained by the procedure, B) Ti foil and TNT electrodes modified with WOx by electrodeposition

2.5.2. PEC Degradation System for Dye Solutions

Then, the TNT-WO_3 electrode was placed into the voltammetric cell as the photoanode, and an ultraviolet A lamp (high intensity long-wave, 365 nm) was positioned at a 20 cm distance from the transparent cell targeting this anode. **Figure 2.8** shows the schematic diagram of the PEC set-up used in this study.

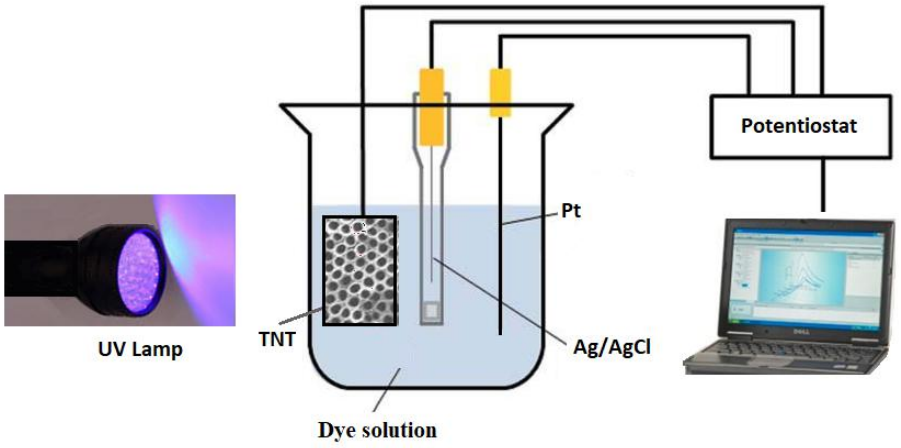

Figure 2.8 Schematic illustrations of experimental set up for PEC studies

The cell was filled with 6.0 mg L^{-1} of azo dye solution and a potential of 0.2 V was applied to the electrode. The performance of the electrode in PEC studies has been evaluated by measuring the absorbance of the 1.0 mL of the solution taken from the cell every 5 min at 480 nm for Orange G, at 525 nm for Rhodamine B and at 660 nm for Methylene Blue by using a UV-Vis spectrophotometer.

3. RESULTS AND DISCUSSION

In the context of the thesis, three different electrodes have been modified with WO_3 to study their catalytic effects towards several reactions. Glassy carbon electrode, pencil graphite electrode and titanium nanotube array have been used for this purpose. Each electrode and their optimization for analytical applications have been given in following subsections.

3.1 ORR Studies with WO_3 Modified Glassy Carbon Electrode

Initial studies were dedicated to developing WOx modified glassy carbon electrode (GCE) to investigate its electrocatalytic behavior against oxygen reduction. This electrode was chosen to compare the results with former studies carried out at GCEs. Besides, the GCE provides a flat surface for enzyme immobilization. After the characterization of the electrode surfaces which give the best signal formation, analytical application of the electrode was searched.

3.1.1. Cyclic Voltammetric Deposition Studies

Initial studies to deposit tungsten oxide onto the glassy carbon electrodes have been carried out in 0.5 M H_2SO_4 medium containing 0.08 M H_2O_2 and 0.15 M Na_2WO_4. The use of peroxide in deposition medium was chosen based on a chapter dealing with electrodeposition of tungsten oxide nanoparticles for sensing applications (Santos et al., 2015). Here, the reaction mechanism is given as

$$2WO_4^{2-} + 4\ H_2O_2 + 2\ H^+ \rightarrow W_2O_{11}^{2-} + 5\ H_2O \qquad \text{(Eq. 3.1)}$$

$$W_2O_{11}^{2-} + 2\ H^+ \rightarrow 2\ WO_3 + 2\ O_2 + H_2O \qquad \text{(Eq. 3.2)}$$

Figure 3.1A shows the cyclic voltammograms obtained by scanning the potential from 1.0 to -0.5 V at a rate of 50 mV s^{-1} for consecutive five cycles. Afterwards, a deep blue color was observed in this study following the deposition step and then, the color has turned to a pale grey color (**Figure 3.1B**).

This blue color was attributed to the bronze formation in peroxide medium. Therefore, the electrode was denoted as GCE/WO_x. Similarly, in a recent thesis study, it was pointed out that tungstate ions in peroxymolybdic tungstate solution are reduced in acidic media to W^{5+} or W^{6+} resulting in H_xWO_3 following injection of H^+ ions into the oxide matrix (Bajunaid, 2021).

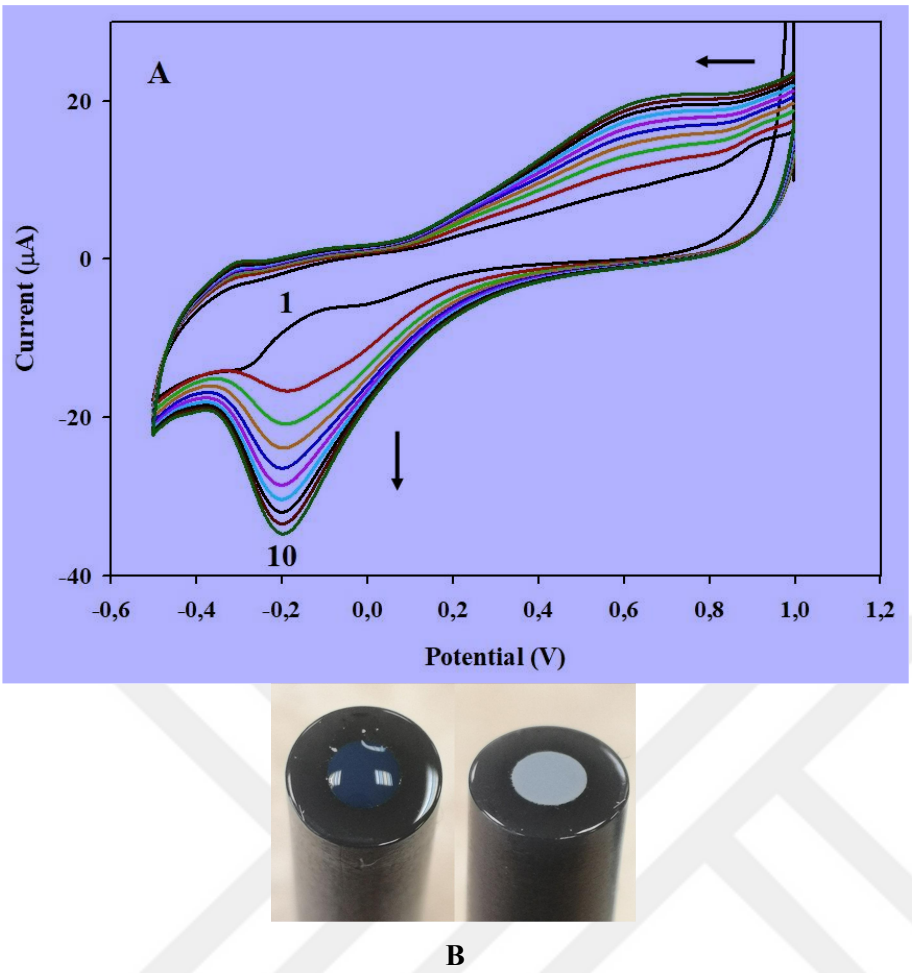

Figure 3.1 A) Cyclic voltammograms obtained for the cell containing 0.15 M Na_2WO_4 in 0.5 M H_2SO_4 containing 0.08 M H_2O_2 at a scan rate of 50 mV s^{-1}, **B)** The images of the electrodes.

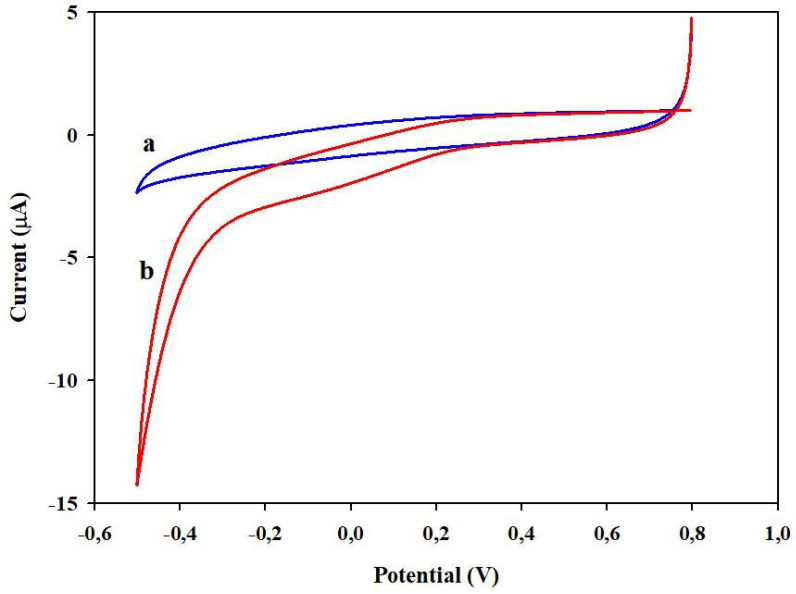

Figure 3.2 Cyclic voltammograms of GCE/WO_x in pH:5.0 BR Buffer a) purged with nitrogen gas and b) saturated with oxygen gas. Potential range: 0.8 – (-0.5) V Scan rate: 50 mVs^{-1}

Here, however, no significant result has been obtained with GCE/WO_x electrode for the ORR. The voltammograms recorded in pH:5.0 BR buffer saturated with oxygen by bubbling through the solution have displayed no significant peak formation (**Figure 3.2**). Background catalytic performance of each electrode was measured by purging nitrogen gas from the buffer solution.

Therefore, it was decided to decorate tungsten oxide film with platinum nanoparticles as is the case of previous studies (Çakar et al., 2013; Özdokur et al., 2019). Prior to the studies with metal-metal oxide composites, electro-deposition and electrocatalytic activity of the GCE modified with Pt nanoparticles (GCE/Pt NPs) was elucidated. In electrodeposition step, the GCE was immersed in 0.001 M Pt^{+2} ions in 0.01 M H_2SO_4 and the potential was cycled between 1.0- -0.5 at a rate of 50 mV s^{-1}. As shown in **Figure 3.3**, the GCE/Pt NPs has displayed a well-known hydrogen adsorption/desorption peak in the potential range of 0.2 – (-0.3) V and the formation and reduction of PtO_2, which were appeared around the same potential in agreement with a former study (Palanisamy et al., 2015).

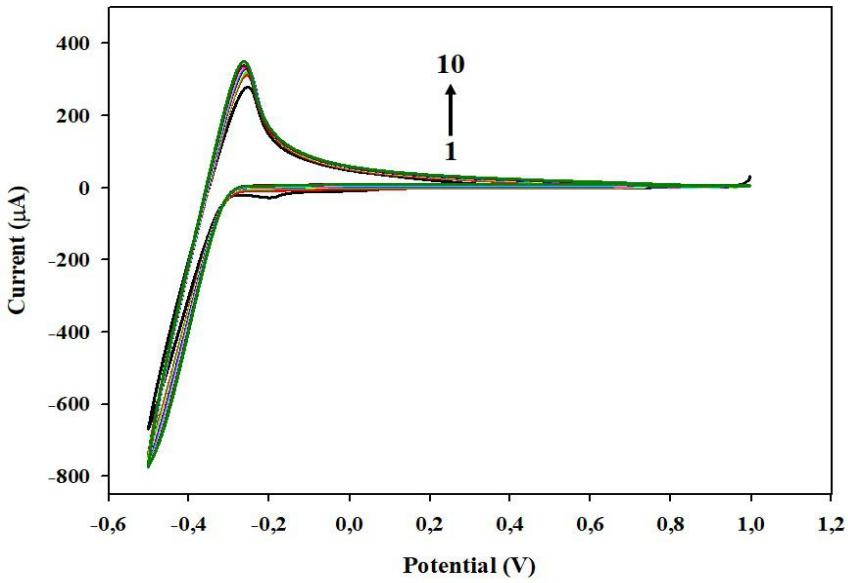

Figure 3.3 Consecutive cyclic voltammograms of GCE in 0.001 M Pt^{2+} ions in 0.01 M H_2SO_4 solution in the potential range of 1.0 – (-0.5) V with scan rate of 50 mVs^{-1}

Electrochemical behavior of the GCE/Pt NP electrode towards oxygen reduction in pH 5.0 BR buffer solution can be seen in **Figure 3.4**. As it is consistent with the voltammogram, no significant effect was observed with GCE/Pt NP electrode towards the ORR.

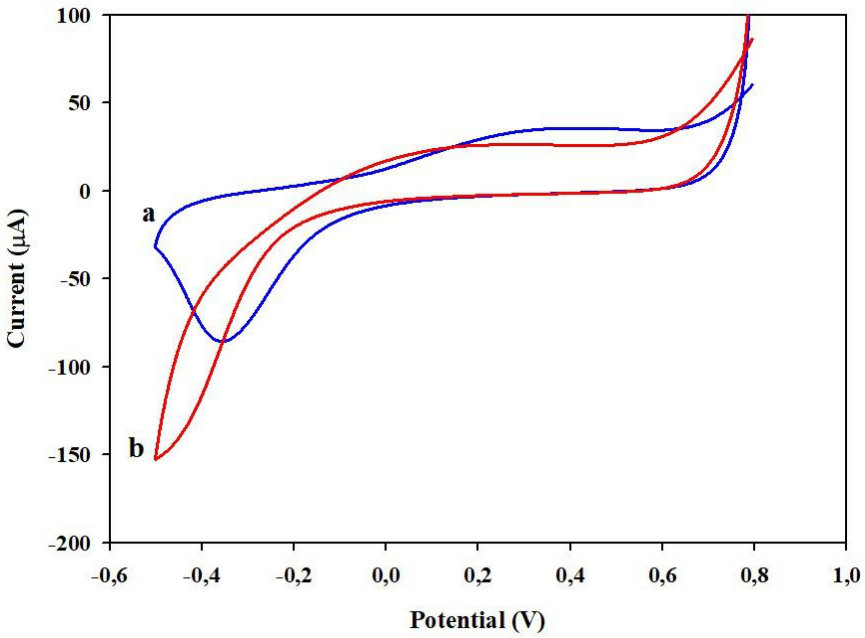

Figure 3.4. The catalytic response of GCE/Pt modified electrode in pH:5.0 BR Buffer a) purged with nitrogen gas and b) saturated with oxygen gas. Scan rate: 50 mVs^{-1}

Further studies were conducted to modify the GCE surfaces with WOx and Pt nanoparticles to reveal any synergetic effect. The role of deposition order of WO_x and Pt on the electrode performance was searched by applying both sequential and simultaneous deposition.

In the first step, the electrode prepared above (GCE/Pt NP) was further modified with WO_x by immersing the electrode into the solution containing 0.05 M WO_4^{2-} ions in 0.01 M H_2SO_4 solution and cycling the potential in the range of 1.0 – (-0.5) V with scan rate of 50 mVs^{-1}. The obtained electro-deposition voltammograms are given in **Figure 3.5**. The electrode was denoted as GCE/Pt NP/WO_x.

Voltammetric responses of as sequentially modified GCE to dissolved oxygen in pH 5.0 BR buffer were as given in **Figure 3.6**. As can be seen at the voltammogram, GCE/Pt/WO_x electrode has displayed a significant catalytic activity for oxygen reduction at 0.17 V with 45 µA current. This clearly indicates the synergetic effect of WO_x and Pt nanoparticles on the GCE surface.

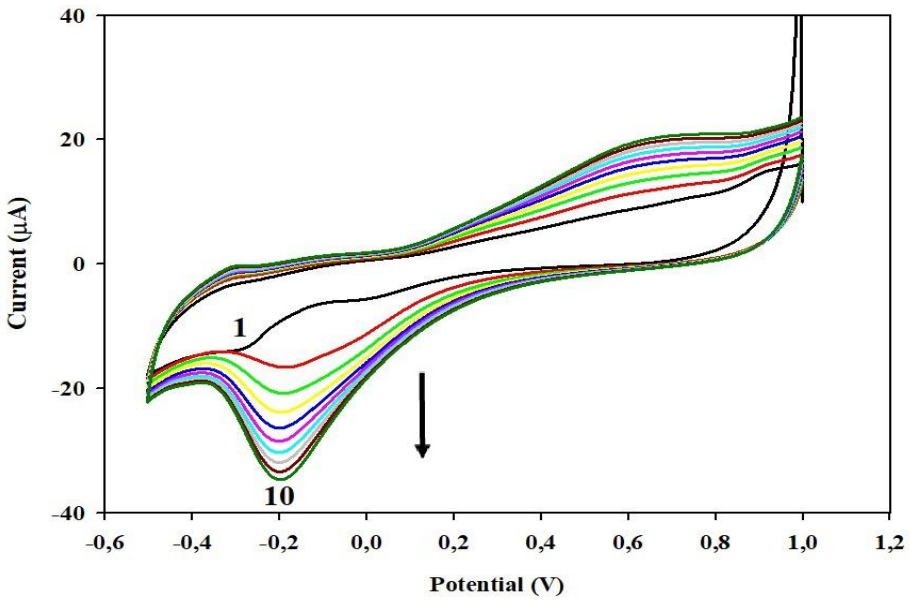

Figure 3.5 Cyclic voltammograms of GCE/Pt electrode in 0.05 M WO_4^{2-} in 10^{-2} M H_2SO_4

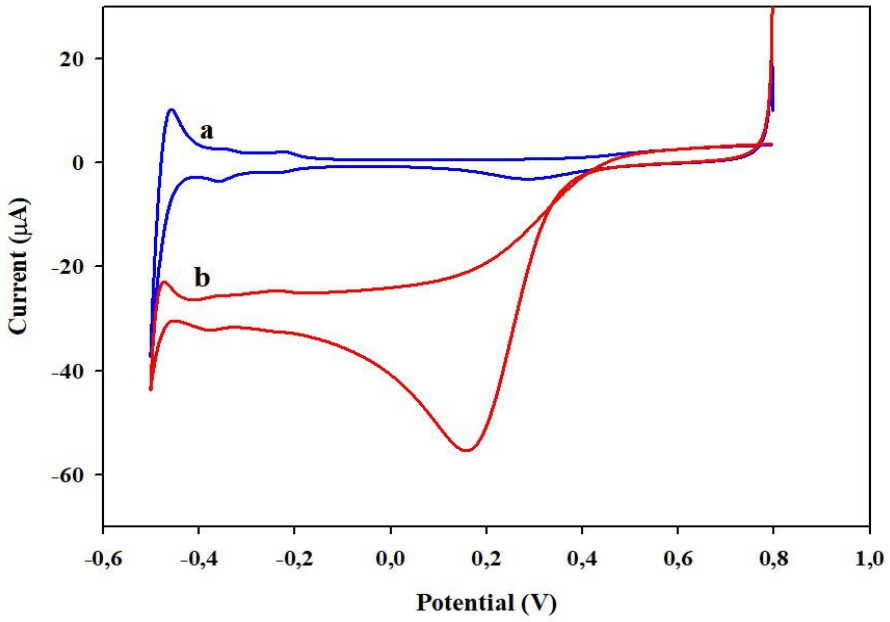

Figure 3.6. The catalytic response of GCE/Pt/WO_x electrode in pH:5.0 BR Buffer a) purged with nitrogen gas and b) saturated with oxygen gas. Scan rate: 50 mVs^{-1}

When we changed the order of deposition, the electrode obtained were denoted as GCE/WOx/Pt NP and its voltammetric response to the ORR in the same buffer solution was given in **Figure 3.7**.

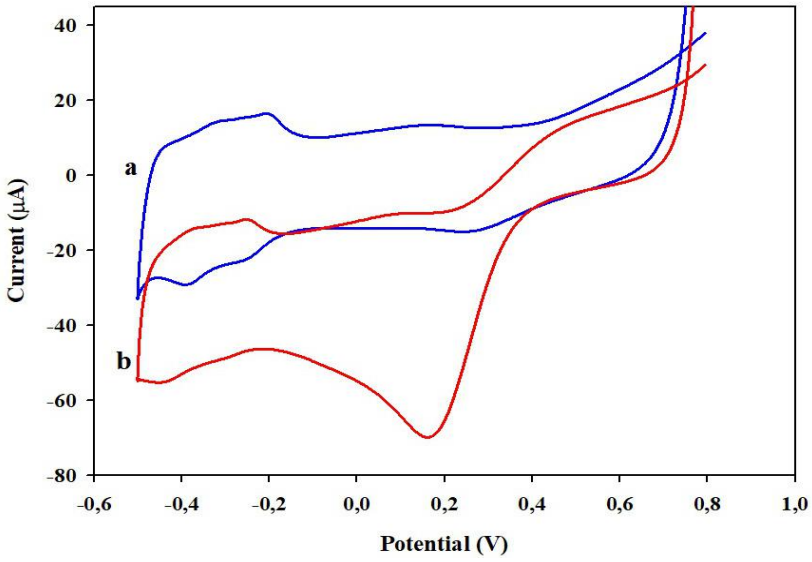

Figure 3.7 The catalytic response of GCE/WO_x/Pt modified electrode in pH:5.0 BR Buffer a) purged with nitrogen gas and b) saturated with oxygen gas. Scan rate: 50 mV s^{-1}

Another experiment was designed to see the effect of co-deposition of WO_x and Pt NPs on to the electrode surface towards the ORR. For this purpose, polished GCE was immersed in 0.01 M WO_4^{2-} ion solution in 0.01 M H_2SO_4 containing 0.001 M Pt^{+2} ions and cyclic voltammograms were recorded in the potential range of -0.5-1.0 V with scan rate of 50 mV s^{-1}. The electro-deposition voltammograms recorded for GCE/WO_x-Pt are given in **Figure 3.8.**

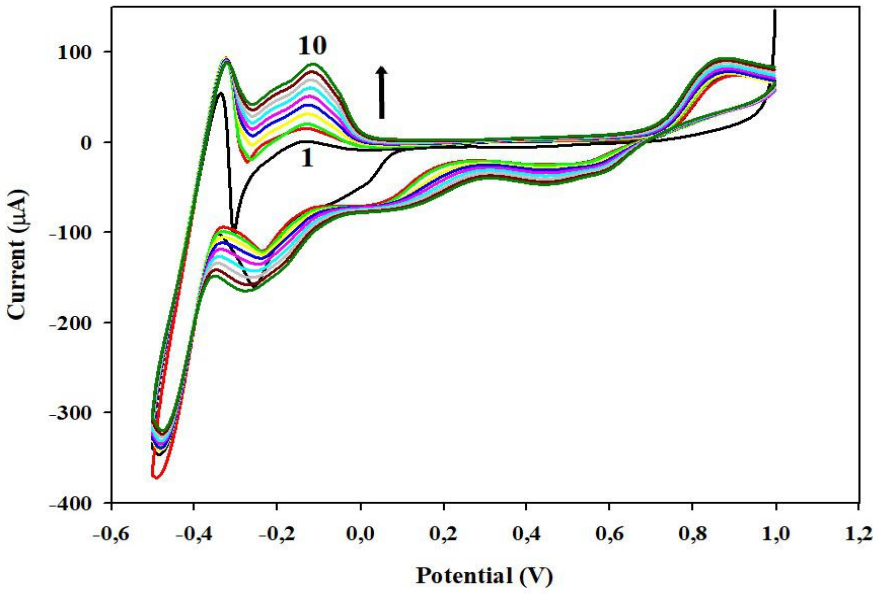

Figure 3.8 Cyclic voltammograms of co-deposition of WOx and Pt nanoparticles on the GCE in the potential range of 1.0 – (-0.5) V with scan rate of 50 mVs^{-1}

The peaks at most negative potentials correspond to the hydrogen adsorption/desorption peaks characteristic to platinum deposits. The main differences of the voltammograms from that of the GCE/Pt NP lie in the cathodic peak around -0.3 V building up with sequential scans and its wide anodic counterpart around -0.15 V.

Another difference in the electrochemical behavior of these two electrodes lies in their electrocatalytic activity towards the ORR. **Figure 3.9** shows the cyclic voltammograms recorded at the GCE/WOx, GCE/Pt, GCE/Pt/WOx and GCE/WOx-Pt electrodes in pH:5.0 BR buffer saturated with oxygen by bubbling through the solution.

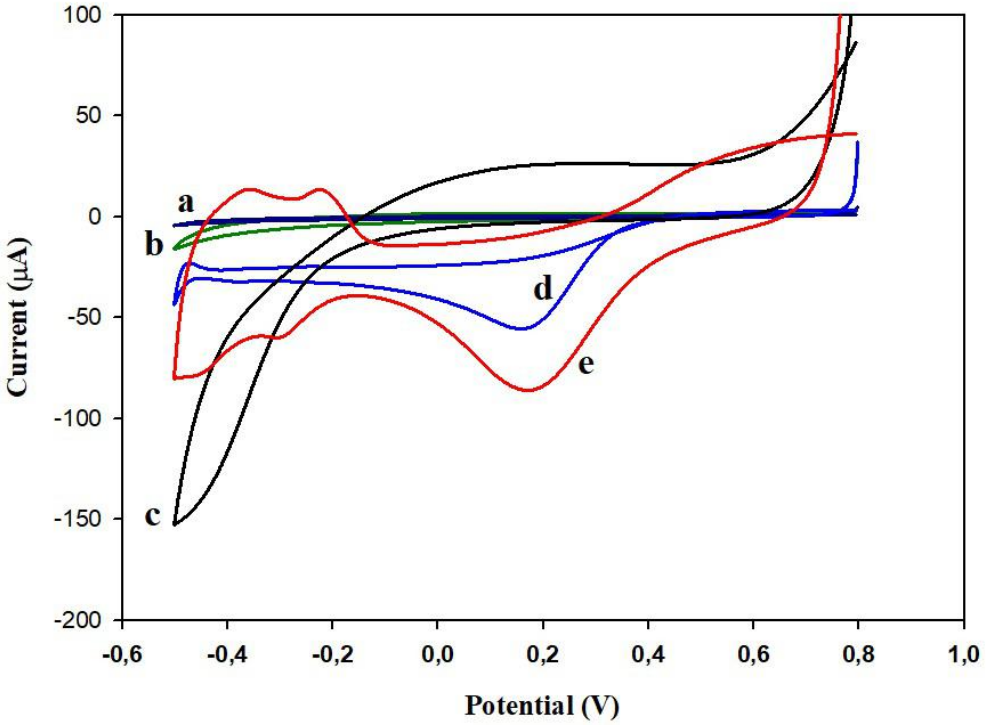

Figure 3.9 Cyclic voltammograms recorded for comparison of a) GCE/WOx, b) GCE/Pt, c) GCE/Pt/WOx and d) GCE/WOx-Pt electrode performances for the ORR in pH:5.0 BR Buffer.

As it is clear from the figure, co-deposited GC/WO_x-Pt electrode has displayed better catalytic activity than the GCE/Pt alone and even better response than the other two electrodes. A significant shift in the peak potential; was observed for the ORR as the peak can be seen at 0.18 V with 58 µA current. Therefore, further studies were carried out based on co-deposited metal/metal oxide film electrode.

The composition of the film might play a significant role on the catalytic activity and therefore, dependence of molar ratio between platinum to tungstate ions was investigated by employing GCEs modified with different molar ratios. For this purpose, Pt^{2+} concentration was kept constant as 0.001 M for each study and tungstate ion concentration was changed from 0.01 M to 0.1 M to maintain the molar ratio of 1:10, 1:25, 1:50, 1:75, 1:100, respectively.

The obtained electro-deposition voltammograms are given in **Figure 3.10**. It is obvious from the figure that as the molar ratio increased, the cyclic voltammogram has changed to that the peak at negative potentials become smaller and the reduction peak at -0.15 V grows larger indicating that WO_x dominates in the film.

Electrocatalytic responses of these electrodes towards dissolved oxygen have been recorded in pH 5.0 BR buffer and given in **Figure 3.11**. As the molar ratio has increased from 1:10 to 1:100, the peak around 0.2 V has increased first indicating the synergetic effect of the binary metals in the film, and then, has displayed a small decrease in height probably due to the lower distribution of platinum on the dominant WO_x film.

Table 3.1 summarizes the peak characteristics, and it was revealed that GC/WOx-Pt electrode prepared with 1:50 molar ratio has the best catalytic activity towards the ORR and this molar ratio was used in further studies.

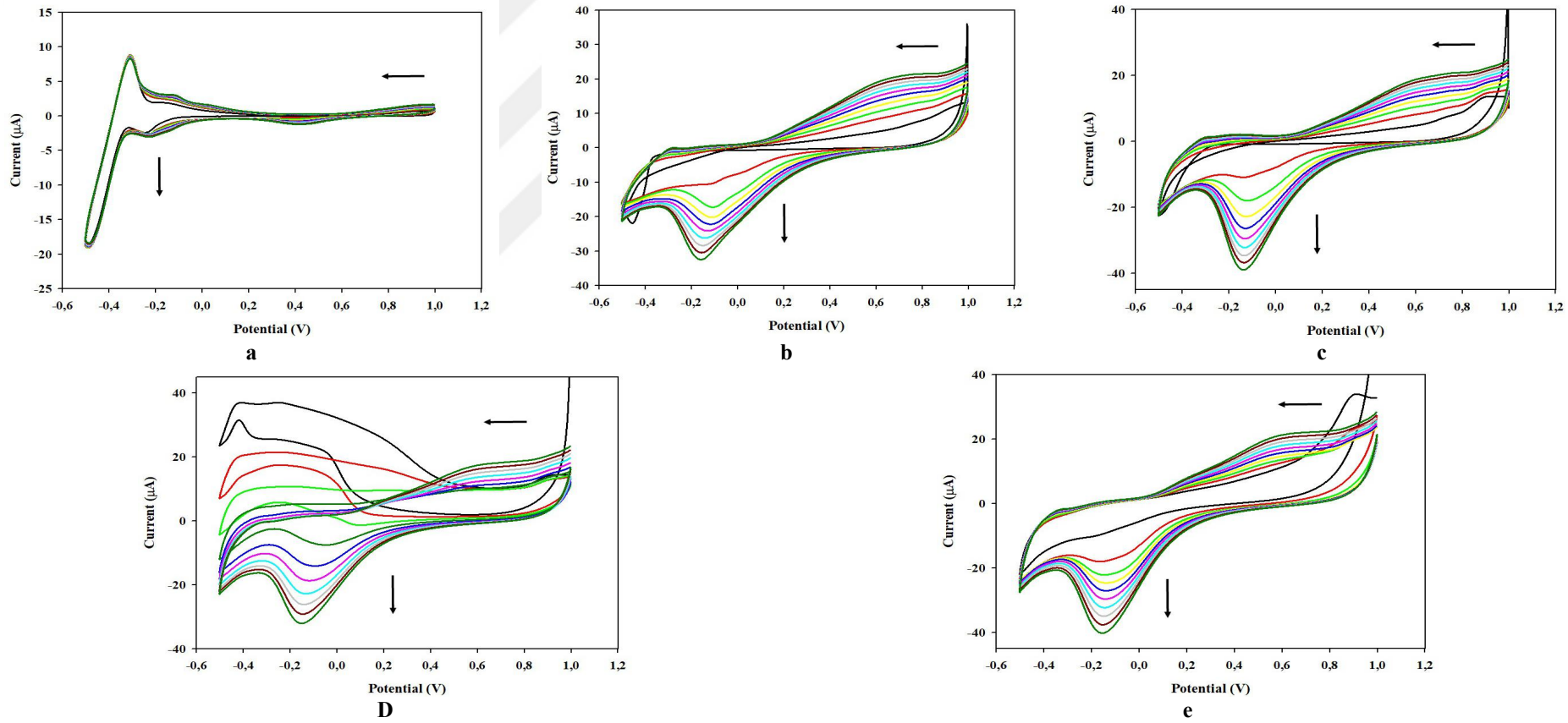

Figure 3.10 Consecutive cyclic voltammograms in deposition of GCE/WOx-Pt from the deposition solution containing 0.001 M Pt^{2+} ions in 0.01 M H_2SO_4 and tungstate ions to maintain the molar ratio of a) 1:10; b) 1:25; c) 1:50; d) 1:75 and e) 1:100 in the potential range of 1.0 – (-0.5) V with scan rate of 50 mVs^{-1}.

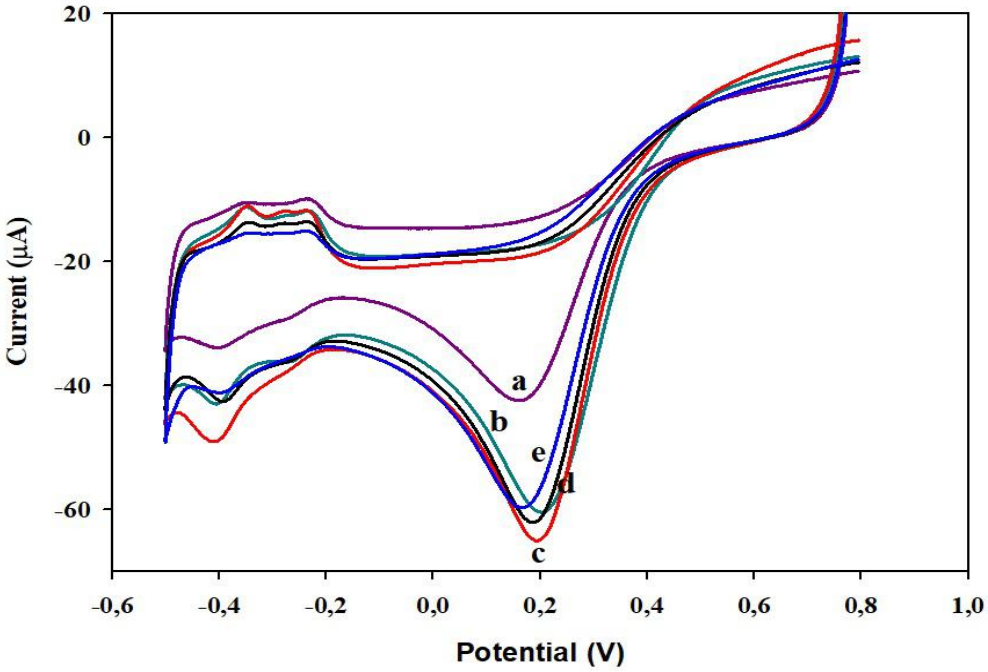

Figure 3.11 The catalytic responses of GCE/WOx-Pt prepared in different molar ratios towards the reduction of oxygen dissolved in pH:5.0 BR Buffer. a) 1:10 b) 1:25 c) 1:50 d) 1:75 e) 1:100 Potential range: 0.8 – (-0.5) V Scan rate: 50 mVs^{-1}.

Table 3.1. Peak characteristics of GCE/WOx-Pt towards the ORR

Pt: WO_4^{2-} Mole Ratio	**Peak Potential (V)**	**Peak Height (µA)**
1:10	0.16	41
1:25	0.21	46
1:50	**0.20**	**49**
1:75	0.19	47
1:100	0.17	44

Another parameter to be optimized is the scan rate since it determines the electrochemical behavior of species generated at the electrode probably due to the change in the diffusion layer thickness on the electrode surface.

Effect of scan rate ranging from 25 to 100 mV s^{-1} were studied for 1:50 mM (Pt: WO_4^{2-}) molar ratio and their responses to the ORR are given in **Figure 3.12.** The peak characteristics were summarized in **Table 3.2**.

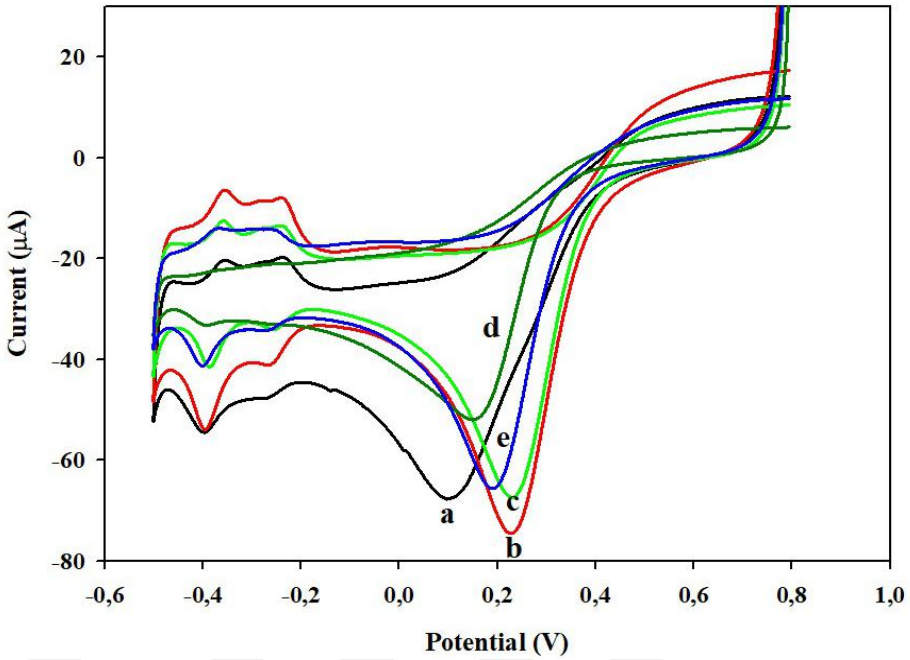

Figure 3.12 The catalytic responses of GC/WOx-Pt modified electrodes in pH:5.0 BR Buffer in the potential range of 0.8 – (-0.5) V at a scan rate of a) 10 b) 25 c) 50 d) 75 e) 100 mV s^{-1}

Table 3.2 Peak height and peak potentials of GCE/WO_x-Pt modified electrodes obtained by differentiating the deposition scan rate.

Scan Rate (mV s^{-1})	Peak Potential (V)	Peak Height (µA)
10	0.12	46
25	**0.23**	**61**
50	0.23	56
75	0.15	42
100	0.19	53

The medium pH on the ORR signal might have an effect the magnitude of the catalytic signal therefore, each GCE/WO_x-Pt electrode has been transferred to the BR buffer in a pH range of 2.0-11 deaerated with O_2 gas. Then, the performance of the electrode towards ORR was investigated. The obtained results are as given below in **Figure 3.13**. As can be followed from the voltammograms, pH of the buffer effects the peak potential for ORR responses of each WOx-Pt/GCE modified surfaces. The peak characteristics were listed in **Table 3.3**.

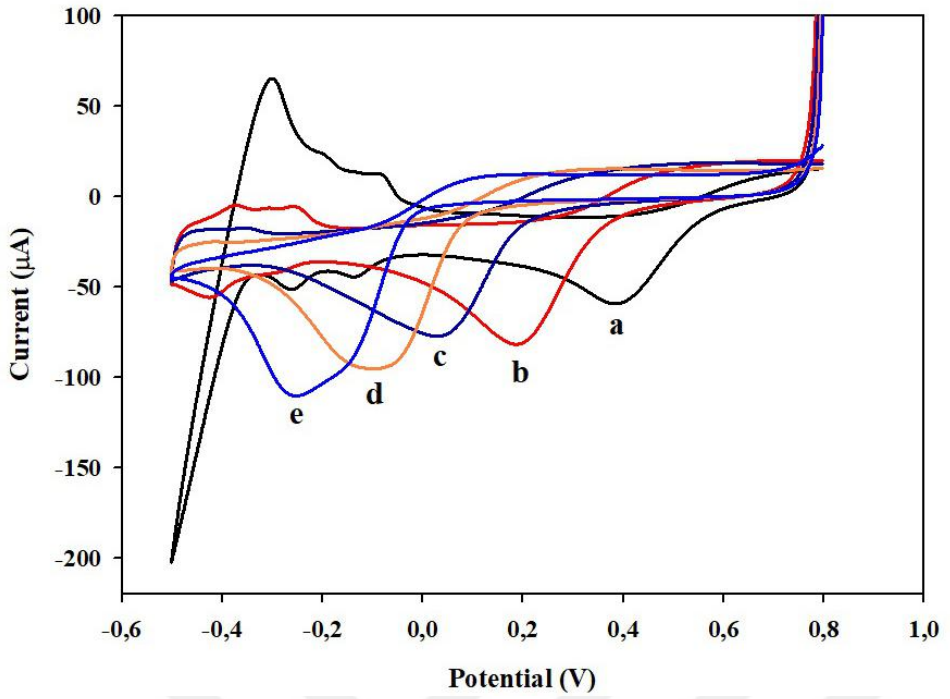

Figure 3.13 Comparison of ORR signals of GCE/WO_x-Pt modified surfaces obtained in BR buffer in a pH range of a) 2.0 b) 5.0 c) 7.0 d) 9.0 and e) 11.0. Scan rate: 50 mVs^{-1}.

Table 3.3 Peak characteristics of the ORR signal obtained at GCE/WO_x-Pt in different pH media

Medium pH	Peak Height (µA)	Peak Potential (V)
2.0	47.84	0.39
5.0	**66.71**	**0.19**
7.0	59.32	0.04
9.0	76.97	-0.08
11.0	84.26	-0.25

According to **Table 3.3** shows that highest peak current was obtained in pH 5.0 BR buffer but, the biggest shift in the peak potential was observed in pH 2.0 medium. So far, the optimal conditions were determined as the co-deposition of Pt and WO_3 from a deposition solution containing 1:50 mole ratio by scanning the potential between 0.8 – (-0.5) V at a rate of 50 mV s^{-1} and then, recording the ORR signal in pH 5.0 buffer system.

In the pursuit of a better electrocatalytic activity, the technique used in electro-deposition step can be changed to pulsed potential deposition technique which has proven better result formation in several cases (Özdokur et al., 2016a; Özdokur et al., 2016b; Akoğulları et al., 2020). Therefore, next experiments were designed to see any difference in electrocatalytic activity.

3.1.2. Pulsed Deposition Studies

The bare GC electrode was polished as described in Experimental Section and then, it was immersed into the 0.01 M H_2SO_4 solution containing 0.050 M WO_4^{2-} and 0.001 M Pt^{2+} ions.

Pulsed deposition procedure applied was given schematically in **Figure 3.14**. Here, the set potentials were chosen as 0.2 and -0.5 V to cover the region where catalytic activity occurs, and corresponding current-time profile can be seen in **Figure 3.15**.

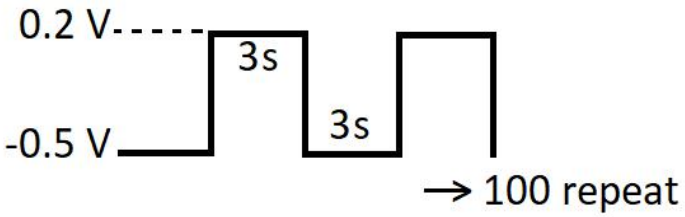

Figure 3.14 Schematic diagram of pulsed deposition parameters

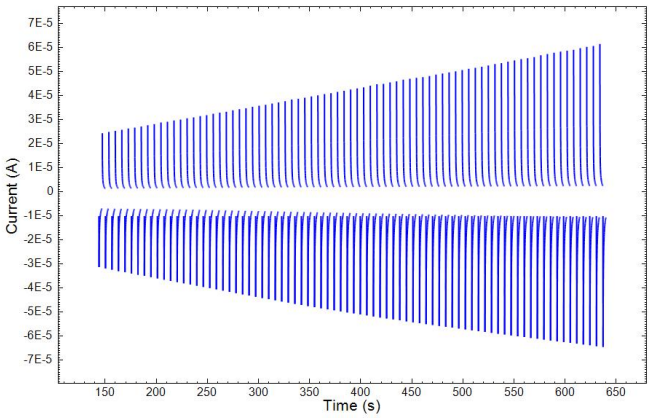

Figure 3.15 Pulsed potential deposition current response by time by changing the potential from 0.2 V to -0.5 V with 3 seconds of pulse duration for 100 times.

The current-time profile displays the current responses in 3 s duration times of the pulses which increases by time. The set potentials and the number of pulses during the deposition might also play a major role on the film thickness and composition. Therefore, several procedures have been tested to see the effect of these parameters on the electrocatalytic activity of GCE/WOx-Pt and GCE/Pt electrode as well. **Table 3.4** summarizes the details of these procedures applied.

Table 3.4 Procedures for preparing GCE/WO_x-Pt and GCE/Pt electrodes by PD technique.

	GCE/WO_x-Pt			
Procedure	**A**	**B**	**C**	**D**
Repeat n times	100	25	50	25
Set Potential-1	0.2	0.2	0.2	-0.8
Set Potential-2	-0.5	-0.2	-0.2	0.8
Duration	3 s	3 s	3 s	3 s
	GCE/WO_x-Pt			**GCE/Pt**
Procedure	**E**	**F**	**G**	**H**
Repeat n times	50	50	50	25
Set Potential-1	-0.6	-1.0	-1.0	1.0
Set Potential-2	0.6	0.0	0.8	-0.5
Duration	3 s	3 s	3 s	3 s

Individual catalytic response of pulsed deposited GCE/WOx-Pt electrodes in pH 5.0 BR buffer were given in **Figure 3.16**. The ORR peak characteristics were listed in **Table 3.5**.

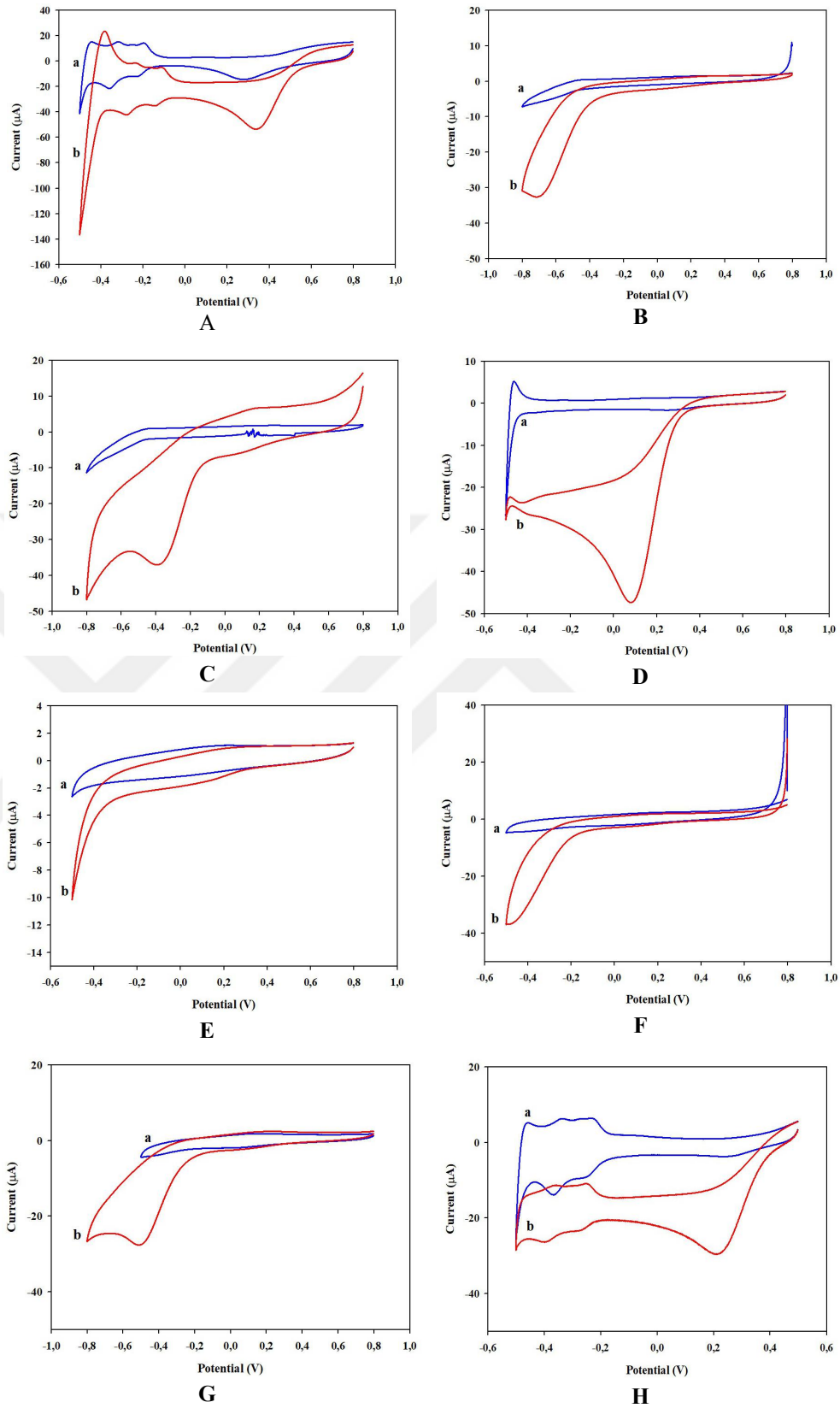

Figure 3.16 The ORR responses of the pulsed deposited GC/WOx-Pt electrodes and GCE/Pt electrode prepared by different procedures. Scan rate: 50 mVs^{-1}.

Table 3.5 The ORR peak characteristics of GCE/WO_x-Pt and GCE/Pt electrodes prepared via pulsed deposition technique.

Electrode	Procedure (Set pot. (V)/n)	Peak Potential (V)	Peak Height (µA)
Bare GCE	-	-0.72	14.24
(CV) GCE/WOx-Pt	**CV (0.8- -0.5/ 10)**	**0.19**	**66.71**
(PD) GCE/WO_x-Pt	**A (0.2- -0.5/ 100)**	**0.34**	**40.05**
	B (0.2- -0.2/ 25)	-0.67	8,0
	C (0.2- -0.2/ 50)	-0.35	15.41
	D (-0.8- 0.8/ 25)	0.09	38.30
	E (-0.6- 0.6/ 50)	-	-
	F (-1.0 – 0.0/ 50)	-0.5	-
	G (-1.0 - 0.8/ 50)	-0.49	12.32
(PD) GCE/Pt NP	**H (1.0 - -0.5/ 25)**	0.20	33.57

Overall results have shown that best results can be obtained with Procedure A where the set potentials were 0.2- -0.5 V and number of pulses were 100. However, CV has resulted better catalytic effect towards the ORR since the peak current is higher more than 50%.

Even though PD technique provides improved ORR signal, comparable results are obtained with cyclic voltammetric deposition and even better responses were obtained in a former study (Kuşcu et al., 2021). This can be explained in a way that mixed valent character of the WO_x, which is responsible for its catalytic activity, becomes more dominant in during potential cycles rather than applying pulse deposition.

The peak characteristics of the ORR obtained by using several transition metal oxides decorated with Pt nanoparticles or Au nanoparticles as another noble metal were collectively given in **Table 3.6**. For elucidating the performances of the electrodes, two parameters are important: the peak potential and the effective surface area. The latter parameter can be determined by several ways; however, the peak current can also give an idea about the electrocatalytic activity of the electrode.

Table 3.6 The ORR peak characteristics of the GCEs modified with transition metal oxides

Electrode Mole ratio (Pt:MeOx)	Deposition Procedure	Peak Pot. (V)	Peak Height (µA)	Reference
Bare GCE	-	-0.72	14.24	This work
GCE/MoOx-Pt (1:90)	**CV** (1.05 - −0.25 V 20 mV s^{-1}, 5 cycles)	0.26	69.19	Çakar et al., 2013
GCE/MnOx-Pt (1:100)	**CV** (-0.25 - 1.05 V 20 mV s^{-1}, 5 cycles)	0.22	29.4	Özdokur et al., 2014
GCE/Pt **GCE/MoOx/Pt**	**CV** (0 - -1.0 V, 50 mV s^{-1}, 20 cycles)	0.011 0.020	50.9 78.1	Yavuz et al., 2015
GCE/MoOx/Pt (2:5)	**PD** (-1.0 - 0 V, 5 s, 20 pulses, sequentially)	0.21	**103.5**	Yavuz et al., 2015
GCE/MnOx-MoOx/Pt (1 (Pt):20 (Mn):2(Mo))	**PD** (0.25- -1.05 V, 5 s, 20 pulses, sequentially)	0.1	80	Özdokur et al., 2016b
GCE/CoOx/Pt (1:100)	**CV** (1.0 – −1.2 V 50 mV s^{-1}, 40 cycles)	0.24	88.2	Kuşçu et al., 2021
GCE/CNT/MnOx-VOx/Au (1(Au): 2 (Mn): 20 (V))	**Mn-V: PD** (0.25 -1.05 V, 5 s, 100 pulses) **Au: CV** (1.0–1.5 V, 15 cycles)	-0.22	51.1	Akoğulları et al., 2020
GCE/WOx-Pt (1:50)	**CV** (0.8- -0.5 V 50 mV s^{-1}, 10)	0.19	**66.71**	This work
GCE/WO_x-Pt (1:50)	**PD** (0.2- -0.5 V, 3s, 100 pulses)	**0.34**	40.05	This work
GCE/Pt NP (1 mM)	**PD** (1.0 - -0.5 V, 3s, 25 pulses)	0.20	33.57	This work

Regarding the peak current, the best results were obtained with pulsed deposited GCE/MoOx/Pt with a 103.5 mA for the ORR (Yavuz et al., 2015). If we compare the peak potentials, the largest shift in potential was obtained with the pulsed-deposited GCE/WOx-Pt electrode developed in this thesis. Considering the -0.72 V obtained for the bare GCE, the peak observed at 0.34 V clearly demonstrated the electrocatalytic activity achieved by this electrode giving more than 1 V of shift in positive direction.

SEM images of the CV and PD deposited electrodes at 2.500 magnifications are given in **Figure 3.17**. Homogenous deposition was observed for PD technique. It can be noticed from Figure 3.17A, bright dots of Pt nanoparticles homogeneously distributed over branched pattern of WOx film can be noticed for CV deposited GCE/WO_x-Pt electrode surfaces. On the other hand, rather spherical deposits were obtained for pulsed deposited GCE/WO_x-Pt electrode surface.

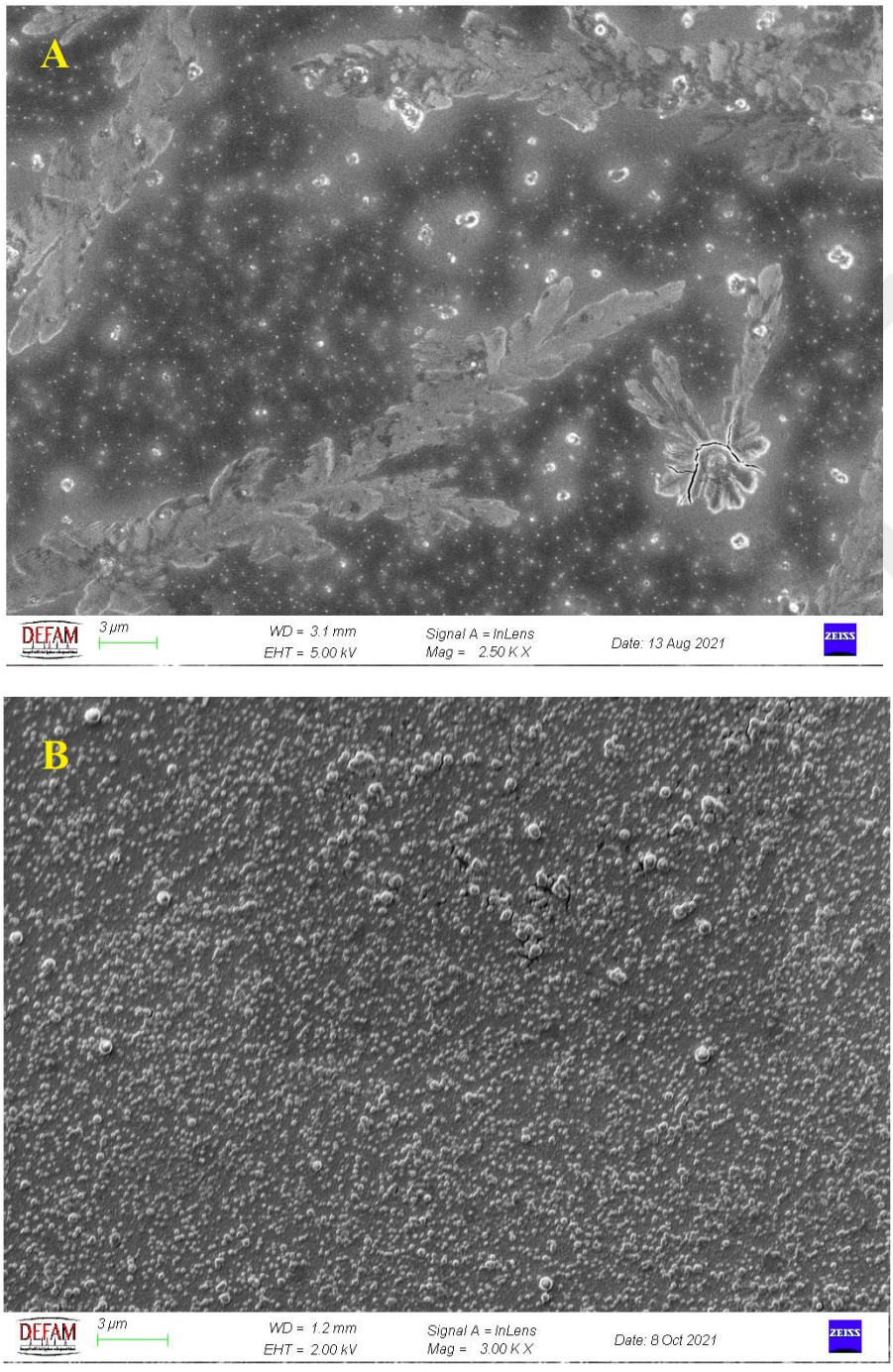

Figure 3.17 The 2.500 times magnified SEM images of A) CV and B) Pulsed deposited GC/WO_x-Pt electrodes

Closer inspection of the surface has revealed the morphological differences in these electrodes prepared by CV and PD techniques (**Figure 3.18**).

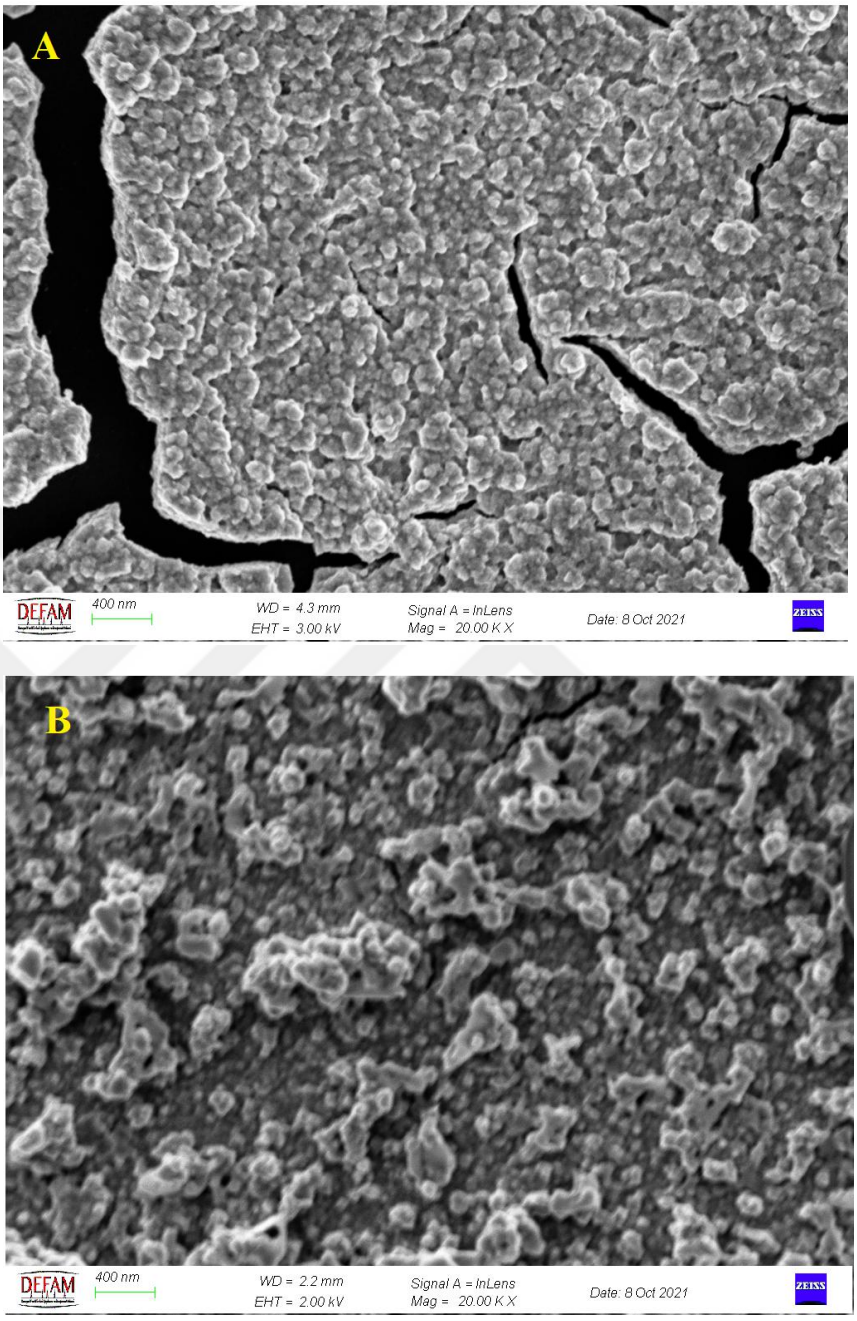

Figure 3.18 The 20.000 times magnified SEM images of A) Cyclic deposited and B) Pulsed deposited GC/WO_x-Pt electrodes

According to the SEM images, it can be elucidated that CV deposition has resulted a layered structure while in PD technique, metal oxide nanoparticles were on the surface. EDX spectra of the electrodes given in **Figure 3.19** has revealed that the surface was partly covered by the metal oxide and carbon contents were higher in PD technique than the CV counterpart.

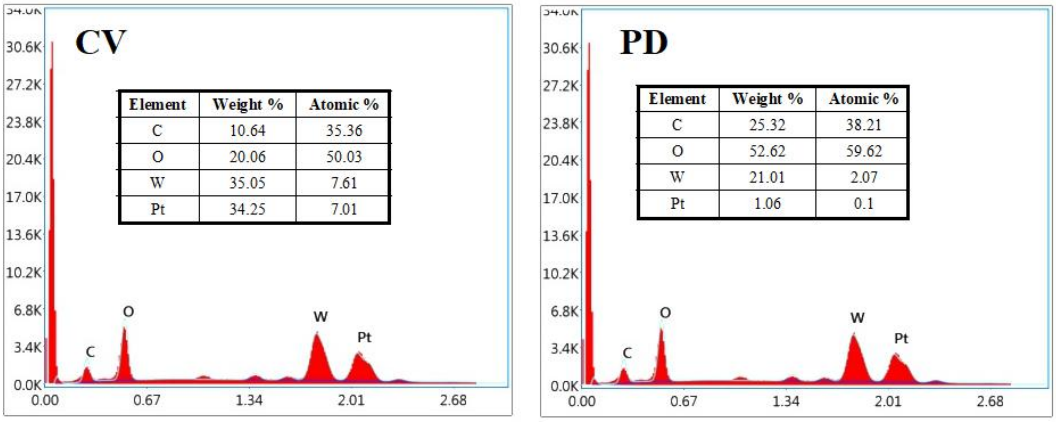

Figure 3.19 The EDX results of the cyclic and pulsed deposited GC/WO_x-Pt electrodes

This result was also consistent with the fact that atomic abundances of W and Pt contents were 7.61% and 7.01% respectively for the CV deposition while the ratios are much lower for pulsed deposition being 2.07% and 0.1%, respectively. These findings may also explain the differences in the performances of the electrodes. Even though much higher current signal was obtained with CV deposited GCE/WOx-Pt electrode, pulsed deposited electrode has displayed better electrocatalytic performance, resulting a shift in peak potential to 0.34 V.

X-ray photoelectron spectroscopy (XPS) was used to obtain information about the surface composition and chemical state of the electrochemical modified electrodes. **Figure 3.20a** shows XPS survey spectrum of GCE/WOx-Pt with the existence of C1s, O1s, W4f, and Pt4f elements.

As shown in **Figure 3.20b**, the XPS spectra of C 1s could be deconvoluted into three peaks: C sp^2 (C=C) at 287.18 eV, C sp^3 (C–C and C-H) at 285.25 eV, and (O-C=O) at 289.18 eV (Pang et al., 2019; Çiftyürek et al., 2019). The π-π* satellite consists of interband transitions in sp^2-hybridized structures and is typical for carbon materials.

As shown in **Figure 3.20c,** the O 1s spectrum of GCE/WOx-Pt can be fitted divided into three peaks: 530.48 eV for lattice oxygen combined with W^{6+}, 532.08 eV for the OH^- which was absorbed on the catalyst surface and 533.98 eV for the H_2O which was absorbed on the GCE/WOx-Pt surface (Xie et al., 2012).

The W 4f XPS spectra of GCE/WOx-Pt showed two main peaks which were attributed to the W $4f_{5/2}$ (38.18 eV) and W $4f_{7/2}$ (35.98 eV) of W^{6+}(WO_3) (Lee et al., 2020; Mukherjee et al., 2020).

Figure 3.20d shows that XPS spectra of W4f core level were fitted into peak doublets with parameters of spin–orbit separation ΔE_P (4f5/2–4f7/2) = 2.2 eV (Xie et al., 2012). A weak peak at 31.08 eV is associated with metallic W. Binding energies of ca. 35.08 and 37.18 eV would be expected for the W^{5+} oxidation state.

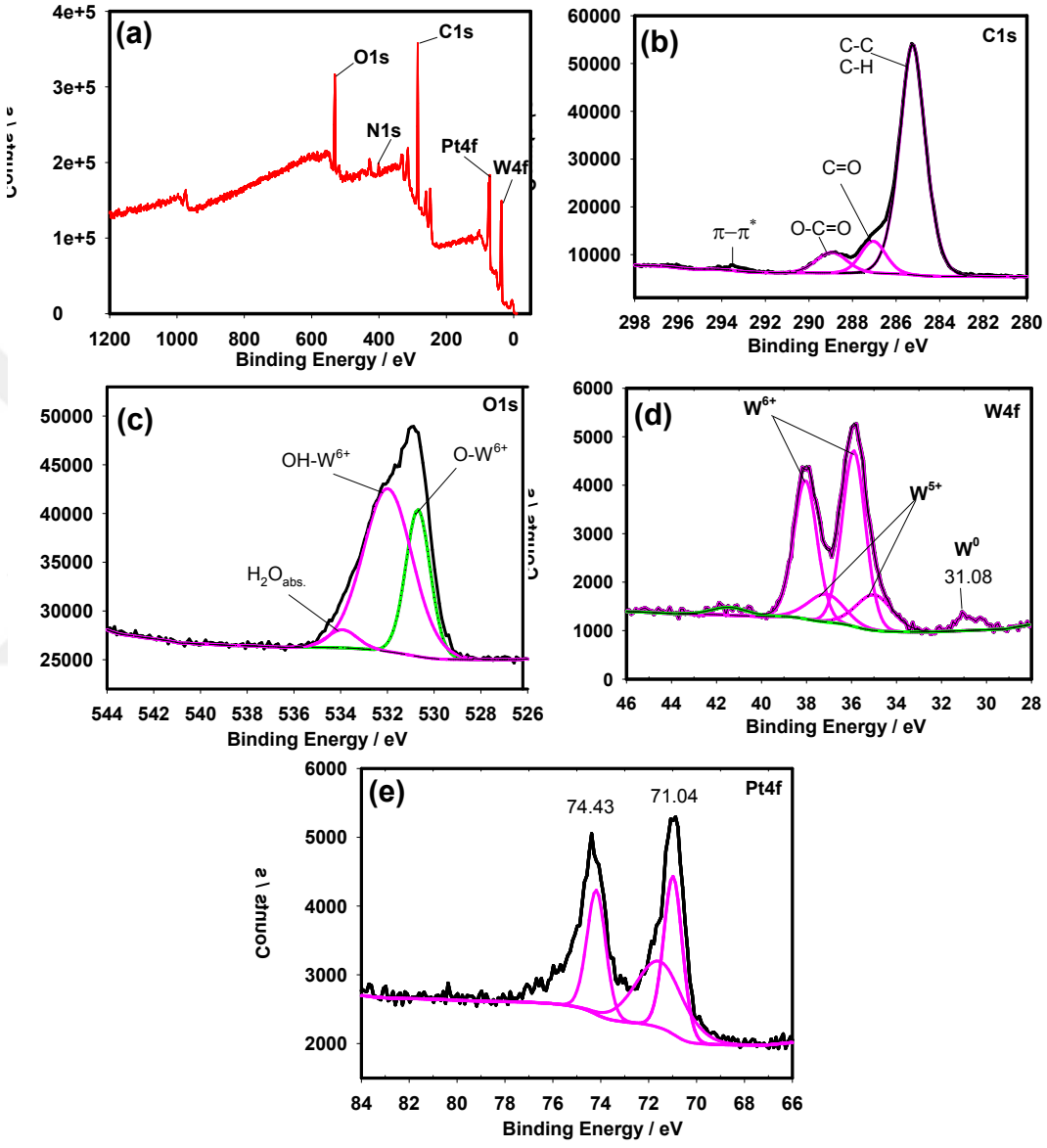

Figure 3.20 XPS spectra for CV deposited GCE/WOx-Pt, (a) survey spectrum (b-f) fitted high-resolution spectra of b) C1s, c) O1s, d) W4f and e) Pt4f.

It is worth mentioning that the bronze nature of electrochemically modified GCE/WOx-Pt composite can be easily characterized by utilizing the binding energies in agreement with a former study (Bajunaid, 2021).

The Pt 4f cores (4 $f_{5/2}$ and 4 $f_{7/2}$) were observed at binding energies of 71.04 and 74.43 eV, respectively (**Figure 3.20e**). Pt 4f region has well-separated spin-orbit components (ΔBE=3.39 eV). Therefore, GCE/WOx-Pt structure was consistent with formation of metallic Pt^0. The positions of the peaks for platinum were consistent with those reported in studies in the literature (Zhao et al., 2021).

3.1.3 Analytical Applications of GCE/WOx-Pt Electrodes

Considering the high electrocatalytic activity of the electrode developed for the ORR, the electrode was utilized in enzymatic and non-enzymatic determination methods for oxygen species in several reactions.

3.1.3.1 Enzymatic Applications of GCE/WOx-Pt Electrode

Catalase enzyme reacts with hydrogen peroxide to give water and oxygen according to the reaction given below. Therefore, a biosensor based on this enzyme constitute an ideal system to test the performance of the electrode developed.

$$2\ H_2O_2 \rightarrow 2\ H_2O + O_2 \qquad \text{(Eq. 3.3)}$$

For this purpose, catalase the biosensor was developed as described in Experimental Section. First of all, GCE/WOx electrode was used as a platform for biosensing studies. **Figure 3.21** shows the chronoamperograms recorded at 0.2 V for addition of 20 µL stock solution of H_2O_2 to be 1 mM in the cell. The peaks indicates the injection points of peroxide solution into the cell and the peak currents in nA levels have been obtained.

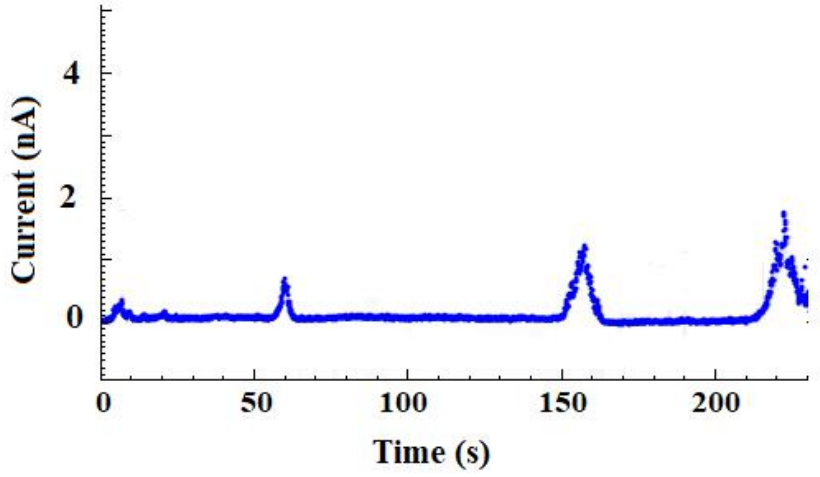

Figure 3.21 Chronoamperograms recorded for the catalase biosensor based on GCE/WOx after the addition of 1 mM H_20_2 to the cell

In the next step, the GCE/WO_x-Pt electrode was utilized as a platform for biosensor and as shown in **Figure 3.22**, very noisy signal has been recorded.

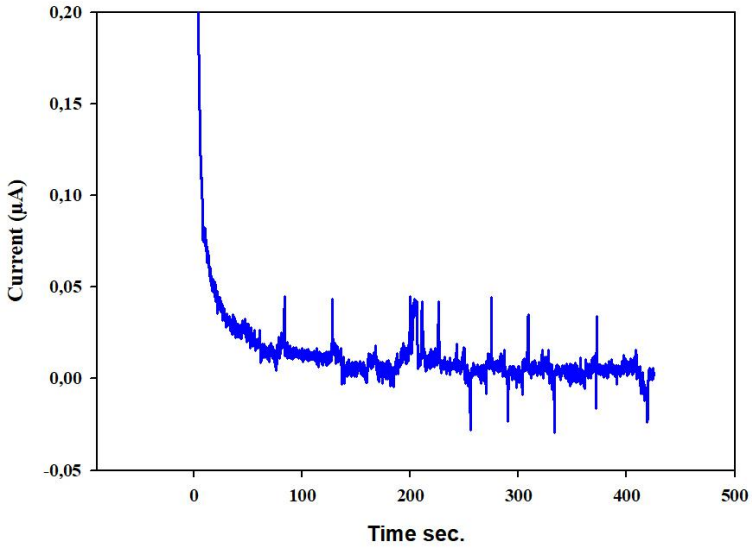

Figure 3.22 Chronoamperograms recorded for the catalase biosensor based on GCE/WO_x-Pt after the addition of 1 mM H_20_2 to the cell

As shown in the figure, very noisy signal formation was observed for the GCE/WO_x-Pt electrode and further studies were conducted to see the electrode response in non-enzymatic peroxide determination.

3.1.3.2 Non-Enzymatic Applications of GCE/WOx-Pt Electrode

Initial studies cover the optimization of the parameters regarding the peroxide peak formation at the WO_x-Pt modified GCE in the presence of hydrogen peroxide. The GCE surface was modified with WO_x and Pt nanoparticles under optimized conditions, and the electrode was immersed in 0.05 M H_20_2 solution. Potential of the electrode was scanned from 1.5 V to -1.5 V for 3 consecutive cycle to specify the reduction potential of hydrogen peroxide.

As shown in **Figure 3.23**, the peak was observed around 0.04 V. To reveal the optimum potential for chronoamperometric measurements, an experiment was designed. The modified electrode was immersed into the 20 mL of pH 7.0 PBS solution in the cell and the potential applied to the working electrode was changed between 0.1 - -0.3 V. Here, the signal might be resulted from the oxygen formed during disproportionation reaction of hydrogen peroxide added into the cell.

As shown in **Figure 3.24**, the current signal was recorded after spiking 100 µL of 1.0 M stock solution of H_2O_2 every 50 s to be 5 mM in the cell. The current

change was more obvious for 0 V and further studies were conducted at this potential.

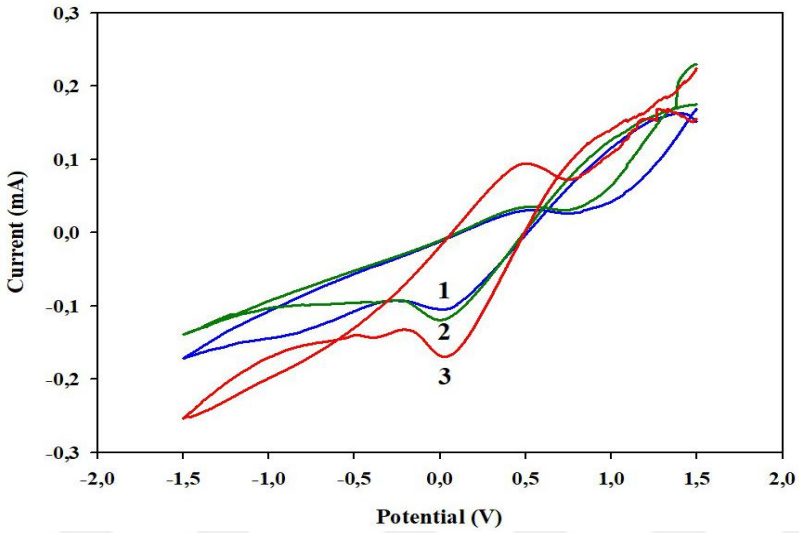

Figure 3.23 Cyclic voltammograms recorded at GCE/WO_x-Pt in 0.05 M H_20_2 solution. Cycle number was indicated on the voltammograms.

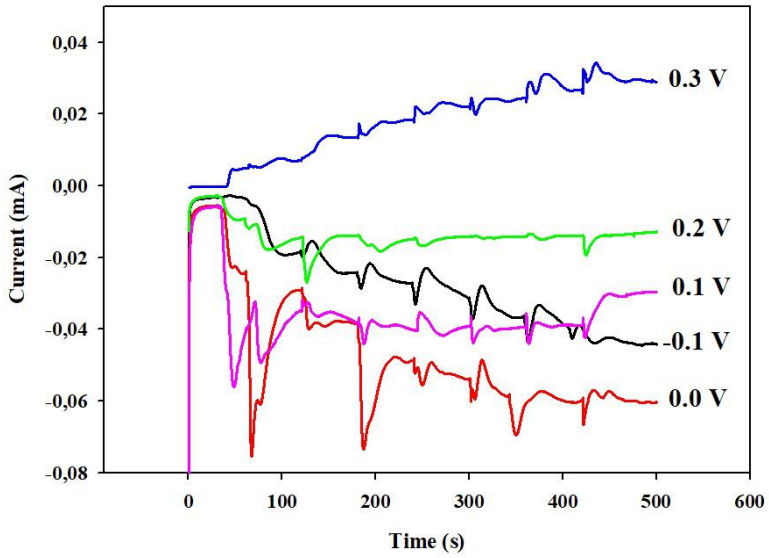

Figure 3.24 Chronoamperograms recorded at GCE/WO_x-Pt at various potentials after injection of 5 mM H_2O_2 at every 60 second.

Another parameter to be optimized is the solution pH. Since transitional metal oxide films are not stable in acidic media, two basic solutions were compared to see any differences in the electrode performances.

Figure 3.25 shows the chronoamperograms recorded at pH 7.0 BR and pH 9.0 boric acid buffer solutions. It was deduced from the figure; the medium pH has a slight effect on the signal formation and further studies were conducted in pH 7.0 BR buffer solutions.

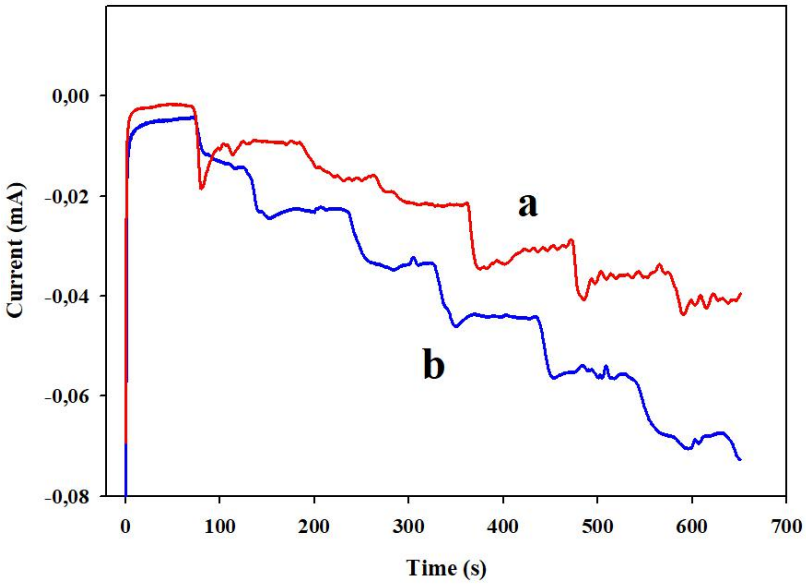

Figure 3.25 Performances of GCE/WO_x-Pt electrode in a) pH 7.0 PBS and b) pH 9.0 Boric acid buffer solutions containing 0.5 mM H_2O_2 in the cell.

Then, quantification studies were conducted and as shown in **Figure 3.26** the chronoamperograms have displayed a continuous decrease in current upon the injection of H_2O_2 solutions for 0.1- 1.0 mM concentration range.

The calibration curve for H_2O_2 was linear in a concentration range.0.2- 1.0 mM with a correlation coefficient of 0.9578. However, as shown in **Figure 3.27** the curve can be divided into two linear segments with different slopes one between 0.2-0.6 mM with a slope of 0.13 µA M^{-1} and the other is in 0.6-1.0 mM with a slope of 0.24 µA M^{-1}. Two segmented calibration curves can be encountered in the literature for voltammetric studies (Benvidi et al., 2015). Here, the slope of the first segment has nearly doubled indicating a kinetic limitation at lower concentrations. This increase can be attributed to the increased activity of the surface in the presence of hydrogen peroxide over a certain concentration. The limit of detection of the method was calculated 0.037 mM by taking the blank signal into account. Reproducibility was calculated for the low, medium, and high concentration levels of the calibration graph. The RSD values were calculated as 4.73%, 2.89% and 3.03% for 0.5, 1.0 and 1.5 mM H_2O_2 concentrations.

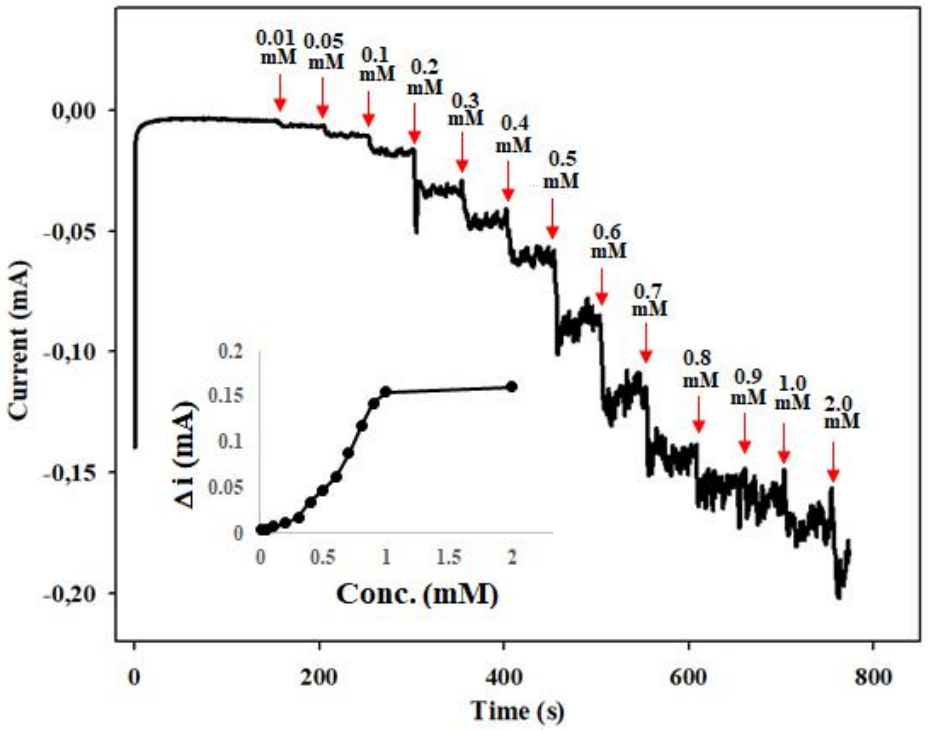

Figure 3.26 Chronoamperograms recorded at 0V by injecting standard solutions of H_2O_2 in a concentration range of 0.1- 2.0 mM under stirring every 60 s.

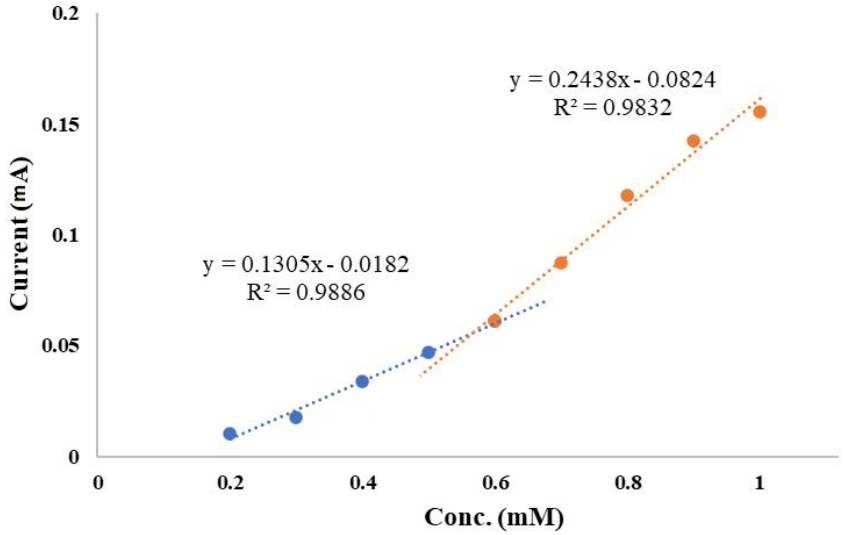

Figure 3.27 Calibration curves for H_2O_2 in a concentration range of 0.1- 1.0 mM.

Overall studies have revealed that the GCE/WO_3-Pt electrode can be a good candidate for the ORR monitoring and its application in peroxide determination in mM regions. Sample analysis with GCE/WOx-Pt electrode was accomplished by using a commercial disinfectant sample obtained from DEFAM known to be including hydrogen peroxide.

The sample was analyzed with the developed non-enzymatic peroxide sensor. Five aliquots of the sample were added hydrogen peroxide to be in the concentration range of 0.5 – 1.5 M was prepared, and the volume was made 10 mL by adding appropriate amount of deionized water as shown in **Figure 3.28**. Standard additions with a volume of 100 µL was spiked into the measurement cell containing 20 mL of PBS pH 7.0 every 50 second and change in current after each addition has been recorded. **Figure 3.29** shows the calibration graph obtained by plotting the measured current data against the concentration.

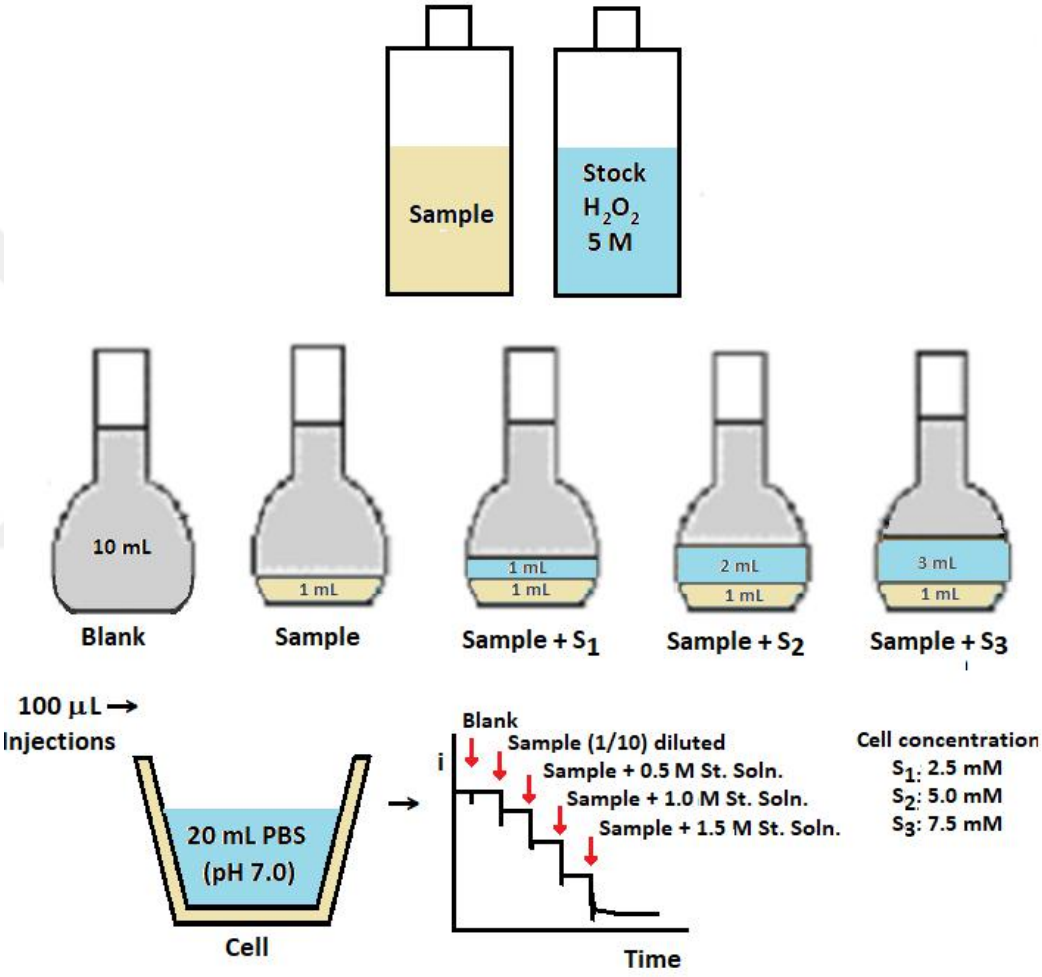

Figure 3.28 Details of standard addition technique used in sample analysis

Commercial disinfectant sample used for sample analysis contains 4.16 mL in liter hydroxide solution (30.0%, suitable for microbiology, d: 1.1 g/mL). Calculated hydrogen peroxide concentration of given amount is equal to 0.04 M. Calibration curve was constructed by adding the background signal to the data series for allowing to calculate the real sample concentration by extrapolation.

The calibration curve for standard addition of disinfectant sample was found linear with a satisfactory correlation coefficient (R^2 = 0.9997). By extrapolating the curve, peroxide content of the sample was calculated as 0.036 M which is very close to the real sample concentration.

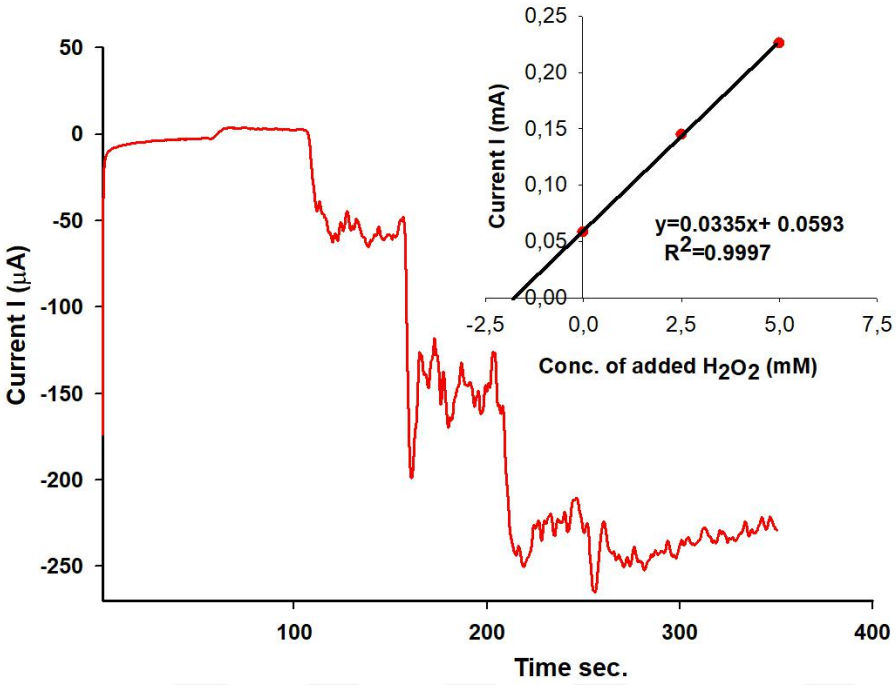

Figure 3.29 Chronoamperograms and standard addition graph for the sample analysis.

Here, the concentration range of standard addition curve might seem wider than the actual calibration curve indicating that subsequent injections may alter the electrode surfaces which is reflected in the current response.

Since ORR is a basic reaction in life processes such as biological interactions and energy converting systems, electrocatalytic performance of the electrodes modified with tungsten oxide towards the ORR was evaluated. To conclude the studies so far, electrochemical synthesis of WO_x on a GCE further decorated with Pt nanoparticles has been elucidated and the synergic effect was attributed to the hyper d- hypo-d interaction of the composite. Multivalent character of the tungsten species in the composite has also contributed to the significant catalytic activity. However, noisy background disabled the enzymatic biosensor studies but, non-enzymatic sensor development has been achieved for hydrogen peroxide determination. The non-enzymatic sensor developed in here presented an alternative way for daily used disinfectant analysis widely used due to Covid 19.

3.2. EIS Studies with Pencil Graphite Electrodes

Another application of the tungsten oxide as a modifier was electrochemical preparation of WO_x species on the disposable pencil graphite electrodes (PGE) in pursue of any catalytic activity in aptasensor studies. PGE/WOx surfaces have served as a platform for an aptamer immobilization specific to Ochratoxin A (OTA). Quantitation was made by Electrochemical impedance spectroscopy (EIS) measurements and after optimization studies, analytical aspects of the method have been searched.

Initially, the PGEs were modified with WO_x by either CV or PD electrodeposition techniques as described in Experimental Section and the obtained electrodes were denoted as PGE/WOx (CV) and PGE/WOx (PD), respectively. Then, the aptamers were immobilized onto the electrode surface following the procedures given in **Figure 2.4** and **Fig. 2.5**. Next heading describes the studies carried out with individual aptasensors.

3.2.1. Studies with 5'-Amino Aptamer

Immobilization of 5'-amino aptamer (5'-Amino-C6-GAT CGG GTG TGG GTG GCG TAA AGG GAG CAT CGG ACA-3') onto the PGE modified with WO_x film was accomplished by treating the electrodes with EDC/NHS solutions as illustrated in **Figure 2.4**. After blocking the residual active sites at the electrode surface with 1% BSA, the performance of the aptasensor for specific and sensory determination of OTA was tested as described **Figure 3.30**.

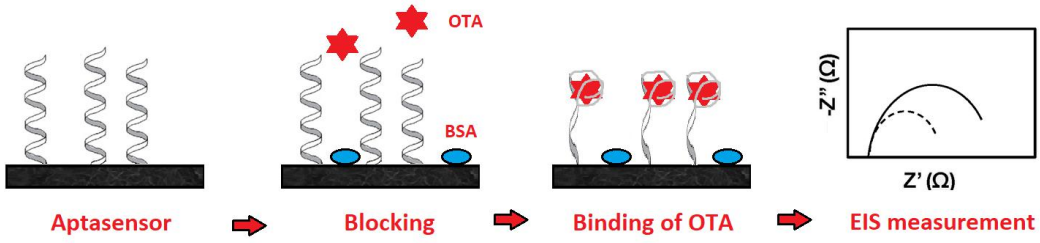

Figure 3.30 Schematic representation of signal formation in Amino-Aptasensor

OTA detections were performed via EIS technique for subsequent 3 measurements. In this technique, the applied potential was chosen on the basis of cyclic voltammograms for each electrode recorded between 0.8- -0.5V. **Figure 3.31** shows the cyclic voltammograms recorded in a cell containing 5 mM $Fe(CN)_6^{3-/4-}$ in pH 7.4 PBS at a scan rate of 50 mV s^{-1}.

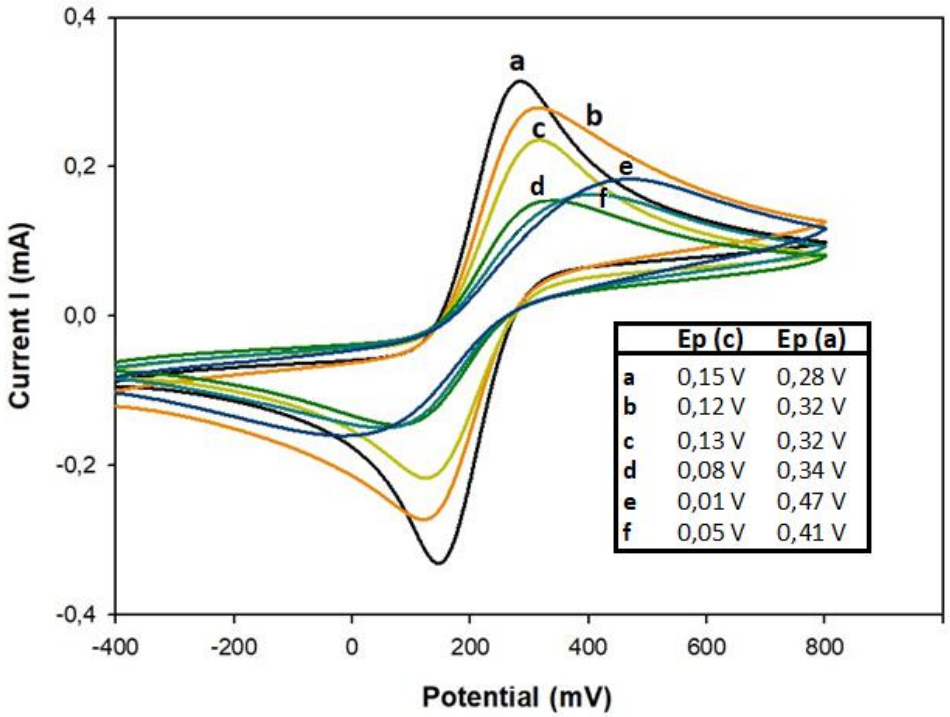

Figure 3.31 Cyclic voltammograms recorded in pH 7.4 BR buffer solution containing 5 mM $Fe(CN)_6]^{3-/4-}$ at a a) bare PGE, b) PGE/WO_x (CV), c) NH_2-Apt-PGE/WO_x, d) After blocking with 1% BSA, and after interaction with e) OTA and f) VEGf .

According to the voltammograms, the anodic peak around 0.28 and its counterpart at 0.15 V has decreased upon deposition of WO_x on the base PGE and shifted in more positive potentials indicating the change in the surface morphology. This decrease has continued further modification with aptamer as expected. Further studies were conducted at 0.24 V and the frequency range was 10.000- 0.05 Hz with an amplitude of 0.01V.

Figure 3.32 shows the Nyquist plots obtained for the electrodes prepared in each step by using both CV and PD deposition techniques from the solutions containing 0.005 M Na_2WO_4 in 0.5 M H_2SO_4 and 0.08 M H_2O_2.

Triplicate measurements were made, and the error bars were included in the graphics. In the next step, the amino aptamer (NH_2-Apt) concentrations were kept constant as 0.2 µM and then, the residual active surfaces were blocked by using 1% BSA. The Nyquist plots were drawn for the electrodes after incubating in 1 nM OTA solution as the target analyte, and in 1 nM ZEA, another mycotoxin, to reveal the effect of non-specific interaction. Larger semicircles have indicated the increased resistances of the electrode surface to the charge transfer due to the surface blockage.

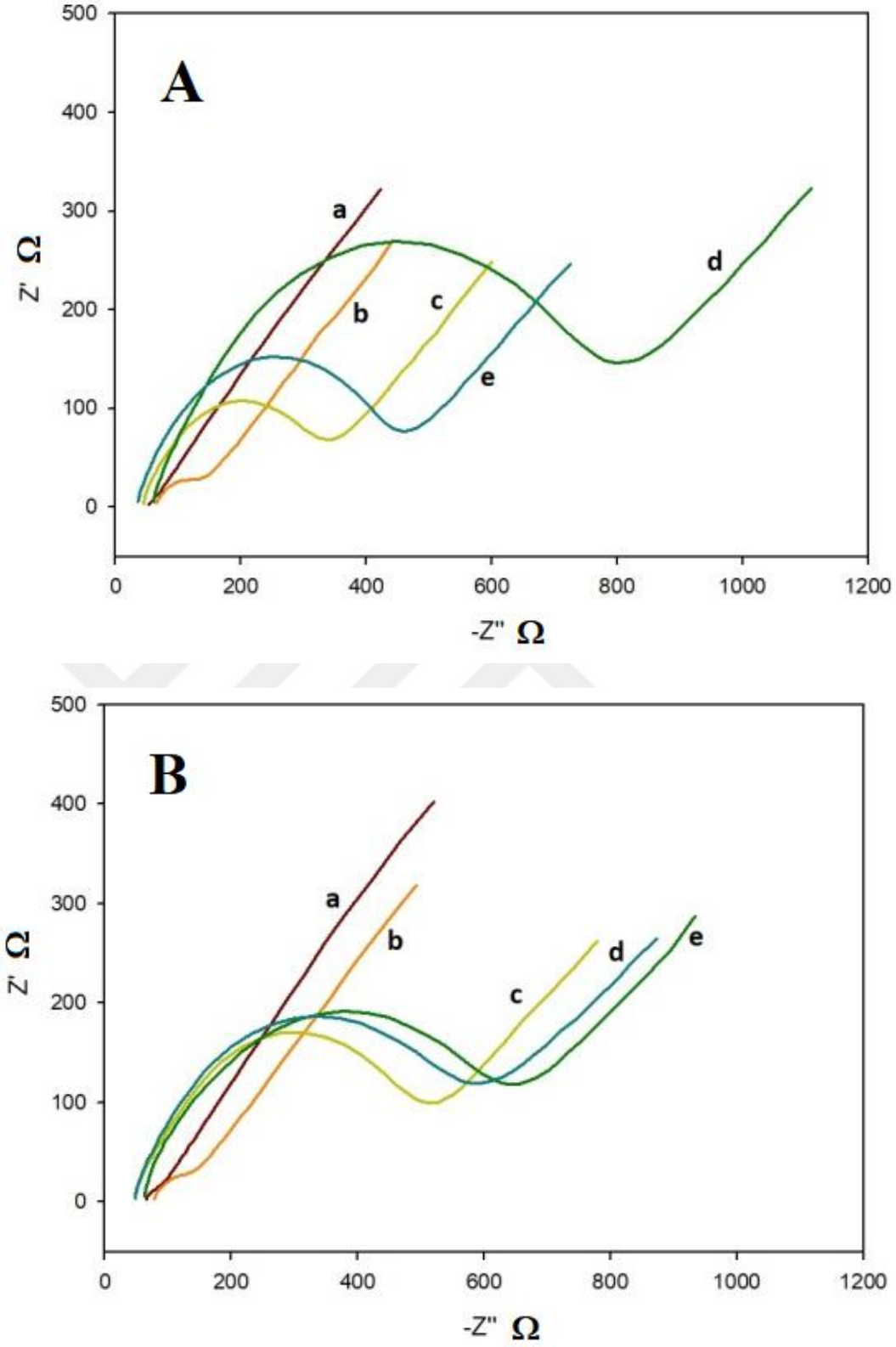

Figure 3.32 The Nyquist graphs of amino-aptasensor based on modification from 0.005 M Na_2WO_4 by using A) CV and B) PD techniques; where a) PGE/WO_x b) NH_2-Apt-PGE/WO_x, c) after blocking with BSA, and after interaction with d) 1 mM OTA and e) 1 mM ZEA.

The charge transfer resistance (R_{ct}) values in ohm for each electrode are determined by the size of the semicircle by fitting the Nyquist plots to a conventional Randles equivalent circuit as described in **Figure 1.8.** The R_{ct} values were determined and plotted for each electrode type in **Figure 3.33**.

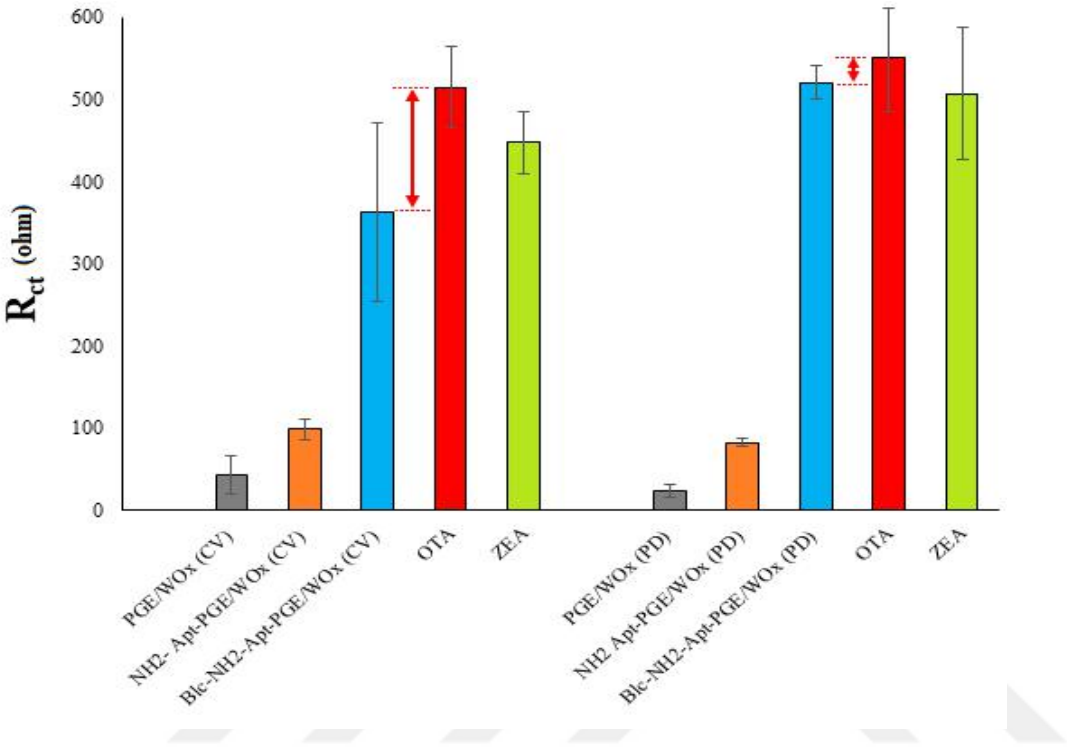

Figure 3.33 The R_{ct} values measured for the amino-aptasensor prepared by depositing from solutions containing 0.005 M WO_4^{2-} ion and applying CV or PD techniques

The observed increase in R_{ct} value after the attachment of the amino aptamer and subsequently with the BSA demonstrates the ability of the aptamer to block the electrochemistry occurring at the underlying graphite electrode. After incubation with the target molecule, OTA, the R_{ct} has increased considerably for the electrode prepared by CV technique. However, after the attachment of the aptasensor to ZEA, the R_{ct} value has decreased indicating weaker interactions.

Here, the actual signal is the difference (ΔR_{ct}) between the R_{ct} value of interaction with the target molecule (red bar) and after the blocking the residual active sites by BSA (blue bar) as pointed out on the figure (Eq. 3.4).

$$\Delta R_{ct} = R_{ct}\,(OTA) - R_{ct}\,(Blocking) \qquad \text{(Eq. 3.4)}$$

Usually, the values of ΔR_{ct} were used to fit a linear curve. Prior to the calibration, optimization studies have been carried out. Main parameters those affect the EIS signal are the tungstate concentration in deposition solution, the technique used in deposition step (CV or PD) and aptamer concentration used in modification step. The procedure was performed for a set of 3 different PGE/WO_x in 3 different tungstate concentrations.

Graphical data obtained from EIS measurements for 0.005, 0.03 and 0.075 M Na_2WO_4 for CV an PD were examined and obtained R_{ct} values were plotted for each step. Charge transfer resistances of the bare PGE were also included for comparison. **Figure 3.34** shows the results obtained for all the electrodes prepared by either CV or PD as described earlier.

As can be seen from the figure, highest signal formation was observed for the electrodes prepared from 0.030 M Na_2WO_4 solution for both CV and PD techniques. Interestingly, very high R_{ct} values were obtained for the aptasensor based on bare electrode. However, from the ΔR_{ct} values given as a bar graph in **Figure 3.35,** modification of the PGEs with WOx has provided a significant increase in the signal and deposition technique also determines the surface characteristics which reflects in the signal size.

For CV deposition, the signal has given a maximum at 0.003 M tungstate concentration and then, decreased for higher concentrations probably due to the excess coverage of the surface. However, progressive increase has been observed for PD technique by increasing the tungstate concentration. It was concluded that the aptasensor prepared by PD technique from a solution containing 0.075 M WO_4^{2-} ion has given the best results. Further studies have been conducted by using this electrode.

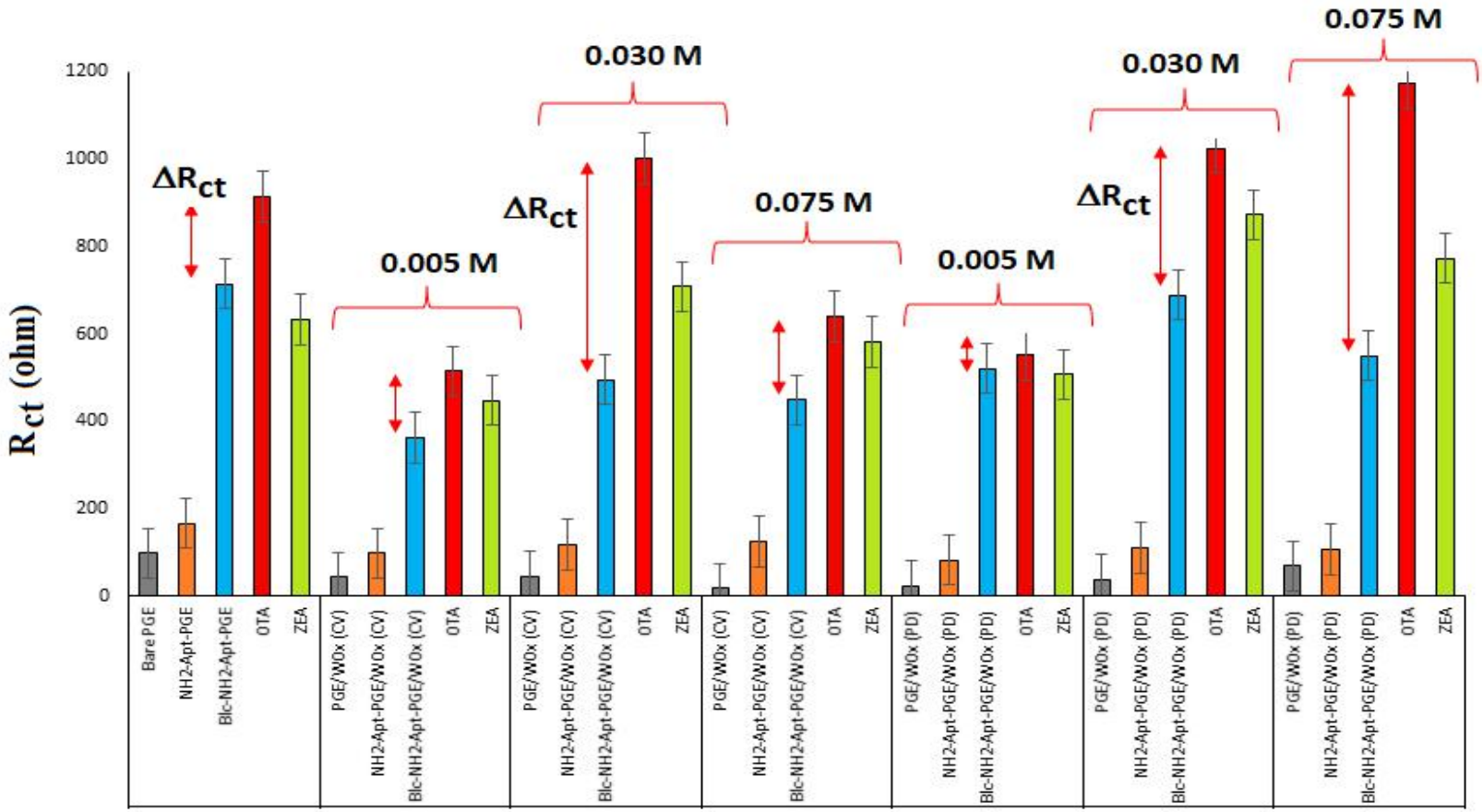

Figure 3.34 The R_{ct} values measured for the amino-aptasensor prepared by depositing from solutions containing 0.005, 0.030 and 0.075 M WO_4^{2-} ion and applying CV or PD techniques.

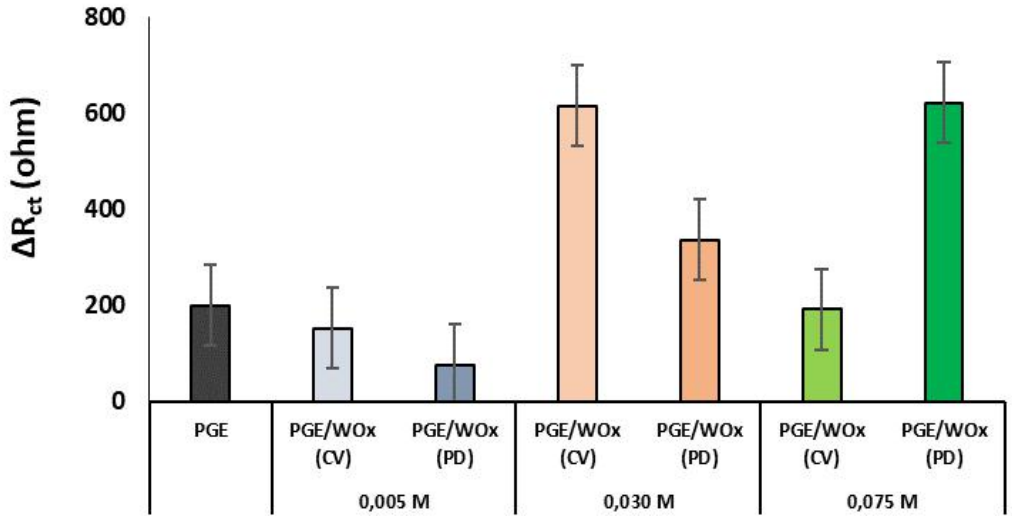

Figure 3.35 The effect of Na_2WO_4 concentrations on the difference in charge transfer resistances of the aptasensors prepared on bare and WOx deposited electrodes by either CV or PD technique.

The binding efficiency of EDC/NHS mechanism in aptamer immobilization stage was tested. As given in **Figure 2.4**, carbon electrodes possess carboxy and hydroxy groups on their surfaces responsible for the interaction with the EDC molecule and covalent attachment of the amino bearing aptamer afterwards. In our cases, since the surface is covered with tungsten oxide film, this interaction might be cumbersome, and the binding might occur due to adsorption.

Therefore, two sets of experiments were performed in the absence of EDC/NHS to observe whether aptamers bind to the modified surface via covalent attachment or via adsorption. **Figure 3.36** shows the R_{ct} values obtained for both sets of electrodes. The differences in R_{ct} levels clearly indicates the efficiency of the EDC/NHS mechanism probably via -OH groups on the metal oxide film.

Another important parameter is the aptamer concentration, and it was optimized by designing a series of experiments by using the aptasensor prepared by PD technique from a solution containing 0.075 M Na_2WO_4 and changing the aptamer concentration in a range of 0.1– 2.0 µM concentrations. Equal concentrations (1 nM) of OTA and ZEA have been used and the R_{ct} values obtained in each step were given in **Figure 3.37** for all the concentration levels. The electrode responses to OTA and ZEA alone were redrawn and given in **Figure 3.38** for clarity.

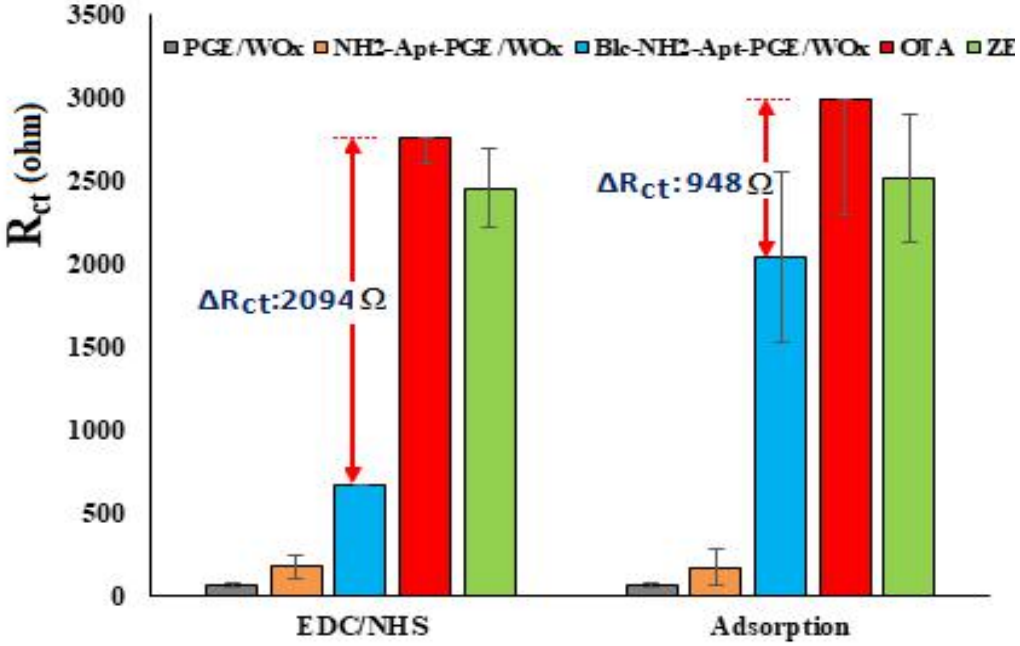

Figure 3.36 The performances of the aptasensors prepared in the absence and presence of EDC/NHS mechanism

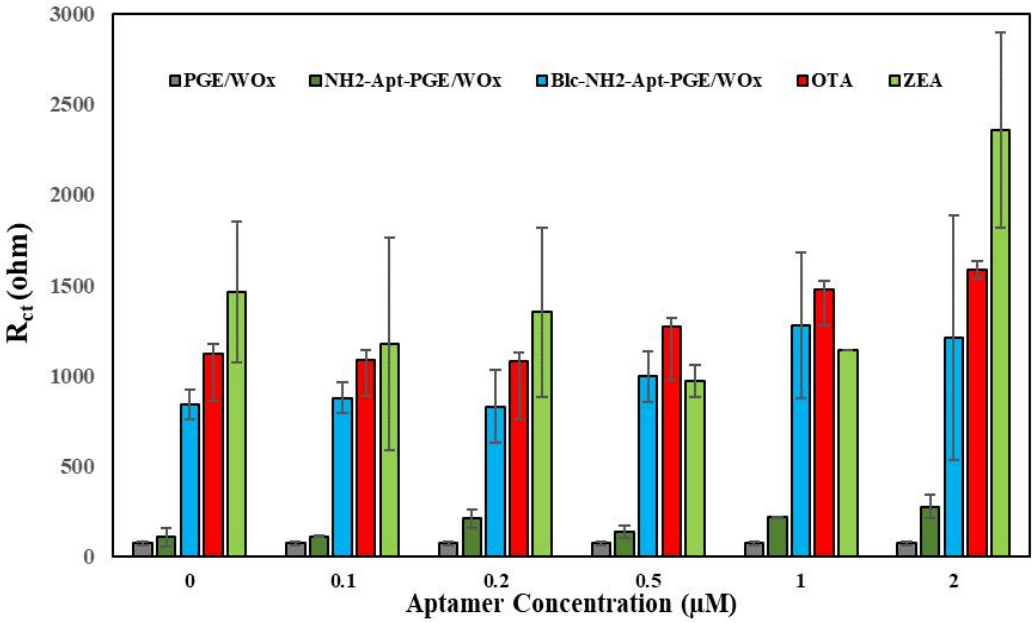

Figure 3.37 The effect of aptamer concentration on the charge transfer resistances of the aptasensors prepared on PGE/WOx (PD) from 0.075 M Na_2WO_4 solution.

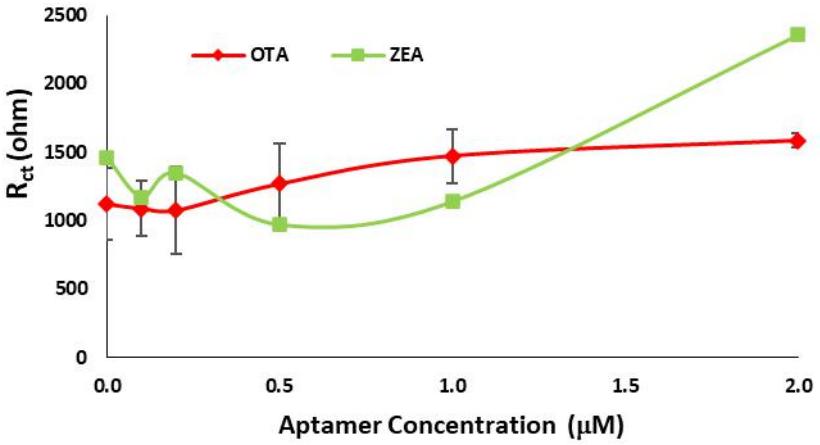

Figure 3.38 The effect of aptamer concentration on the Rct values of OTA and ZEA

According to the figures above, the R_{ct} value has given a rise to 0.5 µM concentrations and then, becomes constant for OTA. However, the electrode response to ZEA, used to reveal any non-specific interactions, was in considerably high in comparison to the target analyte. Therefore, 0.5 M was chosen as the optimum since it provided lower interaction with ZEA molecules as compared to other concentrations.

The last parameter to be optimized is the wash-out time with PBS prior to OTA and ZEA measurements. This parameter was studied for 1 s, 1 min and 5 min under optimized conditions. As shown in **Figure 3.39**, both OTA and ZEA are washed away with longer washing times and the studies have been carried out with 1 s washing time.

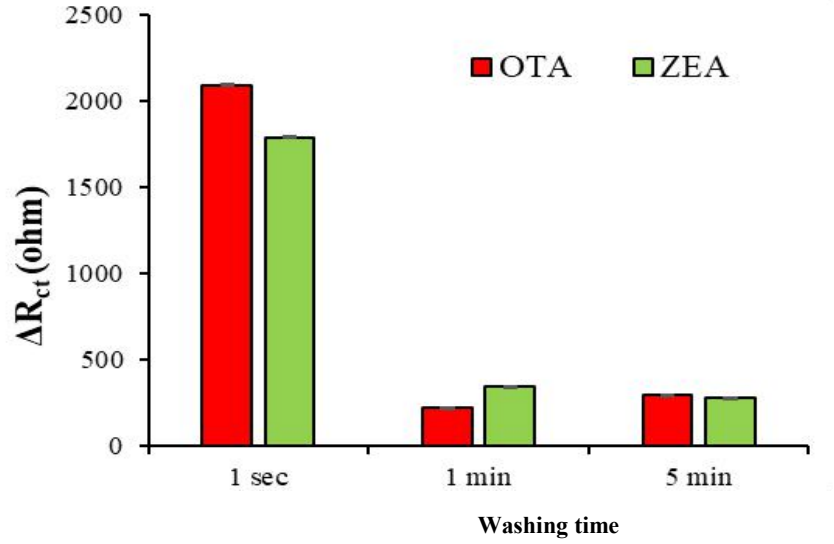

Figure 3.39 The effect of washing time on the R_{ct} values of OTA and ZEA

Under optimal conditions, the electrode surfaces have been closely investigated by Scanning Electron Microscope with in-lens detector and the

images obtained at different magnitudes have been given in **Figure 3.40-3.41**. The electrode type was indicated on the related image and CV and PD deposition.

From the **Figure 3.40A** given below, the bare PGE surfaces exhibited a multilayer structure. Upon depositing the WO_x nanoparticles by cyclic voltammetry, homogenously distributed spherical deposits can be noticed on the graphite layers with a magnification of 20.000 times (**Figure 3.40B**). For pulsed deposited PGE/WOx, rather rare bud-shaped accumulation was observed (**Figure 3.40C**).

Closer inspection of the electrodes prepared in each step are given in **Figure 3.41**. As the stages of the procedure progressed, the close appearance of the electrode surface did not change much, but layer formation was observed, and this formation has become more pronounced with the coating of the biological material such as NH_2-aptamers and OTA even though they are not identified clearly.

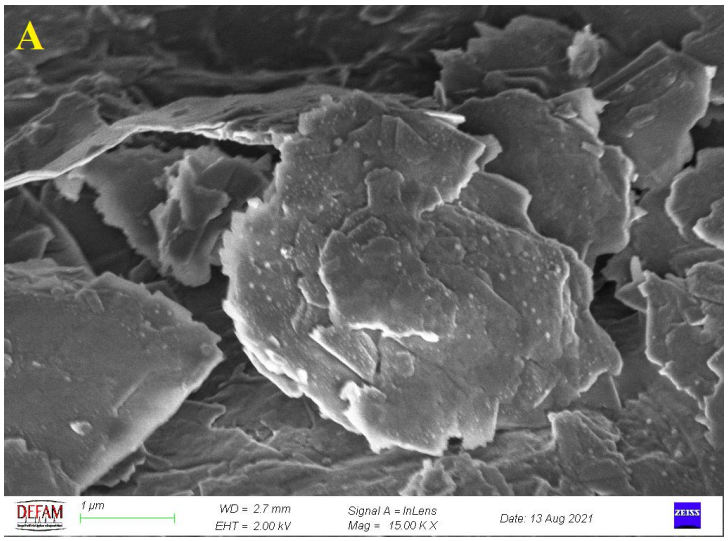

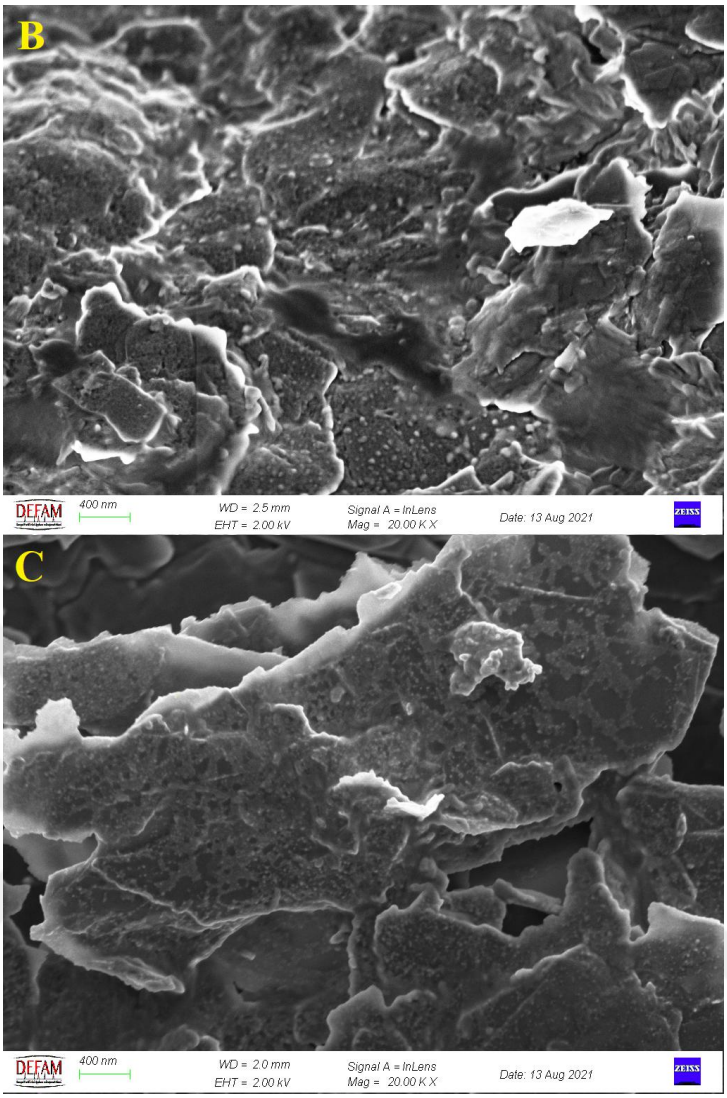

Figure 3.40 The 20.000 times magnified SEM images of A) bare PGE, B) CV and C) Pulsed deposited PGE/WO_x electrodes

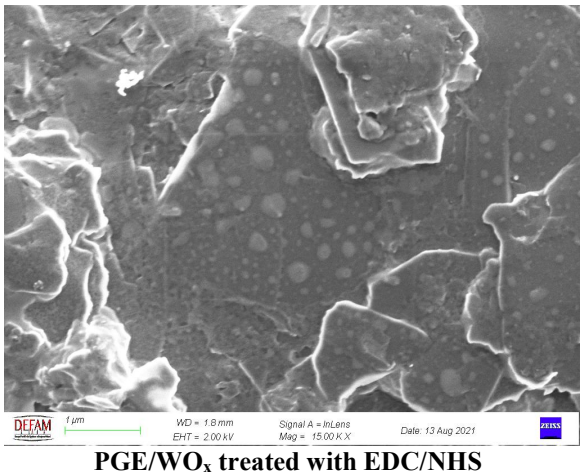

PGE/WO_x treated with EDC/NHS

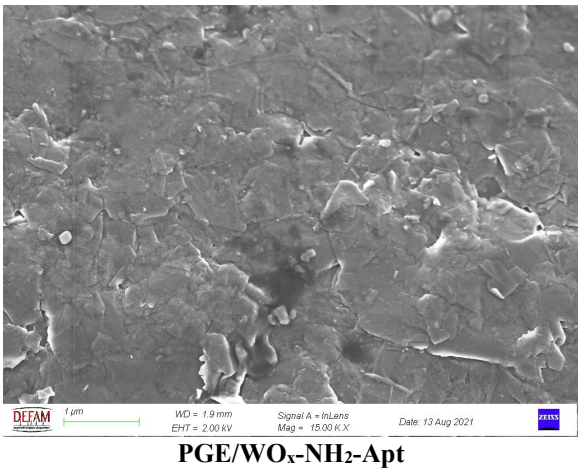

PGE/WO_x-NH_2-Apt

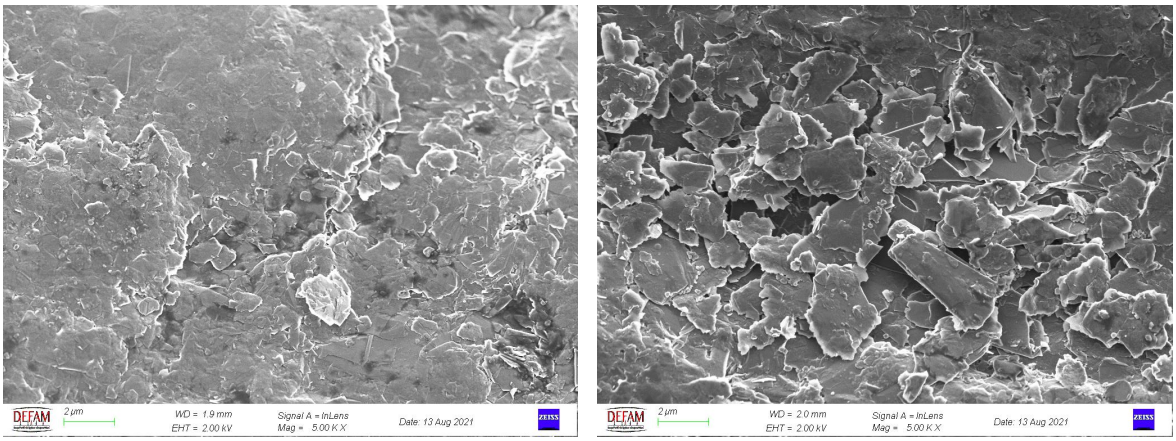

Figure 3.41 SEM images of the electrodes in each stage of the aptasensor fabrication procedure.

Calibration studies have been carried out with a large set of pulsed deposited WO_x modified PGE aptasensors and **Figure 3.42** shows the studies carried out with 1, 2, 5, 10 and 50 nM OTA solutions. Here, the VEGf was used to reveal non-specific interactions. The R_{ct} values were plotted against the OTA concentration, and it was found that linearity was obtained in the range of 1 to 10 nM concentration range with a correlation coefficient of 0.9943 (**Figure 3.43**).

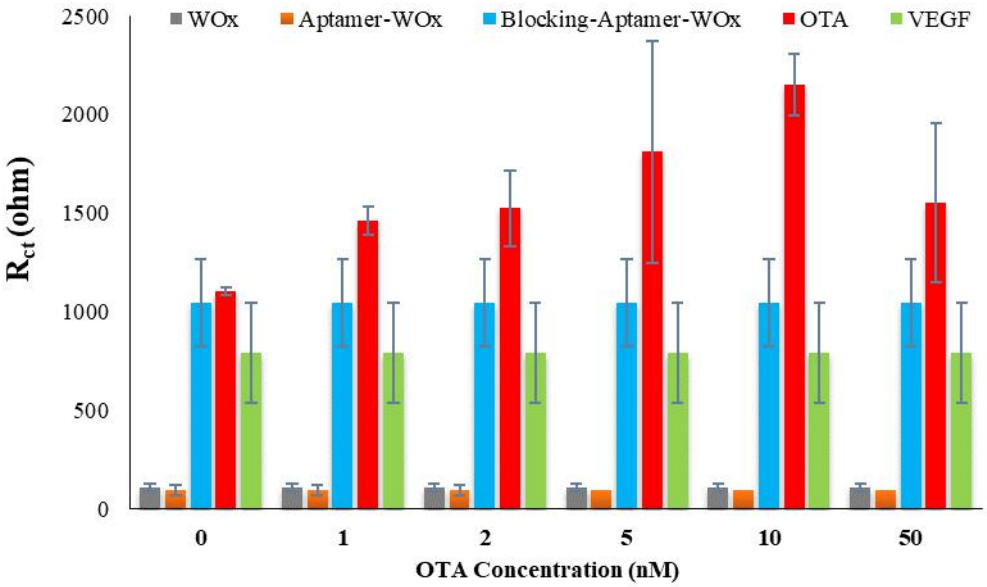

Figure 3.42 The R_{ct} values obtained for the set of OTA solution for calibration and VEGf (1 nM) for non-specific interactions.

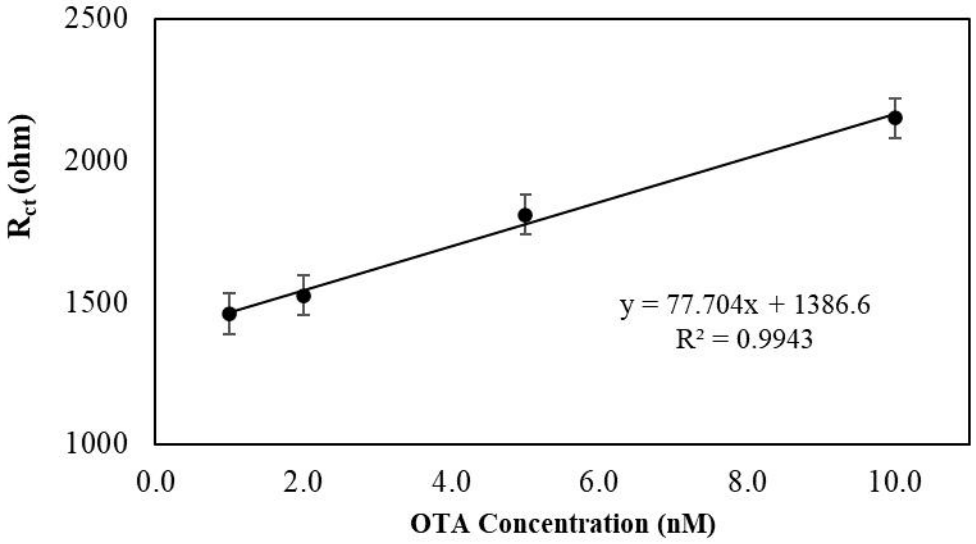

Figure 3.43 Calibration curve for OTA

For lower concentration levels, another set of standard solutions were prepared and ΔR_{ct} values were calculated for 0.05-2.0 nM OTA solutions and plotted against the OTA concentrations as given in **Figure 3.44.**

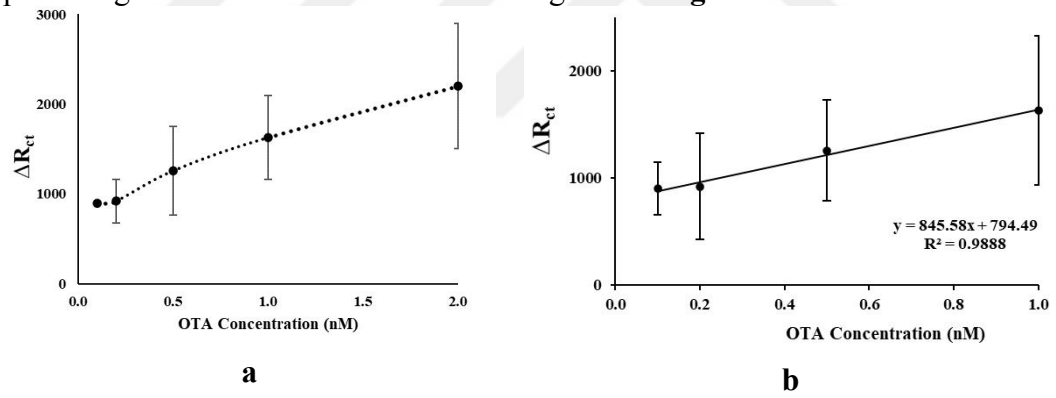

Figure 3.44 a) Effect of OTA concentration on the ΔRct levels measured and b) the calibration curve constructed for OTA

Again, linearity was maintained between 0.1-1.0 nM concentration range with a correlation coefficient of 0.9888. Reproducibility of the method was tested upon triplicate measurements and intermediate precision term was preferred and the RSD values were calculated as 26.7% for 0.1 nM, 19.9% for 0.5 nM and 12.8% for 2.0 nM. These figures might seem high for an analytical method, however, considering each electrode is prepared for single use, these figures are acceptable for an analysis in very low concentration region. The limit of detection (LOD) was calculated as 0.051 nM based on the blank signal added with 3s value and using this in the equation. This LOD level indicates that tungsten oxides represent a novel platform for aptasensor applications as a cost-efficient system.

3.2.2. Studies with 5'-Thiol Aptamer

PGE/WO_x surface was further modified with Au nanoparticles via pulsed deposition technique. As schematically shown in **Figure 3.44**, The Au/WO_x deposited PGE surfaces dipped into the 0.2 µM SH-aptamer solution and kept for 3 hours. Then, the residual active surfaces have been blocked by using 1% mercaptoethanol. The electrodes were incubated in 1 nM OTA solutions for 1 hour and washed with pH 7.4 PBS.

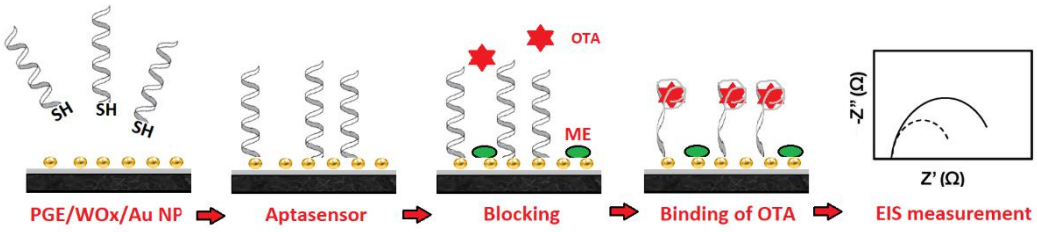

Figure 3.45 Schematic representation of signal formation in Thiol-Aptasensor

The performance of PGE/WOx/Au modified surface was compared against PGE/WOx surface and each aptasensor responses were recorded after incubating them into the 1 nM OTA and 1 nM ZEA solutions.

Figure 3.45 shows the Rct levels plotted for each electrode and it is clear that PGE/WO_x electrode where the NH_2-Apt is immobilized via EDC/NHS mechanism has given much better results.

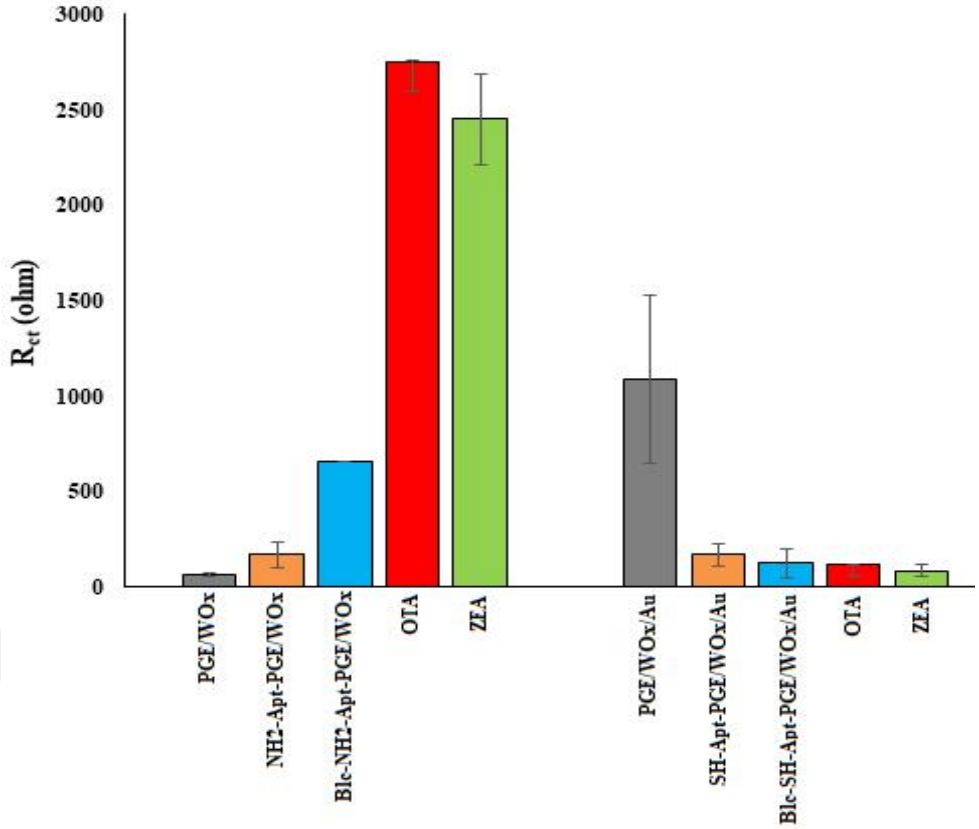

Figure 3.46 Performances of the NH_2-Apt immobilized PGE/WO_x electrode and SH-Apt immobilized PGE/WO_x/Au electrode

Whole studies on aptasensor development have indicated that NH_2-Apt immobilized PGE/WO_x electrode has displayed very sensitive results having an LOD level of sub nanomolar concentrations. Considering the importance of food safety and reliable method, these studies will contribute to the studies on this application areas.

3.3 PEC Studies with Titanium Nanotube Electrode

In recent years, improved photocatalytic activity of TNT doped with tungsten oxide were attributed to several reasons. Indebted to the lower band gap energy, the TNT/WO_3 composite display higher light absorption capacity than the bare TNT and generates more electron and hole pairs. Upon illuminating the TNT/WO_3 composite, these photo-generated electrons can be transferred to the lower lying conduction band of WO_3, while the positive holes move toward the valence band of TiO_2 and reduce the rate of the electron–hole recombination. Furthermore, the TNT/WO_3 composite surfaces are more acidic than pure TNT and therefore, the film enable to absorb more ionic forms (Li et al., 2012).

In this part of the thesis, another catalytic activity of electrochemically deposited WOx film was studied by using titanium nanotube (TNT) electrodes as the support material. Initial studies were devoted to the preparation of TNT, its modification by electrodeposition and investigation of surface morphology. Then, photoelectrocatalytic activity of TNT/WOx has been evaluated on the basis of degradation of azo dyes.

3.3.1 Preparation and Characterization of TNT/WO_3 Electrode

TNT arrays were grown by electrochemical anodization of Titanium foils as described in Experimental Section. The electrode with a surface area of 2.0 cm^2 was placed in the voltammetric cell filled with 50 mL of 0.15 M Na_2WO_4 solution prepared in 0.01 M H_2SO_4 and 0.1 M H_2O_2 as the deposition solution. Three-electrode system was completed with Ag/AgCl reference and Pt wire counter electrode and the potential was cycled between -0.75 - 0.5 V at a rate of 50 mV s^{-1} for 5 times. Cyclic voltammograms are given in **Figure 3.47** where the peak around −0.3 V can be attributed to peroxotungstic acid reduction on the TNT surface. This reduction peak has shifted in positive direction upon depositing the WO_3 layer on the TNT electrode and further increased cycle number.

In consisted with the cyclic voltammograms, closer inspection of the electrode surface has also revealed the cycle numbers used in deposition step have a significant effect on the deposited film thickness. SEM images given in **Figure 3.48** show the difference between the bare TNT and TNT/WOx composite fabricated by cycling the potential for consecutive cycles.

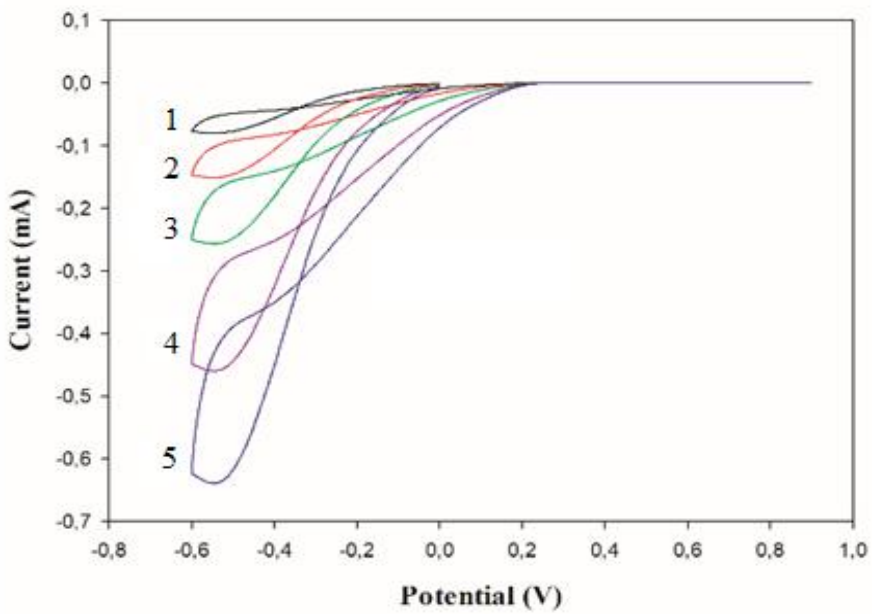

Figure 3.47. Cyclic voltammograms recorded at a scan rate of 50 mV s^{-1} in 0.01 M H_2SO_4 and 0.1 M H_2O_2 mixture containing 0.15 M tungstate ion for five repetitive cycles.

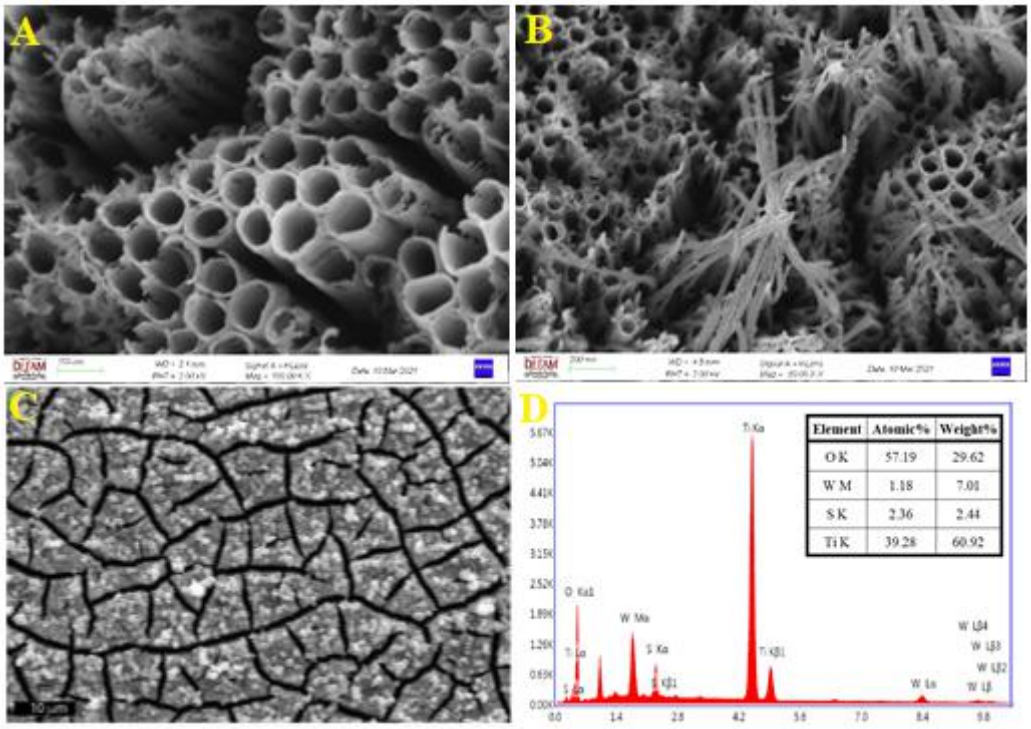

Figure 3.48 SEM images of A) bare TNT and TNT/WO_3 composite electrode prepared by cycling the potential between −0.75 –0.5 V for B) 2 cycles and C) 4 cycles D) EDX spectra of B.

As shown in the figure, the WOx deposits were seen at the edges of the nanotubes for two cycles while for higher cycle numbers, the film has covered the TNT surfaces blocking the active surface area.

Atomic abundance of Ti, W and O contents has been revealed by EDX spectrum of the electrode as 39.28%, 1.18% and 57.19%, respectively. These results are also in good agreement with XPS results given below (**Figure 3.49**).

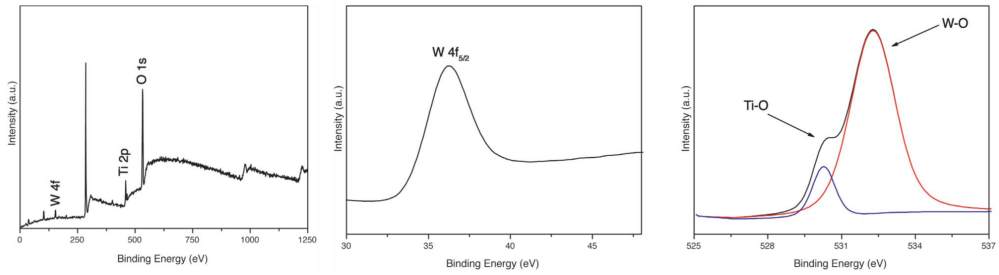

Figure 3.49 A) XPS survey spectra, B) TNT-WO_3 composite electrode and C) the scan of oxygen.

The survey XPS spectrum has revealed the presence of O, Ti and W elements at surface of TNT-WO_3 with atomic compositions 90.06, 7.84 and 1.20 (%), respectively. It was also deduced that the double peaks at 36.2 and 38.2 eV belongs to W4f $_{7/2}$ and W4f $_{5/2}$, respectively, indicating the presence of tungsten as W^{6+} oxidation states in WO_3.

3.3.2 PEC Studies for Screening Dyes

Initially, three azo dyes namely, Orange G (OG), Methylene Blue (MB) and Rhodamine B, (RhB) have been tested and then, the electrode preparation and solution conditions have been optimized for the most promising test material. Then, the WO_x-TNT electrode obtained by cycling the potential for 2 times was placed in the voltammetric cell as the photoanode. A high intensity ultraviolet A lamp was positioned at a 10 cm distance from the transparent cell targeting the anode as given in Experimental Section (**Figure 2.5)**.

In screening studies, the cell was filled with 6.0 mg L^{-1} Orange G, Methylene Blue and Rhodamine B dye solutions for each study and a potential of 0.2 V was applied to the electrode. The performance of the electrode in PEC studies has been evaluated by measuring the absorbance of the 1.0 mL of the solution taken from the cell every 5 min at 480 nm for Orange G, at 525 nm for Rhodamine B and at 660 nm for Methylene Blue by using a UV-Vis spectrophotometer. The absorbances were measured and then, degradation percentages were calculated by using the absorbance ratio to the initial absorbances which corresponds to the C/C^o ratio where C^o is the initial concentration of the dye solution.

Figure 3.50 shows the degradation curves constructed for the azo dyes by using bare TNT electrode and WO_3 modified TNT electrodes as the anode material in PEC system. For the latter electrode, 50 mL of 0.15 M Na_2WO_4 solution prepared in 0.01 M H_2SO_4 and 0.1 M H_2O_2 was used for depositing WO_3 on TNT electrode surface. The potential was cycled twice between 0.9 – (-0.6) V at a rate of 50 mV s^{-1}.

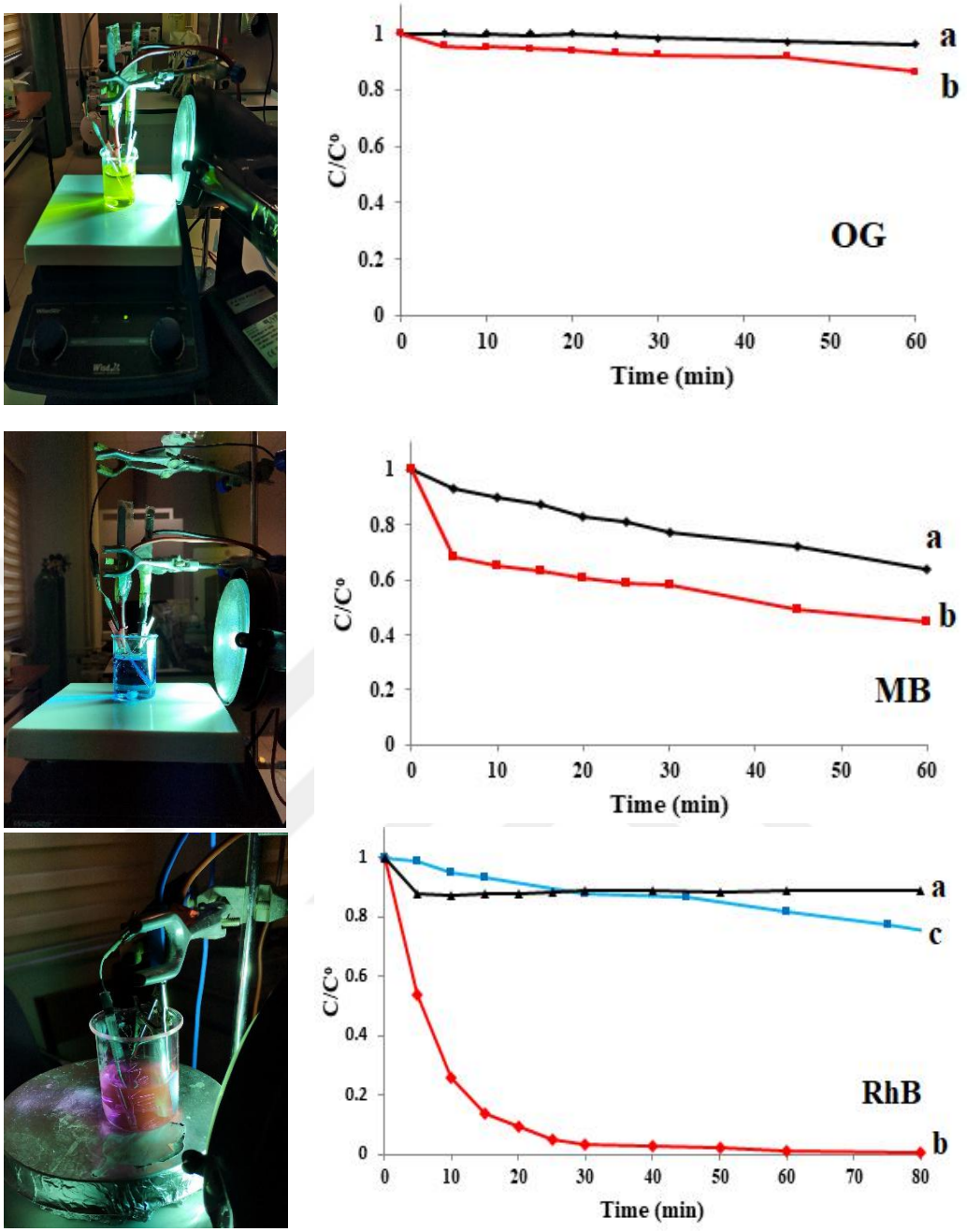

Figure 3.50 The change in the PEC Degradation percentages of the azo dyes by time where the anode material is a) bare TNT and b) TNT/WO_3 electrodes, c) without UV irradiation.

As can be followed from the figure, the degradation of Orange G was very slow due to negative charge repulsion. Methylene blue, on the other hand, strongly absorbs to the electrode surface as reported elsewhere (Yang et al, 2015). Its concentration in the solution was decreased to 68% of its initial value within 5 mins. However, degradation was slowed down afterwards due to the surface coverage in agreement with a former study (Hsieh et al., 2008). These two dyes were not completely degraded even after 60 min but, the best efficiency for PEC

degradation was achieved with Rhodamine B and therefore, further studies have been performed with this dye.

The enhancement of PEC activity can be attributed to the formation of more acidic surfaces enabling the adsorption of RhB molecules which can be readily degraded by the hydroxyl radicals generated. The enhancement of PEC degradation under UV illumination was also tested by using RhB solution. As shown in **Figure 3.51**, the current abruptly increased upon the UV light was on. This can be attributed to the photo-induced charge transfer from electrode to solution.

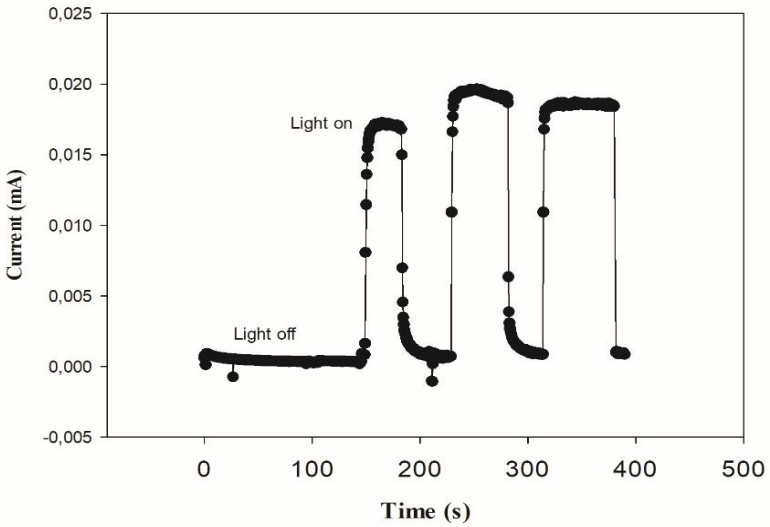

Figure 3.51 Photocurrent profiles of TNT/WO_3 composite electrode in 6 mg L^{-1} RhB solution

Considering that removal efficiency of the PEC system depends on the operating conditions as well as the anode material, the effect of specific parameters have been examined such as WO_4^{2-} ion concentration in deposition solution, cycle number in deposition step. The pH of the dye solution was also studied since their color density and therefore, the absorbance might change with the acidity of the solution.

The performance of the TNT/WO_x composite electrode towards PEC degradation of RhB was investigated for five different tungstate concentrations in deposition solution. **Figure 3.52** shows the percentage of RhB color removal under PEC conditions where the electrode was prepared from deposition solution containing 10-50 mM of Na_2WO_4 in 0.01 M H_2SO_4 and 0.1 M H_2O_2 solution by cycling the potential between 0.9 – (-0.6) V at a rate of 50 mV s^{-1} for 5 times.

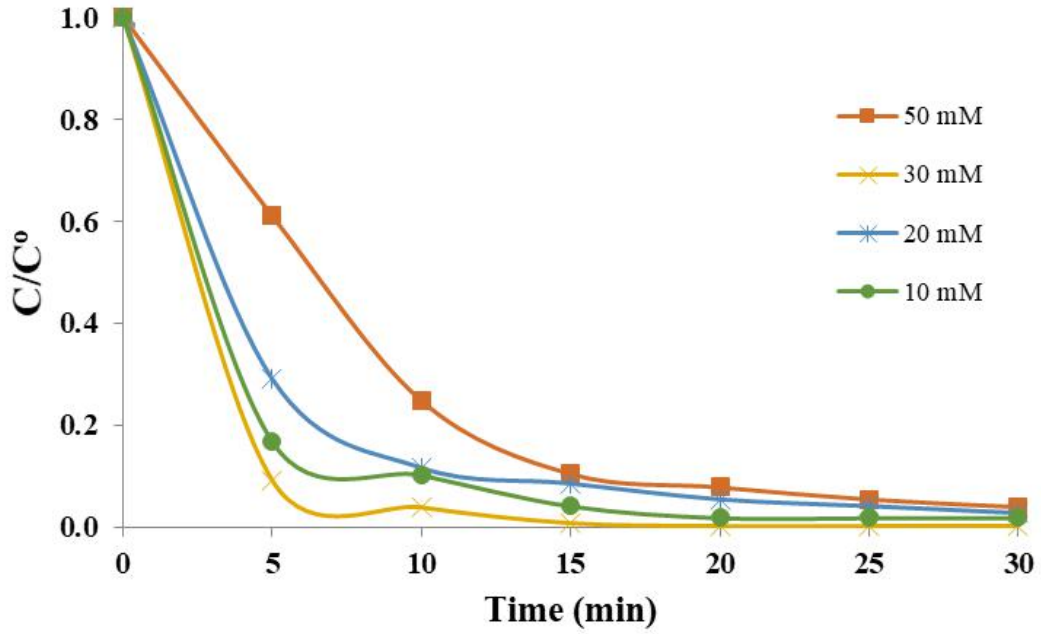

Figure 3.52 The effect of tungstate ion concentration in fabrication of TNT/WO_3 on the PEC degradation efficiency of RhB

As can be deduced from the figure, 15 min would be sufficient for complete removal of the color of 6.0 mg/L RhB. Among the concentrations studied, 30 mM was chosen as this concentration gives the best results. It should be noted that high concentration of tungstate ions results in less PEC activity probably due to the bulk deposition far from the nanoparticle formation.

Another parameter determining the film thickness is the number of repetitive cycles applied for the electrochemical composition. As can be seen from **Figure 3.53**, the best results have been obtained with 2 repetitive cycles in the potential range studied. Here, it is important to note that bare TNT has displayed less performance than WO_x modified TNT electrode. This finding is in agreement with the SEM images given above where the WO_x deposits were seen at the edges of the nanotubes at first and then, the film covers the active surface area blocking its PEC activity.

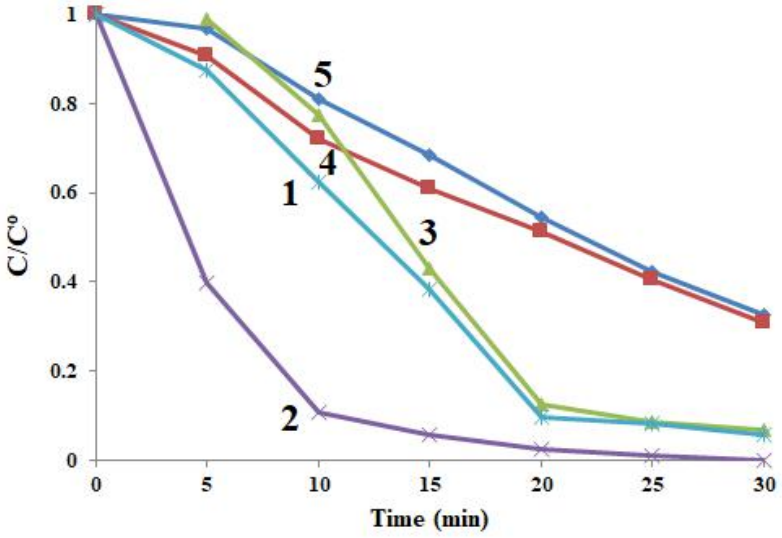

Figure 3.53 The effect of cycle number used in the deposition step on the time dependent degradation efficiency of RhB

Another parameter to be optimized is the solution pH since the color intensity of dye solution might change with medium pH. Besides, hydroxyl radical formation requires low acidity in the medium according to the reaction.

$$H_2O \rightarrow OH^{\cdot} + H^{+} + e^{-} \qquad \text{(Eq. 3.5)}$$

Therefore, the effect of medium pH was studied in a range of 2.0 to 12.0 by using BR buffer system and as shown in **Figure 3.53** no differences was observed in their absorbance values. Further studies were carried out in pH 7.0 medium.

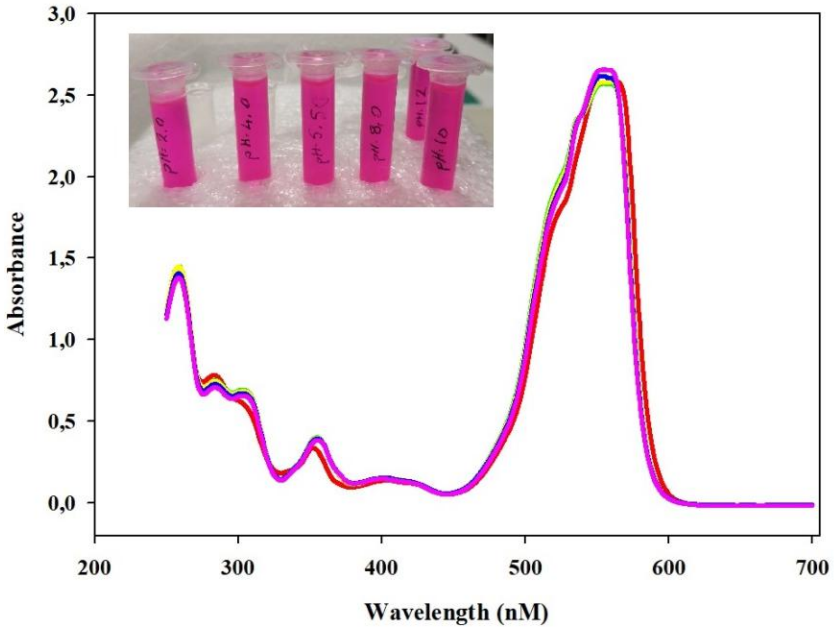

Figure 3.54 The effect of the solution pH on the absorbance of 6 mg L^{-1} RhB solution

3.3.3. Kinetic Study

Under optimized conditions, the PEC degradation of RhB was investigated for different concentrations. **Figure 3.55** shows the decolorization performances of the electrode at three different concentrations and clearly, the process is completed in 15 min for lower concentrations. The kinetic data obtained have indicated that photoelectrochemical degradation of RhB has followed first order kinetics.

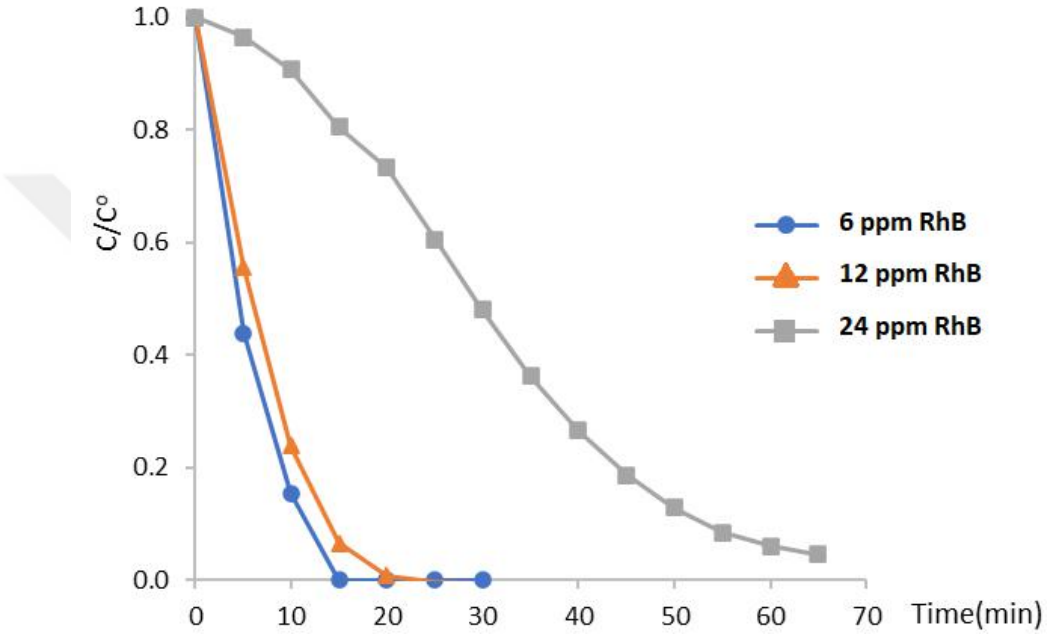

Figure 3.55 PEC degradation of RhB solutions in various concentrations.

Apparent first-order rate constant (min^{-1}) can be expressed as below where t is the irradiation time (min).

$$-ln\ (C/C^o) = k_{PEC}\ t \qquad \text{(Eq. 3.6)}$$

These rate constants can be calculated from the slope of the linear curves. According to the first-order rate constants in **Figure 3.56**, it can be deduced that similar rate constants were obtained for 6 and 12 mg L^{-1} RhB with good correlation coefficients. Much smaller rate constants observed for 24 mg L^{-1} can be attributed to the limited surface area of the electrode.

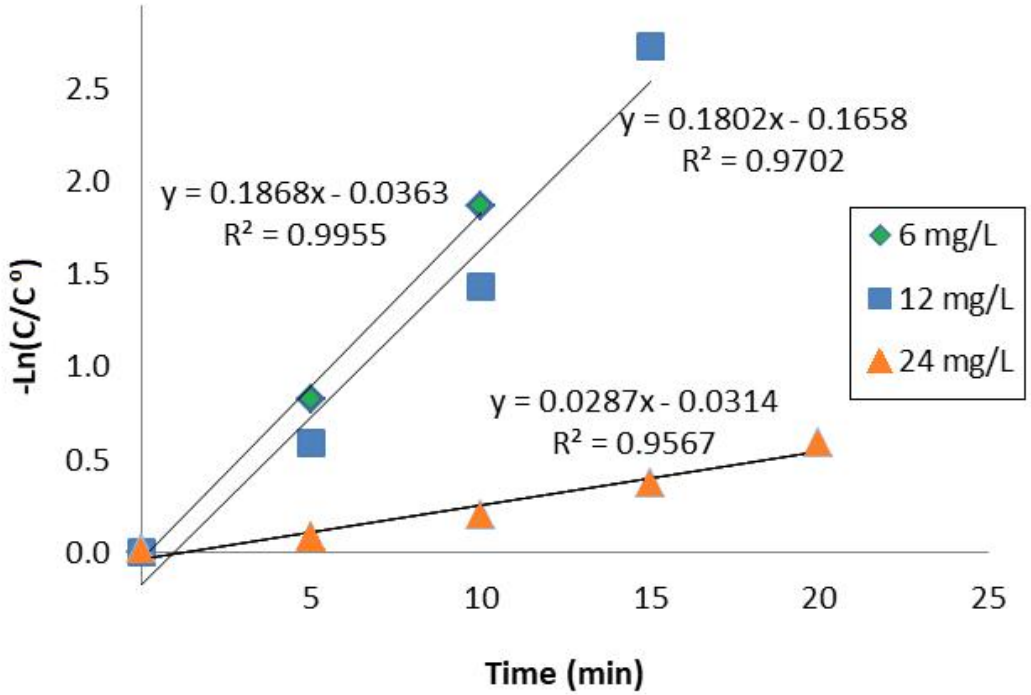

Figure 3.56 First order kinetic of RhB degradation for three different concentrations.

Overall results suggested that degradation efficiency of PEC process strongly depends on the surface characteristics as well as the operating conditions. The synergic interaction between the TNT and WO_3 offers a superior catalytic activity and display a potential for the use in solar irradiation inherited from the chemical properties of the modifier.

3. CONCLUSION

This thesis consisted of three main sections devoted to reveal the catalytic activity of tungsten oxide modified electrodes. In the first section, the studies were focused on the reduction of dissolved oxygen which constitute an electrochemically important reaction, and synergistic effect of platinum nanoparticles deposited onto the WO_x film was tested towards the ORR.

Fabrication conditions of the electrode have been optimized and overall results have shown that cyclic voltammetric deposition has resulted higher peak formation than pulsed deposition. SEM images of the CV deposited electrodes have displayed homogeneous distribution of Pt nanoparticles over the metal oxide film. Pulsed deposited GCE/WO_x-Pt electrode on the other hand, has given better response after GCE/MoO_x/Pt in terms of peak potential.

A catalase-based biosensor was designed to monitor this ORR signal for peroxide determination however, chronoamperograms have displayed rather noisy background and therefore, a non-enzymatic method for hydrogen peroxide determination was developed. Hydrogen peroxide can be determined in micromolar levels by this means and the method was successfully applied to a commercial disinfectant analysis used in pandemic conditions.

In the second part of the thesis, a disposable electrode; pencil graphite (PGE) modified with WO_x film was used as a support for aptasensor studies. Previous studies in the lab have revealed that transition metal oxides provide an appropriate platform for immunosensing and aptasensing technologies based on EIS measurements in the presence of 5 mM $[Fe(CN)_6]^{3-/4-}$ ions in the cell. The charge transfer resistance (R_{ct}) values for each electrode were determined by the size of the semicircle by fitting the Nyquist plots to a conventional Randles equivalent circuit.

In the light of these studies, an aptasensor based on WO_3 nanoparticles was fabricated for ochratoxin A detection. WO_3 nanoparticles have been electrodeposited onto the PGEs by using different deposition techniques and under optimized conditions, two different aptamers have been bounded to the electrode surface by different strategies.

Performances of the NH_2-Apt immobilized PGE/WO_x electrode and SH-Apt immobilized PGE/WO_x/Au electrode was compared and better results have been obtained with the former electrode.

Covalent binding efficiency of NH_2-Apt by EDC/NHS mechanism was confirmed by comparing the results obtained with NH_2-Apt bound to the electrode surface through adsorption. The differences in R_{ct} levels clearly indicated the efficiency of the EDC/NHS mechanism probably via -OH groups on the metal oxide film. Then, the solution parameters (tungstate ion concentration, pH and aptamer concentration) along with operating conditions have been optimized for OTA detection. Selectivity was ensured by using another mycotoxin, ZEA and the calibration graphs have been constructed in nanomolar levels.

In the final part of the thesis, another challenge in the electrocatalytic activity search, tungsten oxide film has been electrodeposited on the titanium nanotubes (TNT) and then, by setting the potential at an appropriate value, the composite film was applied for the PEC degradation of several azo dyes. The application conditions of this binary-oxide film to Rhodamine B degradation have been optimized and kinetic studies were also carried out to clarify the degradation mechanism. In conclusion, synergic interaction between the TNT and WO_3 offers a superior catalytic activity and display a potential for the use in solar irradiation inherited from the chemical properties of the modifier.

Overall studies can be evaluated as different aspects of electrocatalytic activities of tungsten oxide have been clarified in this thesis to contribute the studies of this kind in the literature.

REFERENCES

Açıkyıldız et al., 2014. Electrocatalysis and the Production of Nanoparticles, Açıkyıldız, M., Gürses, A., Korucu, M.E., Güneş, K., *Modern Electrochemical Methods in Nano, Surface and Corrosion Science*, *Intech Open Book Series,* DOI: 10.5772/58340

Akoğulları et al., 2020. Pulsed deposited manganese and vanadium oxide film modified with carbon nanotube and gold nanoparticle: chitosan and ionic liquid-based biosensor, Akoğulları, S., Çınar, S., Özdokur, K.V., Aydemir, T., Ertaş, F.N., Koçak, S., *Electroanalysis*, 32: 445-453

Azzouz et al., 2021. Nanomaterial-based aptasensors as an efficient substitute for cardiovascular disease diagnosis: future of smart biosensors, Azzouz, A., Hejji, L., Sonne, C., Kim, K.-H., Kumar, V., *Biosensors and Bioelectronics,* in press, https://doi.org/10.1016/j.bios.2021.113617.

Benvidi et al., 2015. Electrochemical deposition of gold nanoparticles on reduced graphene oxide modified glassy carbon electrode for simultaneous determination of levodopa, uric acid and folic acid. Benvidi A., Firouzabadi A. D., Ardakani M. M., Mirjalili B. B. F., Zare R. *Journal of Electroanalytical Chemistry*, 736: 22–29.

Benvidi et al., 2017. Developing an electrochemical sensor based on a carbon paste electrode modified with nanocomposite of reduced graphene oxide and $CuFe_2O_4$ nanoparticles for determination of hydrogen peroxide, Benvidi, Nafar, A.T., Jahanbani, S., Tezerjani, M.D., Rezaeinasab, M., Dalirnasab, S., *Materials Science and Engineering C* 75:1435–1447

Beyene et al., 2004. (Bio)sensors based on manganese dioxide modified carbon substrates: retrospections, further improvements and applications, Beyene, N.W., Kotzian P., Schachl, K., Alemuc, H., Turkusic, E., Copra, A., Moderegger, H., Svancara, I., Vytras, K. Kalcher, K. *Talanta* 64: 1151–1159

Bajunaid, 2021. Electrodeposition of Hydrogen Molybdenum Tungsten Bronze Films and Electrochemical Reduction of Carbon Dioxide. Bajunaid, M. *East Tennessee State University*, https://dc.etsu.edu/etd/3857.

Cao et al., 2017. Combination of photocatalytic and electrochemical degradation of organic pollutants from water, Cao, D., Wang, Y., Zhao, X., *Current Opinion in Green and Sustainable Chemistry*, 6: 78–84

Chen et al., 2017. A novel aptamer- metal ions- nanoscale MOF based electrochemical biocodes for multiple antibiotics detection and signal amplification, Chen, M., Gan, N., Zhou, Y., Li, T., Xu, Q., Cao, Y., Chen, Y., *Sensors and Actuators B*, 242: 1201–1209

Chou et al., 2006. Electrodeposition synthesis and electrochemical properties of nanostructured-MnO_2 films, Chou, S., Cheng, F., Chen, J., *Journal of Power Sources,* 162: 727–734

Cubero-Leon et al., 2017. Determination of Ochratoxin A in Black and White Pepper, Nutmeg, Spice Mix, Cocoa, and Drinking Chocolate by High-Performance Liquid Chromatography Coupled with Fluorescence Detection: Collaborative Study, Cubero-Leon, E. Bouten, K., Senyuva, H., Stroka1, J., *Journal of AOAC International*, 100 (5) 1458-1468

Çakar et al., 2013. Molybdenum oxide/platinum modified glassy carbon electrode: A novel electrocatalytic platform for the monitoring of electrochemical reduction of oxygen and its biosensing applications, I. Çakar, K.V. Ozdokur, B. Demir, E. Yavuz, D.O. Demirkol, S. Koçak, S. Timur, F.N. Ertaş, *Sensors and Actuators B* 185: 331– 336

Çırak et al., **2017.** Synthesis, surface properties, crystal structure and dye sensitized solar cell performance of TiO_2 nanotube arrays anodized under different voltages, Çırak, B.B., Karadeniz, S.M., Kılınç, T., Çağlar, B., Ekinci, A.E., Yelgin, H., Kürekçi, M., Çırak, Ç. *Vacuum* 144: 183–189.

Çiftyürek et al., 2019. Spectroscopic Understanding of SnO_2 and WO_3 Metal Oxide Surfaces with Advanced Synchrotron Based; XPS-UPS and Near Ambient Pressure (NAP) XPS Surface Sensitive Techniques for Gas Sensor Applications under Operational Conditions, Ciftyürek, E., Šmíd, B., Li, Z., Matolín, V., Schierbaum K., ***Sensors,*** 19: 4737.

Derina et al., 2020. Non-enzymatic electrochemical approaches to cholesterol determination, Derina, K., Korotkova, E., Barek, *J. Journal of Pharmaceutical and Biomedical Analysis* 191: 113538

Dong et al., 2020. A review on WO_3 based gas sensors: morphology control and enhanced sensing properties, C. Dong, R. Zhao, L. Yao, Y. Ran, X. Zhang, Y. Wang, *Journal of Alloys and Compounds*, 820: 153194.

Dong et al., 2021. Metal oxide based non-enzymatic electrochemical sensors for glucose detection, Dong, Q., Ryu, H., Lei, L., *Electrochimica Acta* 370: 137744

Duca and Koper, 2020. Surface and Interface Science: Volume 8: Interfacial Electrochemistry, Duca, M. and Koper, M.T.M., *Fundamental Aspects of Electrocatalysis*, Book Editor: K. Wandelt, Vol. 8, Chapter 59, https://doi.org/10.1002/9783527680603.ch59

El-Deab, 2012. Platinum nanoparticles–manganese oxide nanorods as novel binary catalysts for formic acid oxidation, El-Deab, M.S., *J Adv. Res.* 3: 65–71

EU regulation, 2010. Setting Maximum Levels for Certain Contaminants in Foodstuffs as Regards Aflatoxins, European Union Commission Regulation No 165/2010, *Amending Regulation (EC)* No 1881/2006, 2010.

Evtugyn et al., 2013. Electrochemical Aptasensor for the Determination of Ochratoxin A at the Au Electrode Modified with Ag Nanoparticles Decorated with Macrocyclic Ligand, Evtugyn, G., Porfireva, A., Sitdikov, R., Evtugyn, V., Stoikov, I., Antipin, I., Hianik, T., *Electroanalysis* 25:1847- 1854

Feng et al., 2005. The fabrication and switchable super hydrophobicity of TiO_2 nanorod films, X. Feng, J. Zhai, L. Jiang, *Angew Chem.* 117: 5245-5248.

Foura et al., 2017. Fe-Doped TiO_2 Supported on HY Zeolite for Solar Photocatalytic Treatment of Dye Pollutants. Foura, G.; Chouchou, N.; Soualah, A.; Kouachi, K.; Guidotti, M.; Robert, D. *Catalysts*, 7: 344-360.

Gamry, 2021. https://www.gamry.com/application-notes/EIS/basics-of-electrochemical-impedance-spectroscopy/ (Access date Sep 2021)

Gan et al., 2007. Electrocatalytic oxidation of methanol on carbon nanotubes/ graphite electrode modified with molybdenum oxide nanoparticles, Y. Gan, H. Hui, Z. Wen-kui, *Transactions of Nonferrous Metals Soc.* 17: 214–219.

Garcia-Segura and Brillas, 2017. Applied photoelectrocatalysis on the degradation of organic pollutants in wastewaters, Garcia-Segura S. Brillas, E., *Journal of Photochemistry and Photobiology C: Photochemistry Reviews* 31: 1–35

Ghorbani, et al., 2019. Application of various optical and electrochemical aptasensors for detection of human prostate specific antigen: A review, Ghorbani, F., Abbaszadeh, H., Ezzati, J., Dolatabadic, N., Aghebati-Malekid, L., Yousefi, M., *Biosensors and Bioelectronics* 142: 111484.

Girault, 2004. Analytical and Physical Electrochemistry, Girault, H.H., *Fundamental Sciences,* EPFL Press, Distributed by Mercel Dekker Inc.

Goud et al., 2018. Progress on nanostructured electrochemical sensors and their recognition elements for detection of mycotoxins: A review, Goud, K.Y., Kailasa, S.K.,1, Kumar,V., Tsang, Y.F., Lee, S.E., Gobib, K.V., Kim, K.H., *Biosensors and Bioelectronics*, 121: 205–222

Gökçe et al., 2020. Aptamer-modified pencil graphite electrodes for the impedimetric determination of ochratoxin A, Gökçe, G., Aissa, S.B., Nemčeková, K., Catanante, N., Raouafi, N., Marty, J.L., *Food Control* 115. 107271

Guo et al., 2015. A comprehensive review on synthesis methods for transition-metal oxide nanostructures, Ting Guo, Ming-Shui Yao, Yuan-Hua Lin, Ce-Wen Nan, *Cryst Eng Comm*, 17: 3551-3585

Guo et al., 2021. Aptamer-Based Biosensor for Detection of Mycotoxins, Guo, X., Wei, X., Zhang, J., Saive, M., Fauconnier, M.L., Wang, J., *Prime Archives in Chemistry.* Ed. Lakem, A.E. Hyderabad, India: Vide Leaf.

Guaraldo et al., 2016. Hydrogen production and simultaneous photoelectrocatalytic pollutant oxidation using a TiO_2/WO_3 nanostructured photoanode under visible light irradiation, Guaraldo, T.T., Gonçales, V.R., Silva, B.F. de Torresi, S.I.C., Zanoni M.V.B. *Journal of Electroanalytical Chemistry* 765: 188–196

Gutierrez et al., 2018. Analytical Applications of Cu@Ptpd/C Nanoparticles for the Quantification of Hydrogen Peroxide, Gutierrez F.A., Giordana I.S., Fuertes V.C., Montemerlo A., Sieben J.M., Alvarez A.E., Rubianes M.D., Rivas G. A. *Microchemical Journal* 141: 240–246

Güler, 2008. Determination of Ochratoxin A and Fumonisin Production In Figs, Güler, F.K., PhD. Thesis (PhD), *İstanbul Technical University, Institute of Science and Technology*, 2008

Gürel and Ertaş, 2010. Elektrokimyanın Temel İlkeleri, Nişli, G. and Ertaş, F.N., *Emin Dikman 1. Uygulamalı Elektrokimya Lisansüstü Yaz Okulu Kitabı*, E.Ü. Fen Fak. Kimya Böl**.** 14-17 Eylül 2010 İzmir. pp. 1-17.

Hernandez-Pichardo et al., 2015. The role of the WO_3 nanostructures in the oxygen reduction reaction and PEM fuel cell performance on WO_3-Pt/C electrocatalysts. Hernandez-Pichardo, M.L.,Gonzalez-Huerta, R.G., del Angel, P., Tufino- Velazquez, M., Lartundo, L., *Int. J. Hydrogen Energy,* 40: 17371–17379.

Hsieh et al., 2008. Impact of mesoporous pore distribution on adsorption of methylene blue onto titania nanotubes in aqueous solution, Hsieh, C.T., Fan, W.S., Chen, W.Y., Microporous and Mesoporous Materials 116: 677–683.

https://www.rsc.org, 2021, https://www.rsc.org/periodic-table/element/74/tungsten, Access date March 2021.

Huang et al., 2014. Enhanced Photoelectrocatalytic and Photoelectrochemical Properties by High-Reactive TiO_2/$SrTiO_3$ Hetero-Structured Nanotubes with dominant {001} Facet of Anatase TiO_2, Huang, J.R. Tan, X., Yua, T., Zhao, L., Hub, W-L., *Electrochimica Acta* 146: 278–287.

In et al., **2007.** Effective visible light-activated B-doped and B,N-codoped TiO_2 photocatalysts. S. In, A. Orlov, R. Berg, F. García, S. Pedrosa-Jimenez, M.S. Tikhov, D.S. Wright, R.M. Lambert. *Journal of American Chemical Society*, 129: 13790–13791.

Jia et al., 2016. Construction of graphite/TiO_2/nickel foam photoelectrode and its enhanced photocatalytic activity, Jia, J., Li, D., Cheng, X., Wan, J., Yu, X., *Applied Catalysis A: General* 525: 128–136

Karaca and Koçak, 2021. Fabrication and characterization of enhanced hydrazine electrochemical sensor based on gold nanoparticles decorated on the vanadium oxide, ruthenium oxide nanomaterials, and carbon nanotubes composites, Karaca, S., Koçak, S., *Turkish Journal of Chemistry*, 45: 1210-1223

Khater et al., 2017. Biosensors for plant pathogen detection, Khater, M., Escosura-Muñiza, A., Merkoçi, A., *Biosensors and Bioelectronics* 93: 72–86

Kırlangıç et al., 2021. Development of Transition Metal Oxide Film Coated Platforms for Aptamer Based Electrochemical Detection of Ochratoxin A, Kirlangiç, I.A., Kara, P., Ertaş, F.N., *Journal of The Electrochemical Society*, 168: 057516

Kıvrak et al., **2020.** Aptamer-based electrochemical biosensing strategy toward human non-small cell lung cancer using polyacrylonitrile/polypyrrole nanofibers, Kıvrak, E., Yardımcı, A.I., Ilhan, R., Kırmızıbayrak, P.B., Yılmaz, S., Kara, P., *Analytical and Bioanalytical Chemistry,* 412:7851–7860

Kim et al., 2015. Efficient visible light-induced H_2 production by Au@CdS/TiO_2 nanofibers: Synergistic effect of core-shell structured Au@CdS and densely packed TiO_2 nanoparticles. M. Kim, Y.K. Kim, S.K. Lim, S. Kim, S.I. In, *Applied Catalysis B Environmental*. 166–167, (2015) 423–431.

Koçak et al., 2013. Electrochemical deposition and behavior of mixed-valent molybdenum oxide film at glassy carbon and ITO electrodes, Koçak, S., Ertaş, F.N., Dursun, Z., *Applied Surface Science* 265: 205– 213

Kothavale et al., 2020. Photoelectrocatalytic degradation of Rhodamine B using N doped TiO_2 thin Films, Kothavale, V.P, Patil, T.S., Patil, P.B., Bhosale, C.H., *Materials Today: Proceedings* 23: 382–388

Kumar et al., 2018. Effect of Brownian motion on reduced agglomeration of nanostructured metal oxide towards development of efficient cancer biosensor, S. Kumar, Ashish, S. Kumar, S. Augustine, S. Yadav, B. K. Yadav, R. P. Chauhan, A. K. Dewan, B. D. Malhotra, *Biosensors and Bioelectronics*, 102: 247–255

Kumar et al., 2021. A review of recent advances in non-enzymatic electrochemical creatinine biosensing, Kumar, R.K.R., Shaikh, M.O., Chuang, C-H., *Analytica Chimica Acta*, in press.

Kuşci et al., 2018. Development and characterization of zirconium oxide and palladium nanoparticle composite electrodes and investigation of their electrocatalytic applications, Kuşci, C., Özdokur, K.V., Koçak, S., Ertaş, F.N., *IV. International Ege Composite Materials Symposium Book*, 6-8 September 2018, İzmir, Turkey.

Kuşçu et al., 2020. Development of cobalt oxide film modified electrode decorated with platinum nanoparticles as a biosensing platform for phenol, Kuşcu, C., Özdokur, K.V., Koçak, S., Ertaş, F.N., *International Journal of Environmental Analytical Chemistry*, 100(8): 873–881.

Kühl and Strasser, 2016. Oxygen Electrocatalysis on Dealloyed Pt Nanocatalysts, Kühl, S., Strasser, P., *Topics in Catalysis,* 59:1628–1637.

Lee et al., 2013. Morphology and composition control of manganese oxide by the pulse reverse electrodeposition technique for high performance supercapacitors, S.H. Lee, H. Lee, M.S. Cho, J.D. Nam, Y. Lee, *J. Mater. Chem. A,* 1: 14606–14611 pp.

Li et al., 2012. Multi-functionalized biosensor at WO_3 –TiO_2 modified electrode for photoelectrocatalysis of norepinephrine and riboflavin, Li, Y., Hsu, P.C., Chen, S.M. *Sensors and Actuators B: Chemical* 174: 427–435

Li et al., 2015. Bimetallic Au@Pt@Au core–shell nanoparticles on graphene oxide nanosheets for high-performance H_2O_2 bi-directional sensing, Li, X-R, Xu, M-C., Chen, H-Y., Xu, J-J, *Journal of Materials Chemistry B,* 3 (2015) 4355.

Li et al., 2020. Effect of hydrogen spillover on the surface of tungsten oxide on hydrogenation of cyclohexene and N-propylcarbazole. Li, P., Dong, Y., Ding, Y., Zhang, H., Yang, M. Cheng, H., *International Journal of Hydrogen Energy*, 46(5), 3945–3953.

Liu et al., 1999. Atomic force microscopy imaging of molybdenum oxide film electrodeposited on a carbon electrode, Liu, S., Zhang, Q., Wang, E., Dong, S., *Electrochemistry Communications,* 1: 365–369.

Manikandan et al., 2017. High performance supercapacitor and non-enzymatic hydrogen peroxide sensor based on tellurium nanoparticles, Manikandan, M., Dhanuskodi, S., Maheswari, N., Muralidharan, G., Revathi, C., Kumar, R.T.R., Rao, G.M., *Sensing and Bio-Sensing Research* 13: 40–48

Medina et al., 2021. Current role of modern chromatography and mass spectrometry in the analysis of mycotoxins in food, Medina, D.A.V., Borsatto, J.V.B., Maciel, E.V.S., Lanças, F.M., *Trends in Analytical Chemistry* 135: 116156

Mor et al., 2006. Use of highly ordered TiO2 nanotube arrays in dye-sensitized solar cells, G. K. Mor, K. Shankar, M. Paulose, O. K. Varghese, C. A. Grimes, *Nano Lett.,* 6: 215-218.

Mukherjee et al., 2020. Mechanism of thiol-induced color change of tungsten oxide nanoparticles, Mukherjee, A., Sengupta, S.K., Steeves, D.M., Soares, J.W., Whitten, J.E, ***Chemical Physics Letters***, 752: 137568.

Munoz et al., 2017. Trends in electrochemical impedance spectroscopy involving nanocomposite transducers: Characterization, architecture surface and bio-sensing, Munoz, J., Montes, R., Baeza, M., *Trends in Analytical Chemistry* 97: 201-215.

Nakayama et al., 2005. Electrodeposition of manganese and molybdenum mixed oxide thin films and their charge storage properties, Nakayama, A., Tanaka, A., Sato, Y., Tonosaki, T., Ogura, K. *Langmuir*, 21: 5907–5913 pp.

Nakiboğlu, 2010. Elektroanalitik Kimyada Katalitik Tepkimeler, Nakiboğlu, N., *Emin Dikman 1. Uygulamalı Elektrokimya Lisansüstü Yaz Okulu Kitabı*, Ege Üni. Fen Fak. Kimya Böl.14-17 Eylül 2010 İzmir. p.p. 139-158.

Naresh and Lee, 2021. A Review on Biosensors and Recent Development of Nanostructured Materials-Enabled Biosensors. Naresh, V. and Lee, N., *Sensors* 21: 1109.

Özdokur et al., 2014. Pyranose oxidase and Pt–MnOx bionanocomposite electrode bridged by ionic liquid for biosensing applications, Ozdokur, K.V., Demir, B., Yavuz, E., Ulus, F., Erten, Ç., Aydın, İ., Demirkol, D.O., Pelit, L., Timur, S., Ertaş, F.N. *Sensors and Actuators B,* 197: 123–128 pp.

Özdokur et al., 2016a. Development of pulsed deposited manganese and molybdenum oxide surfaces decorated with platinum nanoparticles and their catalytic application for formaldehyde oxidation**,** Özdokur, K.V., Tatlı, A.Y., Yılmaz, B., Koçak, S., Ertaş, F.N. *Int. Jornal of Hydrogen Energy*, 41: 5927–5933 pp.

Özdokur et al., 2016b. A novel ethanol biosensor on pulsed deposited MnOx-MoOx electrode decorated with Pt nanoparticles, Özdokur, K.V., Demir, B., Atman, E., Tatlı, A.Y., Yılmaz, B., Demirkol, D.O., Koçak,S., Timur, S., Ertas, F.N., *Sensors and Actuators B* 237: 291–297 pp.

Özdokur et al., 2018. Fabrication, characterization and catalytic applications for dissolved oxygen of palladium decorated copper molybdenum oxide modified glassy carbon electrode, Özdokur, K.V., Koçak, S., Çırak, Ç., Çağlar, B., Koçak, Ç.C., Ertaş, F.N., IV. *International Ege Composite Materials Symposium Book*, 6-8 September 2018, İzmir, Turkey.

Özdokur et al., 2019. Nanostructured Metal-Metal Oxides and Their Electrocatalytic Applications, Özdokur, K.V., Koçak S., Ertaş, F.N. Chapter in *Advanced Coating Materials* Ed, Li, L., Yang, Q., Wiley Interscience, 2019. ISBN: 9781119407560.

Quaino et al., 2014. Volcano plots in hydrogen electrocatalysis – uses and abuses, Quaino, P., Juarez, F., Santos, Schmickler, E., Beilstein W., *J. Nanotechnol*, 5: 846–854.

Palanisamy et al., 2015. An electrochemical facile fabrication of platinum nanoparticle decorated reduced graphene oxide; application for enhanced electrochemical sensing of H2O2. Palanisamy, S., Lee, H.F., Chen, S-M, Thirumalraj, B. *RSC Advances,* 5: 105567–105573.

Palmas et al., 2021. Trend in using TiO2 nanotubes as photoelectrodes in PEC processes for wastewater treatment, Palmas S, Mais L, Mascia M, Vacca A, *Current Opinion in Electrochemistry*, in press.

Pang et al., 2019. Formation of high-performance Cu-WOx@C tribasic composite electrode for aqueous symmetric supercapacitor. Pang, S., Gong, L., Du, N., Luo, H., Yu, K., Gao, J., Zheng, Z. Zhou, B. ***Materials Today Energy***, 13, 239–248.

Peleyeju and Viljoen, 2021. WO3-based catalysts for photocatalytic and photoelectrocatalytic removal of organic pollutants from water – A review, Peleyeju, M.G., Viljoen, E.L., *J of Water Process Engineering* 40: 101930.

Rahimi and Shakerian, 2013. Ochratoxin A in dried figs, raisings, apricots, dates on Iranian retail market, Rahimi, E. and Shakerian, A., *Health*, 5 (12): 2077-2080

Rahman et al., 2010. A Comprehensive Review of Glucose Biosensors Based on Nanostructured Metal-Oxides, M. Rahman, A.J.S. Ahammad, J.-H. Jin, S. J. Ahn, J.-J. Lee, Sensors, 10: 4855-4886

Rajput et al., 2021. Photoelectrocatalysis as a high-efficiency platform for pulping wastewater treatment and energy production, Rajput, H., Kwon, E.E., Younis, S.A., Weon, S. Jeon, T.H., Choi, W., Kim, K-H, *Chemical Engineering Journal* 412 (2021) 128612

Randviir and Banks, 2013. Electrochemical impedance spectroscopy: an overview of bioanalytical applications, Randviir, E.P. and Banks, C.E., *Analytical Methods*, 5 (2013) 1098

Reithmaier et al., 2011. Nanotechnological Basis for Advanced Sensors, Ed. J.P. Reithmaier, P. Paunovic, W. Kulisch, C. Popov, P. Petkov, Springer, Ed. J.P. Reithmaier.

Riboni et al., 2013. WO_3 –TiO_2 vs. TiO_2 photocatalysts: effect of the W precursor and amount on the photocatalytic activity of mixed oxides, F. Riboni , L.G. Bettini , D.W. Bahnemann , E. Selli , *Catalysis Today* 209: 28–34.

Rozman et al., 2020. Flexible electrochromic tape using steel foil with WO3 thin film, Rozman, M., Zener, B., Matoh, L., Godec, R.F., Mourtzikou, A., Stathatos, E., Bren, U., Luksic, M. *Electrochim. Acta* 330: 135329

Santos et al., 2015. Electrodeposition of WO_3 Nanoparticles for Sensing Applications, L., Neto, J.P., Crespo, A., Baião, P. Barquinha, P., Pereira, L.,

Martins, R., Fortunato, E., Chapter in Electroplating of Nanostructures, Santos, Ed. M. Aliofkhazraei, IntechOpen, DOI: 10.5772/61216. Available from: https://www.intechopen.com/chapters/49175

Seh et al., 2017. Combining theory and experiment in electrocatalysis: Insights into materials design, Seh, Z.W., Kibsgaard, J., Dickens, C.F., Nørskov, C.J.K., Jaramillo, T.F., *Science* 355, 4998.

Shinde and Jun, 2020. Review on recent progress in the development of tungsten oxide-based electrodes for electrochemical energy storage, Shinde, P.A. and Jun, S.C. *ChemSusChem* 13: 11–38.

Si et al., 2014. Electrochemical Oxygen Reduction Reaction, Si, F., Zhang, Y., Yan, L., Zhu, J., Xiao, M., Liu, C., Xing, W., Zhang, J., 4th chapter in the Book *Rotating Electrode Methods and Oxygen Reduction Electrocatalysts,* Ed. Wei Xing, p.p. 133-170, Elsevier.

Sun et al., 2015. Modification of TiO_2 nanotubes by WO_3 species for improving their photocatalytic activity, Sun, H., Dong, B., Su, G., Gao, R., Liu, W., Song, L., Cao, L., *Applied Surface Science* 343: 181–187

Tang et al., 2006. MnO_x/CeO_2 mixed oxide catalysts for complete oxidation of formaldehyde: effect of preparation method and calcination temperature, X. Tang,X., Li, Y., Huang, X., Xu, Y., Zhu, H., Wang, J., Shen, W. *Appl. Catal. B,* 62: 265–273 pp.

Tang et al., 2018. Graphene Modified TiO_2 Composite Photocatalysts: Mechanism, Tang, B.; Chen, H.; Peng, H.; Wang, Z.; Huang, W. Progress and Perspective. *Nanomaterials*, 8: 105-132.

Tural et al., 2003. Enstrümental Analysis I, H. Tural, H.İ. Gökçel, F.N. Ertaş, *Ege Üniversitesi Fen Fakültesi Yayınları*, No 186.

Wang, 2006 "Analytical Electrochemistry", Wang, J. John Wiley & Sons, 3rd Ed.

Wang and Dong, 1994. Electrocatalytic properties of mixed-valence molybdenum oxide thin film modified microelectrodes, Wang, B., Dong, S., *J. Electroanal. Chem.,* 379: 207–214 pp.

Wang et al., 2013. Visible-light photoelectrocatalytic degradation of rhodamine B over planar devices using a multi-walled carbon Nanotube-TiO_2 composite,

Wang, Q., Shang, J., Song, H., Zhu, T., Ye, J., Zhao, F., Li, J., He, S., *Materials Science in Semiconductor Processing* 16: 480–484

Wang et al., 2015. Integration of membrane filtration and photoelectrocatalysis using a TiO_2/carbon/Al_2O_3 membrane for enhanced water treatment. Wang, G., Chen, S., Yu, H., Quan, X., *Journal of Hazardous Materials* 299: 27–34

Wang et al., 2018. Transition-metal-oxide-based catalysts for the oxygen reduction reaction, Wang, Y., Li, J., Wei, Z. *J. Mater. Chem. A,* 6: 8194–8209 pp.

Wang et al., 2020. Electrochemically self-doped WO_3/TiO_2 nanotubes for photocatalytic degradation of volatile organic compounds, Wang, X. Sun, M. Murugananthan, M. Zhang, Y. Zhang, L. *Applied Catalysis B: Environmental* 260: 118205.

Wu et al., 2012. Ultrasensitive one-step rapid detection of ochratoxin A by the folding-based electrochemical aptasensor, Wu, J., Chu, H., Mei, Z., Deng, Y., Xue, F. Zheng, L., Chen, W., *Analytica Chimica Acta* 753: 27– 31

Xie et al., 2012. XPS studies on surface reduction of tungsten oxide nanowire film by Ar+ bombardment. Xie, F.Y., Gong, L., Liu, X., Tao, Y.T., Zhang, W.H., Chen, S.H., Meng, H., Chen, J., *Journal of Electron Spectroscopy and Related Phenomena*, 185(3–4):112–118,

Xie et al., 2020. In-situ phase transition of WO_3 boosting electron and hydrogen transfer for enhancing hydrogen evolution on Pt, Xie, C., Chen, W., Du, S., Yan, D., Zhang, Y., Chen, J., Liu, B., Wang, S. *Nano Energy*, 104653.

Yang et al., 2015. Hydrothermal synthesis of TiO_2–WO_3–bentonite composites: conventional versus ultrasonic pretreatments and their adsorption of methylene blue, Yang, C., Zhu, Y., Wang, J., Li, Z., Su, X., Niu, C., *Applied Clay Science,* 105–106: 243–251

Yang et al., 2017. Nanoporous PdCu alloy as an excellent electrochemical sensor for H_2O_2 and glucose detection, Yang, H., Wang, Z., Li, C., Xu, C., *Journal of Colloid and Interface Science* 491: 321–328

Yang et al., 2021. Aptamer-functionalized carbon nanomaterials electrochemical sensors for detecting cancer relevant biomolecules, Yang, Y., Yang, X., Yang, X., Yuan, Q., *Carbon* 129: 380-395

Yao et al., 2012. Decolorization of Rhodamine B in a thin-film photoelectrocatalytic (PEC) reactor with slant-placed TiO_2 nanotubes electrode, Yao, Y., Li, K., Chen, S., Jia, J., Wang, Y., Wang, H., *Chemical Engineering Journal* 187: 29– 35

Yavuz et al., 2015. Electrochemical Preparation, Characterization of Molybdenum-Oxide/Platinum Binary Catalysts, and Its Application to Oxygen Reduction Reaction in Weakly Acidic Medium, E. Yavuz, K.V. Özdokur, I. Çakar, S. Koçak, F.N. Ertaş, *Electrochimica Acta* 151: 72–80

Žalnėravičius et al., 2019. Nanoplatelet MoS_2 arrays decorated with Pt nanoparticles for nonenzymatic detection of hydrogen peroxide, Žalnėravičius, R., Gedminase, A., Ruzgas, T., Jagminas, A. *Journal of Electroanalytical Chemistry* 839: 274–282

Zejli et al., 2018. Label free aptasensor for ochratoxin A detection using polythiophene-3-carboxylic acid, Zejli, H.,. Goud, K.Y., Marty, J.L., *Talanta* 185: 513–519

Zeng et al., 2017. Preparation of vertically aligned WO_3 nanoplate array films based on peroxotungstate reduction reaction and their excellent photoelectrocatalytic performance, Zeng, Q., Li, J., Bai, J., Li, X., Xia, L., Zhou, B., *Applied Catalysis B: Environmental* 202: 388–396.

Zhang and Chen, 2017. Recent advances in graphene-based nanomaterials for fabricating electrochemical hydrogen peroxide sensors, Zhang, R., Chen, W., *Biosensors and Bioelectronics* 89: 249–268.

Zhao et al., 2019. Boosting the performance of WO_3/n-Si heterostructures for photoelectrochemical water splitting: from the role of Si to interface engineering, Zhao, Y., Brocks, G., Genuit, H., Lavrijsen, R., Verheijen, M.A., Bieberle-Hütter, A. *Laser Phys. Rev*. 9: 1900940.

Zhao et al., 2021. Hydrogenation of naphthalene to decalin catalyzed by Pt supported on WO_3 of different crystallinity at low temperature. Zhao, T.,

Zhao, B., Niu, Y., Liang, Y., Liu, L., Dong, J., Li, X. *Journal of Fuel Chemistry and Technology*, 49(8:1181–1189.

Zheng, 2011. Nanostructured Tungsten Oxide-Properties, Synthesis and Applications, Zheng H., *Advanced Functional Materials*, 21: 2175-2196

Zheng et al., 2014. Visible light photoelectrocatalytic degradation of methyl orange using anodized nanoporous WO_3, Zheng, Q., Lee, C., *Electrochimica Acta,* 115: 140– 145

Zoski, 2007. Handbook of Electrochemistry, Zoski, C.G., Elsevier, 1st Ed.

Zhou et al., 2006. Electro-catalytic effect of manganese oxide on oxygen reduction at teflon bonded carbon electrode, D. Zhou, X. Lu, D. Liu, *Trans. Nonferrous Met. Soc. China,* 16: 217–222 pp.

ACKNOWLEDGEMENT

I am sincerely thankful to my supervisors, Prof. Dr. F. Nil ERTAŞ and Prof. Dr. Süleyman KOÇAK for their endless guidance and encouragement during my whole thesis period.

My dearest supervisor, Prof. Dr. F. Nil ERTAŞ; I am very thankful to your endless support during my thesis period. Treating me like a daughter of your own beyond your consultancy, I am very grateful to your understanding, warm and kind support.

My second supervisor, Prof. Dr. Süleyman KOÇAK; My endless thanks to you for your encouragement, share of knowledge and experience since the first day I met with the world of electrochemistry.

My dearest judge members, Prof. Dr. Nuri NAKİBOĞLU and Prof. Dr. Zekerya DURSUN; I would like to thank you very much for your support and valuable suggestions for the qualified progress of my thesis studies.

I would like to express my sincere gratitutes to Ass. Prof. Dr. Hasan ERTAŞ for his sincere guidance throughout the studies.

My dearest friend and colleague Assist. Dr. K. Volkan ÖZDOKUR; I am very thankful to your sincere friendship and endless support for my thesis studies.

I would like to thank to Prof. Dr. Çağrı Çırak, Prof. Dr. Bülent Çağlar for their support and for the opportunity to do some of my research at Binali Yıldırım University.

Dear Prof. Dr. Pınar KARAKADAYIFÇILAR, I would like to thank you for giving me opportunity to work at Ege University Faculty of Pharmacy Analytical Chemistry Laboratory and for your valuable contributions to my thesis within the scope of OTA studies.

My dearest friend Ph.D Student İrem AYDIN KIRLANGIÇ; Thank you very much for your valuable support during my thesis work.

I am grateful to my role model, my dear mother, Fatma ÇAKAR, for her contributions to my presence of today. I am proud of you because I am the daughter of a strong mother who takes the bad luck of being at a time when she is prevented from being a teacher during her education life, and does her best for the education of her children with an endless patience.

I would like to thank to my father Fevzi ÇAKAR, my brother İlker ÇAKAR and all my dear family members for always supporting me in my whole education life.

I would like to thank to my dear husband Oğuzhan DAVASLIOĞLU for his endless support and patience during my doctorate studies and for his belief in me.

I would like to thank to my dear friend Şebnem Gül İLARSLAN for her support and love, with whom I started the doctorate together and I believe we will finish together within this year.

My dear friends, Elif DAVASLIOĞLU, Celal DEĞERLİ, Burak BERAN, Seda ZİĞEN, FETHİYE ALERT group members and all my friends, whose names I can't mention, I am grateful to for your support and encouragement during this process.

Finally, I would like to thank to Ege University Research Foundation (BAP) for financially supporting my thesis studies (2018-FEN-036).

İrem ÇAKAR DAVASLIOĞLU

Ekim, 2021, İzmir

ÖZGEÇMİŞ

Kişisel Bilgiler	
Öğrenci Adı	İrem ÇAKAR DAVASLIOĞLU
TC Kimlik No	
Tel No	
e-mail	
Eğitim Bilgileri	
Lisans	Ege Üniversitesi Kimya Bölümü, 2005-2009
Yüksek Lisans	Fen Bilimleri Enstitüsü Analitik Kimya Bölümü, 2009-2013
YL Tez Adı	The Preparation of Polyoxomolybdate Modified Electrodes and Analytical Applications
Doktora Tezine Bağlı Yayın ve Bildiriler	
Uluslararası Kongre Sunumları	
. Tungsten Oxide Modified Electrodes: A Promising Platform for Biosensors, ***İrem Çakar Davaslıoğlu,*** K. Volkan Özdokur, Süleyman Koçak, F. Nil Ertaş (Poster) ***NYNA 2018, 3-5 Temmuz 2017, Barselona***	
. The Use of Tungsten Oxide Modified Titanium Nanotube Electrodes as a Platform for Photoelectrochemical Degradation, ***İrem Çakar Davaslıoğlu***, K. Volkan Özdokur, Süleyman Koçak, Çağrı Çırak, Bülent Çağlar, F. Nil Ertaş (Sözel) ***KOMPEGE 06-08 Eylül 2018, İzmir***	
. Electrocatalytic Activity of Tungsten Oxide Modified Electrodes Decorated with Platinum Nanoparticles Toward Oxygen Reduction Reactions and Analytical Applications, ***İrem Çakar Davaslıoğlu***, K. Volkan Özdokur, Süleyman Koçak, F. Nil Ertaş (Poster) ***ICABC, Antalya, 27-30 Mart 2019***	
. Development of Tungsten Oxide Modified Pencil Graphite Electrode as a Novel Platform for Ochratoxin-A Detection, ***İrem Çakar Davaslıoğlu***, İrem Aydın Kırlangıç, Pınar Kara, Süleyman Koçak, F. Nil Ertaş (Sözel) ***ICABC, Antalya, 11-14 Mart 2020***	
SCI Yayın	
WO_3 decorated TiO_2 nanotube array electrode: Preparation, characterization and superior photoelectrochemical performance for Rhodamine B dye degradation, ***İrem Çakar Davaslıoğlu***, K. Volkan Özdokur, Süleyman Koçak, Çağrı Çırak, Bülent Çağlar, Burcu Bozkurt Çırak, F. Nil Ertaş, Journal of Molecular Structure 1241 (2021) 130673	